

STATIC ERROR MODELING OF SENSORS
APPLICABLE TO OCEAN SYSTEMS

JEREMY AH-CHONG

**STATIC ERROR MODELING
OF SENSORS APPLICABLE TO OCEAN SYSTEMS**

by

Jeremy Ah-Chong

A Thesis Submitted to the Faculty of

The College of Engineering

in Partial Fulfillment of the Requirements for the Degree of

Master of Science

Florida Atlantic University

Boca Raton, Florida

May 2003

STATIC ERROR MODELING
OF SENSORS APPLICABLE TO OCEAN SYSTEMS

by

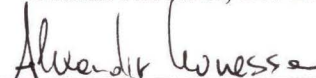
Jeremy Ah-Chong

This thesis was prepared under the direction of the candidate's thesis advisor, Dr. P. Edgar An, Department of Ocean Engineering, and has been approved by the members of his supervisory committee. It was submitted to the faculty of the College of Engineering and was accepted in partial fulfillment of the requirements for the degree of Master of Science.


SUPERVISORY COMMITTEE:



Thesis Advisor, Dr. Edgar An



Dr Alexander Leonessa



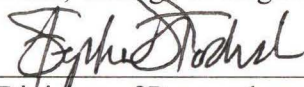
Dr. Frederick Driscoll



 Chairman, Department of Ocean Engineering



Dean, College of Engineering



Division of Research and Graduate Studies

4/18/03

Date

ACKNOWLEDGEMENTS

I would like to express my gratitude to my advisor, Dr. Edgar AN for his valuable help on conducting the thesis and for giving me the opportunity to work on this project. I must thank the department of Ocean Engineering of Florida Atlantic University for all the facilities accorded to the students and the support I received throughout this study.

I extend my thanks to Dr. Driscoll and Dr. Leonessa for their useful comments during the thesis correction.

A thanks goes also to the AUV laboratory for providing the data necessary to the project realization.

Je voudrais remercier ma mere, mon pere, Jessie, Popo et la derniere petite merveille Hugo pour leur soutien durant ces deux dernieres annees.

ABSTRACT

Author: Jeremy Ah-Chong
Title: Static Error Modeling of Sensors applicable to Ocean Systems
Institution: Florida Atlantic University
Thesis Advisor: Dr. P. Edgar An
Degree: Master of Science
Year: 2003

This thesis presents a method for modeling navigation sensors used on ocean systems and particularly on Autonomous Underwater Vehicles (AUV). An extended Kalman filter was previously designed for the implementation of the Inertial Navigation System (INS) making use of Inertial Measurement Unit (IMU), a magnetic compass, a GPS/DGPS system and a Doppler Velocity Log (DVL). Emphasis is put on characterizing the static sensor error model. A "best-fit ARMA model" based on the Aikake Information Criterion (AIC), Whiteness test and graphical analyses were used for the model identification. Model orders and parameters were successfully estimated for compass heading, GPS position and IMU static measurements. Static DVL measurements could not be collected and require another approach. The variability of the models between different measurement data sets suggests online error model estimation.

TABLE OF CONTENTS

LIST OF ACRONYMS	viii
LIST OF TABLES	ix
LIST OF FIGURES	x
1 INTRODUCTION.....	1
1.1 PROBLEM STATEMENT	2
1.2 OBJECTIVES	3
1.3 THESIS OUTLINE.....	4
2 BACKGROUND	5
2.1 MORPHEUS SENSOR SUITE	5
2.2 AUTOCORRELATION TECHNIQUES	9
2.2.1 Autocorrelation Function.....	9
2.2.2 Cross-Correlation Coefficient	10
2.2.3 The Yule-Walker Equation.....	11
2.2.4 The Partial Autocorrelation function.....	13
2.3 STOCHASTIC PROCESSES	16
2.3.1 Signal Characteristics.....	17
2.3.2 Noise Characteristics.....	18

2.3.3	<i>Autoregressive model</i>	21
2.3.4	<i>Moving Average model</i>	22
2.3.5	<i>Autoregressive-Moving Average model</i>	24
2.3.6	<i>Autoregressive-Integrated Moving Average model</i>	25
2.4	AUTOCORRELATION FUNCTION INTERPRETATION	26
2.4.1	<i>Interpretation of the Autocorrelation function</i>	26
2.4.2	<i>Interpretation of the Partial Autocorrelation function</i>	27
2.4.3	<i>Simple ACF and PACF patterns</i>	28
3	SENSOR ERROR MODELING	33
3.1	BOX-JENKINS BUILDING BLOCKS	34
3.2	ESTIMATION STAGE	35
3.2.1	<i>Least Square Estimation</i>	36
3.3	SELECTING THE MODEL ORDER	38
3.3.1	<i>The Akaike information theoretic criterion (AIC)</i>	39
3.3.2	<i>Mehra Whiteness Test (WT)</i>	40
4	RESULTS AND ANALYSIS	42
4.1	DATA COLLECTION	42
4.2	TCM2 MAGNETOMETER COMPASS HEADING	48
4.2.1	<i>Steady state measurement:</i>	48
4.2.2	<i>Order and parameter estimation:</i>	52
4.2.3	<i>Conclusion</i>	67
4.3	GPS SENSOR NOISE CHARACTERISTICS	69
4.3.1	<i>Steady state measurement</i>	69

4.3.2	<i>Order and Parameter estimation</i>	73
4.3.3	<i>Conclusion</i>	77
4.4	IMU SENSOR NOISE CHARACTERISTICS	80
4.4.1	<i>Accelerometer characteristics</i>	80
4.4.2	<i>Gyroscope characteristics</i>	89
5	CONCLUSIONS	99
	REFERENCES	101
	APPENDIX A	105
	APPENDIX A – 1	106
	APPENDIX A – 2	107
	APPENDIX A – 3	110
	APPENDIX A – 4	111

LIST OF ACRONYMS

ACF	= Autocorrelation Function
AR	= Autoregressive
ARIMA	= Autoregressive Integrated Moving Average
ARMA	= Autoregressive Moving Average
DVL	= Doppler Velocity Log
GPS/DGPS	= Global Positioning System / Differential Global Positioning System
IMU	= Inertial Measurement Unit
INS	= Inertial Navigation System
MA	= Moving Average
PACF	= Partial Autocorrelation Function

LIST OF TABLES

Table 2.1: Sensor error characteristics [7]	8
Table 2.2: Guideline for Box-Jenkins model identification [32].....	29
Table 4.1: Data collection dates.....	43
Table 4.2: Steady State Data collected	43
Table 4.3: Results of heading model error order selection	67
Table 4.4: Standard deviation of the heading signal.....	68
Table 4.5: Results of GPS model error order selection	79
Table 4.6: Standard deviation of the GPS signals.....	79
Table 4.7: Acceleration whiteness test.....	81
Table 4.8: Results of acceleration model error order selection	88
Table 4.9: Standard deviation of the accelerometer signals	88
Table 4.10: Angular rates characteristics.....	89
Table 4.11: Results of angular rate model error order selection.....	98
Table 4.12: Standard deviation of the angular rate signals.....	98

LIST OF FIGURES

Figure 2.1: GPS/DGPS equipped Morpheus AUV 1	5
Figure 2.2: Bio Inspired Propulsion System Morpheus AUV 2	6
Figure 2.3: Random process	17
Figure 2.4: AR process	22
Figure 2.5: MA model.....	23
Figure 2.6: ARMA model.....	25
Figure 2.7: Time series signals	29
Figure 2.8: AR signal order 1 autocorrelations.....	30
Figure 2.9: MA signal order 1 autocorrelations.....	31
Figure 2.10: ARMA order (1,1) autocorrelations	31
Figure 2.11: White noise signal autocorrelations	32
Figure 3.1: Box-Jenkins building blocks	35
Figure 4.1: Compass measurements case 1.....	44
Figure 4.2: GPS measurements case 1	45
Figure 4.3: Compass measurements case 2.....	45
Figure 4.4: Compass and DVL measurements case 3.....	46
Figure 4.5: IMU measurements case 3	46

Figure 4.6: Compass measurements case 4.....	47
Figure 4.7: IMU measurements case 4	47
Figure 4.8: TCM2 case 2 (a) and case 1 (b) compass heading	48
Figure 4.9: TCM2 case 2 (a) and case 1 (b) heading ACF	48
Figure 4.10: Case 1 (a) and Case 2 (b) DVL-CTD Temperature.....	50
Figure 4.11: Case 1 (a) and Case 2 (b) Temperature Vs Heading	50
Figure 4.12: Lab case 2 heading residual AIC (above) and WT (below)	53
Figure 4.13: Residual characteristics for best AIC (6,0,10) (a) and WT (10,0,8) (b).....	54
Figure 4.14: Residual characteristics for order (4,0,4)	55
Figure 4.15: Differentiated heading residual case 2 AIC (above) and WT (below).....	56
Figure 4.16: Residual of differentiated heading case 2 AIC-WT (6,1,10)	57
Figure 4.17: Signal Case 4 heading (a) and ACF (b).....	58
Figure 4.18: Lab case 4 residual AIC (above) and WT (below).....	59
Figure 4.19: Case 4 heading residual statistics and fitting model ACF (10,0,9)	60
Figure 4.20: Differenced case 4 residual AIC (above) and WT (below).....	61
Figure 4.21: Case 4 differenced heading residual statistics AIC (a) and (1,1,1) (b)	62
Figure 4.22: Case 1 Heading residual AIC (above) and WT (below)	63
Figure 4.23: Case 1 Heading residual (10,0,5) and (8,0,7)	64
Figure 4.24: Case 1 Heading residual (4,0,2)	64
Figure 4.25: Differenced Case 1 heading residual AIC (above) and WT (below)	65
Figure 4.26: Case 1 Heading residual (a) (4,1,6) and (b) (8,1,8).....	66
Figure 4.27: GPS latitude (left) and Longitude (right) [min]	69
Figure 4.28: GPS HDOP.....	71

Figure 4.29: GPS Latitude (left) and Longitude (right) statistics	72
Figure 4.30: GPS Latitude residual AIC (above) and WT (below)	73
Figure 4.31: GPS Latitude residual statistics (a) (2,0,2) and (b) (10,0,10).....	74
Figure 4.32: GPS Latitude residual statistics (a) (1,0,1) and (b) (2,0,0).....	75
Figure 4.33: GPS Longitude residual AIC (above) and WT (below)	76
Figure 4.34: GPS Longitude residual statistics AIC (5,0,5) (a) & WT (10,0,0) (b)	77
Figure 4.35: GPS Longitude residual statistics (2,0,0)	77
Figure 4.36: X, Y, Z Acceleration signals time series (left) and PSD (right).....	82
Figure 4.37: X, Y, Z Acceleration signals ACF (left) and PACF (right)	82
Figure 4.38: X-acceleration residual AIC (above) and WT (below)	83
Figure 4.39: X acceleration residual statistics (a) AIC and (b) WT	84
Figure 4.40: Y-acceleration residual AIC (above) and WT (below)	85
Figure 4.41: Y acceleration signal residual statistics (a) AIC and (b) WT	86
Figure 4.42: Z-acceleration residual AIC (above) and WT (below).....	86
Figure 4.43: Z-axis acceleration residual statistics (a) AIC & (b) WT.....	87
Figure 4.44: Z-axis acceleration residual statistics (2,0,1)	87
Figure 4.45: Gyroscope signals (left) and PSD (right)	90
Figure 4.46: Gyroscope signals ACF (left) and PACF (right).....	91
Figure 4.47: Yaw rate residual AIC (above) and WT (below)	92
Figure 4.48: Yaw rate residual statistics (a) (5,0,9) and (b) (2,0,2).....	93
Figure 4.49: Roll angular rate AIC and WT	94
Figure 4.50: Roll rate residual statistics (3,0,3) and (8,0,10).....	95
Figure 4.51: Roll rate residual statistics (2,0,2)	95

Figure 4.52: Pitch angular rate AIC and WT	96
Figure 4.53: Pitch rate residual statistics (a) (3,0,4) and (b) (7,0,10)	97
Figure 4.54: Pitch rate residual statistics (2,0,2).....	97

1 INTRODUCTION

Autonomous Underwater Vehicles (AUVs) are small, unmanned and untethered submarines providing a simple, low-cost solution to collect various underwater data [6].

These vehicles have been very useful for many undersea applications including scientific, commercial and military applications. Specifically, the main interest of AUVs resides in mine-countermeasure applications. While current approaches requires the use of humans in endangered area for mine detection, classification, identification and marking [24], the growing capability of AUVs' navigation positioning accuracy enables the use of automated vehicles in place of humans, thereby significantly reducing the risk of life.

Since the early 90's the Department of Ocean Engineering at Florida Atlantic University has been strongly involved in the development of shallow-water AUVs [6] [7] [26], and has been participating in many research programs sponsored by American institutions including the Office of Naval Research, the National Science Foundation, the Florida Department of Transportation, the Florida Sea Grant Program, NASA, the U.S. Coast Guard, and the U.S. NAVSEASYS COM.

An Inertial Navigation System (INS) has been designed for the latest generation of FAU AUVs, the Morpheus [6]. It uses several sensors with more or less accurate information and a complementary full-state Extended Kalman Filter to estimate the AUV's heading and position. To rely on the information given, an extensive data processing is required to

reduce the critical source of errors in the navigation estimation. Satisfactory results of the order of 1% navigation accuracy have been obtained while using the INS [7].

Another powerful and sophisticated post-processed filter has been developed for the previous generation of AUVs, the Ocean Explorer (OEX). This system uses an error-state Extended Kalman Filter, based on the complementary characteristics of some redundant navigation measurements. This filter used in conjunction with the post-processing Rauch-Tung –Striebel smoother [4] has proven to be a very efficient tool to compensate for the sensors dropouts and long-term drift errors. This post-processed filter can also be used for the Morpheus AUV data measurements.

1.1 Problem Statement

Navigation is the act of determining the course or the heading of movement of a vehicle at all times. The major problem that arises in underwater navigation is the absence of an accurate source of positioning. While air or outdoor land vehicle navigation can rely on GPS fixes throughout the entire mission, underwater navigation suffers from the absence of this position information. Instead it relies on other dynamics and orientation sensors such as Doppler Velocity Log and TCM2 compass to determine the vehicle's position underwater. This technique of determining position by computing distance traveled on a given course is called dead reckoning.

An inertial navigation system INS has been designed for the Morpheus [7] and with the aid of redundant information capable of removing the major sources of errors in positioning, more particularly in the compass heading bias. However, this system using a

full-state Kalman Filter has shown some limitations regarding the long-term drifts caused by inertial measurement integrated bias. Therefore, a complementary error state Kalman Filter was then ideally suited to remove this long-term drift [6]. The problem when using an error state filter is on how to model the sensor errors accurately. For this, a 1st order Gauss-Markov process [4], which states that the sensor error outputs are time-correlated was previously used. Nevertheless, practical analyses have shown that the sensor errors exhibit a more complex model. Modeling the sensor errors is an important step in underwater navigation and will be investigated in this thesis.

1.2 Objectives

The objective of this thesis is to enhance the navigation accuracy of the Morpheus Autonomous Underwater Vehicle. Sensor measurements are usually accompanied with a disturbing term, which prevents the exact estimation of the true process. To improve this navigation accuracy, a lot of emphasis should then be put on identifying these error terms. This sensor error modeling aims to characterize the sensor residual outputs in steady-state situation. The analysis results will enable the characterization of the sensor errors by an adequate Gauss-Markov process [4] [31]. The error model will then be a useful tool for the Inertial Navigation System of the AUV using a sensor error-state Extended Kalman Filter [6].

1.3 Thesis outline

The rest of this thesis is organized as follows:

In chapter 2, the navigation system currently in use on the Morpheus AUV will be described. Particularly, we will describe the on board sensors and their error characteristics. Autocorrelation techniques in data analysis are reviewed [13] [14] followed by some known models in system identification [8] [9]. Chapter 3 describes the sensor error modeling methodology. Least-square model identification [24] is detailed as well as the criteria of fit used for diagnostic checking. In chapter 4, the results of static sensor measurement analysis are presented and discussed with the introduced methods. Chapter 5 summarizes the main conclusions from the project, and gives recommendations for further work on the project. Appendix A tabulates the results of the model estimation of the sensor error models so far obtained.

2 BACKGROUND

This chapter describes the navigation sensors currently used on the Morpheus AUV. A literature review on the autocorrelation techniques is included [13] [14] as well as the signal characteristics and autoregressive and moving average models [9] [10]. Several important tools on the autocorrelation functions graphical interpretation are also detailed.

2.1 MORPHEUS SENSOR SUITE

Morpheus is a class of autonomous underwater vehicle (AUV) developed by the department of Ocean Engineering at Florida Atlantic University. It is composed of modular and replaceable payloads depending on the need for specific applications. In Figure 2.1, a Morpheus is surfacing for GPS fixes. This AUV will be referenced in this thesis as AUV 1. Figure 2.2 shows a Bio Inspired Propulsion System of the Morpheus AUV, this AUV will be referenced in this thesis as AUV 2. One of the payloads has been equipped with additional fins for control enhancement.



Figure 2.1: GPS/DGPS equipped Morpheus AUV 1



Figure 2.2: Bio Inspired Propulsion System Morpheus AUV 2

Two types of data are collected using the following sensors:

- Environmental: oceanographic (Conductivity Temperature and Depth CTD sensor), acoustic (sonar), visual (video)
- Vehicle: attitude (gyroscope), acceleration (accelerometer), heading (compass), velocity (Doppler Velocity Log DVL sensor), satellite aided positioning (Global Positioning System GPS, Differential Global Positioning System DGPS) and underwater acoustic positioning (Ultra Short Baseline USBL and Long Baseline LBL).

The navigation system of the Morpheus uses four types of instruments to estimate the position of the vehicle [6] [7]. They are a magnetometer compass for the heading, a GPS/DGPS sensor, a Doppler Velocity Log and an Inertial Measurement Unit IMU. The IMU encompasses a set of three accelerometers and a set of three ring-laser gyroscopes.

2.1.1.1 TCM2 Navigation Compass

Precision Navigation, Inc manufactures and provides the TCM2 electronic compass module. This module outputs the heading, pitch and roll angles and the 3-D magnetic field strengths surrounding the vehicle. The instrument uses the attitude information

(pitch and roll angles) to transform the magnetic field in the Euler frame (i.e. the projection of the body frame onto the horizontal frame) and compute the heading [28].

2.1.1.2 *Motorola VP Oncore GPS receiver*

The *VP Oncore* receiver from *Motorola* [35] collects GPS/DGPS data information and processes them to output the absolute position of the AUV. The position accuracy depends on the number of satellites transmitting time signals to the receiver. Usually four to six orbiting satellites are available.

The major error sources in GPS measurements can be assigned to: satellite clock errors, ephemeris error, receiver errors and atmospheric or ionospheric delay. In addition, the accuracy of GPS data were purposely degraded by the U.S. Department of Defense using “Selective Availability” to prevent hostile force from taking advantage of this positioning means. A Differential GPS positioning can significantly enhance the accuracy of positioning by using an extra referenced emitter source in a ground location.

2.1.1.3 *RDI Navigator Doppler Velocity Log*

The Navigator Doppler Velocity Log instrument is provided by *RD Instruments*. It outputs the vehicle velocity in the forward, starboard and downward directions and with respect to seabed. The velocity is computed based on the frequency shift between outgoing and incoming signals [29].

2.1.1.4 *IMU X100CX Inertial Measurement Unit*

The IMU X100CX from *Crossbow* encompasses three gyroscopes and three linear accelerometers mounted in strap down configuration. The tri-axial accelerometer measures the acceleration in three mutually perpendicular directions [30]. It actually

reads the force applied on a spring mass along the three independent axes on a different accelerometer unit. The displacement of the mass will be then read as a force and converted in acceleration via gravity unit. Because of the gravitational earth attraction, a constant acceleration will always be read on the tri-axial accelerometer. Besides, the frequency rate attainable for the IMU of 100 [Hz] enables instant vehicle attitude estimation but is usually limited to steady state due to the acceleration sensitivity to attitude changes, this shortcoming motives the reason to discard the pool acceleration data. The ring-laser block assembly outputs angular rates namely the yaw, roll and pitch rates. The quantities, angular rates and acceleration can be integrated with respect to time to obtain attitude and velocity then position respectively.

Table 2.1 presents the characteristics of the navigation sensors used on the Morpheus AUV 1 [7].

Unit	Measurement	Accuracy	Bias	Update Rate	Range
Crossbow IMU	Gyroscope	-	Gyro drift <2.25[°/hr ^{1/2}]	100 Hz	± 100 [°/s]
	Accelerometer	± 0.25 [mg]	Acc bias: ± 0.5 [mg]		± 2 [g]
TCM2	Heading	± 0.2 μT	~ 5 °	8-40 Hz	0-359.9°
	Roll	± 0.2°	-		± 20°
	Pitch				
DVL	Speed (x, y, z)	± 0.2% ± 0.4%	0.003 m/sec	4 Hz	-
GPS	Latitude Longitude	GPS: < 25 m DGPS: 1-5 m	~ 0.2 m negligible	1 Hz	-

Table 2.1: Sensor error characteristics [7]

2.2 AUTOCORRELATION TECHNIQUES

Autocorrelation functions ACF are valuable tools for evaluating of how a process is related to itself from one time step to another. Recent methods have been proposed for stationary process analysis [9] [10] [31] [32] using the complementary characteristics of the partial autocorrelation function PACF with the ACF. These two statistical properties have shown to be very useful in the development of a process model, its identification and in the checking diagnosis (section 3.4) [9] [10] [13]. This chapter will describe these two functions and more particularly the derivation of the PACF from the Yule-Walker equation [4] [25].

2.2.1 Autocorrelation Function

From the definition given in [1], an auto-correlation function $R_{xx}(\tau)$ of a quantity $x(t)$ is a time average of the product of a quantity at time t with the same quantity at time $(t + \tau)$ over a period T :

$$R_{xx}(\tau) = E[x(k).x(k + \tau)] = \lim_{T \rightarrow \infty} \frac{1}{T} \int_0^T x(t)x(t + \tau)dt \quad (2.1)$$

Where τ is the time lag, and $E[.]$ represents the expected value of the term inside the brackets. The autocorrelation function at lag 0 is equivalent to the mean square value estimated by:

$$\bar{x}^2 = R_{xx}(0) = \lim_{T \rightarrow \infty} \frac{1}{T} \int_0^T x^2(t)dt \quad (2.2)$$

Noting that $|R_{xx}(\tau)| \leq R_{xx}(0)$, it follows that the maximum possible values of $R_{xx}(\tau)$ occur at $\tau = 0$.

For convenience, we will use the normalized autocorrelation function.

$$r(\tau) = \frac{R_{xx}(\tau)}{R_{xx}(0)} = \frac{\int_0^T x(t)x(t+\tau)dt}{\int_0^T x^2(t)dt} \quad (2.3)$$

The autocorrelation function (ACF) will then vary between -1 and +1, with values near ± 1 indicating stronger correlation. For the analysis in this thesis, the time series data are subtracted from their mean. The function used is also called auto-covariance.

2.2.2 Cross-Correlation Coefficient

Cross-correlation coefficients at each lag k measure the degree of correlation between neighboring data observations in a time series.

Let $x_N = (x_1, \dots, x_N)$ and $y_N = (y_1, \dots, y_N)$ be some given time-series data, the correlation coefficient function is estimated in discrete time as follows:

$$\rho_{xy} = \frac{C_{xy}}{\sigma_x \sigma_y} \quad (2.4)$$

C_{xy} is the covariance of x and y , defined by the equation:

$$\begin{aligned} C_{xy} &= E[(x(k) - \mu_x)(y(k) - \mu_y)] = E[x(k) \cdot y(k)] - E[x(k)]E[y(k)] \\ C_{xy} &= \int \int_{-\infty}^{\infty} (x - \mu_x) \cdot (y - \mu_y) \cdot p(x, y) dx dy \end{aligned} \quad (2.5)$$

Where (σ_x, σ_y) and (μ_x, μ_y) represent respectively the standard deviation and mean for the time series x_n and y_n .

2.2.3 The Yule-Walker Equation

We can characterize an autoregressive process (section 2.3.3) as a linear combination of previous observations plus a Gaussian random noise [4] [20]:

$$u_n = \sum_{k=1}^p a_k \cdot u_{n-k} + v_n \quad (2.6)$$

Where u_n is an observation at time step n , v_n is the portion of measurement which cannot be predicted from previous measurements, and a_k the corresponding autoregressive parameters of order p .

We can represent the autoregressive process by a sum of p linear terms:

$$u_n = a_1 \cdot u_{n-1} + a_2 \cdot u_{n-2} + \dots + a_{n-1} \cdot u_{n-p+1} + a_p \cdot u_{n-p} + v_n \quad (2.7)$$

Evaluating the auto-correlation function for the autoregressive process by multiplying (2.7) with u_{n-p} and then taking the expectation term by term, we obtain:

$$\begin{aligned} E[u_{n-p} \cdot u_n] &= a_1 \cdot E[u_{n-p} \cdot u_{n-1}] + a_2 \cdot E[u_{n-p} \cdot u_{n-2}] + \dots \\ &\dots + a_{n-1} \cdot E[u_{n-p} \cdot u_{n-p+1}] + a_p \cdot E[u_{n-p} \cdot u_{n-p}] + E[u_{n-p} \cdot v_n] \end{aligned} \quad (2.8)$$

Where the autocorrelation function at lag p is given by:

$$R_{uu}(p) = E[u_{n-p} \cdot u_n] \quad (2.9)$$

Since v_n is a white noise process, $E[u_{n-p} \cdot v_n] = 0$. Thus we can write:

$$R_{uu}(p) = a_1 \cdot R_{uu}(p-1) + a_2 \cdot R_{uu}(p-2) + \dots + a_{n-1} \cdot R_{uu}(1) + a_p \cdot R_{uu}(0) \quad (2.10)$$

Since $R_{uu}(p) = R_{uu}(-p)$, we obtain the following set of equations:

$$\begin{aligned}
R_{uu}(1) &= a_1 \cdot R_{uu}(0) + a_2 \cdot R_{uu}(1) + \dots + a_{n-1} \cdot R_{uu}(p-2) + a_p \cdot R_{uu}(p-1) \\
R_{uu}(2) &= a_1 \cdot R_{uu}(1) + a_2 \cdot R_{uu}(0) + \dots + a_{n-1} \cdot R_{uu}(p-3) + a_p \cdot R_{uu}(p-2) \\
&\vdots \\
R_{uu}(p-1) &= a_1 \cdot R_{uu}(p-2) + a_2 \cdot R_{uu}(p-3) + \dots + a_{n-1} \cdot R_{uu}(0) + a_p \cdot R_{uu}(1) \\
R_{uu}(p) &= a_1 \cdot R_{uu}(p-1) + a_2 \cdot R_{uu}(p-2) + \dots + a_{n-1} \cdot R_{uu}(1) + a_p \cdot R_{uu}(0)
\end{aligned} \tag{2.11}$$

In vector-matrix notation:

$$\begin{bmatrix} R_{uu}(1) \\ R_{uu}(2) \\ \vdots \\ R_{uu}(p-1) \\ R_{uu}(p) \end{bmatrix} = \begin{bmatrix} R_{uu}(0) & R_{uu}(1) & R_{uu}(2) & \dots & R_{uu}(p-2) & R_{uu}(p-1) \\ R_{uu}(1) & R_{uu}(0) & R_{uu}(1) & \dots & R_{uu}(p-3) & R_{uu}(p-2) \\ \vdots & \vdots & \vdots & \ddots & \vdots & \vdots \\ R_{uu}(p-2) & \dots & \dots & \dots & R_{uu}(0) & R_{uu}(1) \\ R_{uu}(p-1) & \dots & \dots & \dots & R_{uu}(1) & R_{uu}(0) \end{bmatrix} \begin{bmatrix} a_1 \\ a_2 \\ \vdots \\ a_{p-1} \\ a_p \end{bmatrix} \tag{2.12}$$

Normalizing each autocorrelation term by $R_{uu}(0)$ and defining r_p as:

$$r_p = \frac{R_{uu}(p)}{R_{uu}(0)} \tag{2.13}$$

We obtain the **Yule-Walker equation**:

$$\begin{bmatrix} r_1 \\ r_2 \\ \vdots \\ r_{p-1} \\ r_p \end{bmatrix} = \begin{bmatrix} 1 & r_1 & r_2 & \dots & r_{p-2} & r_{p-1} \\ r_1 & 1 & r_1 & \dots & r_{p-3} & r_{p-2} \\ \vdots & \vdots & \vdots & \ddots & \vdots & \vdots \\ r_{p-2} & \dots & \dots & \dots & 1 & r_1 \\ r_{p-1} & \dots & \dots & \dots & r_1 & 1 \end{bmatrix} \begin{bmatrix} a_1 \\ a_2 \\ \vdots \\ a_{p-1} \\ a_p \end{bmatrix} \tag{2.14}$$

$$\text{Or, compactly } \rho_p = R_p \cdot \alpha_p \tag{2.15}$$

With

$$\rho_p = [r_1 \quad r_2 \quad \dots \quad r_{p-1} \quad r_p]^T \tag{2.16}$$

$$\alpha_p = [a_1 \quad a_2 \quad \dots \quad a_{p-1} \quad a_p]^T \tag{2.17}$$

$$R_p = \begin{bmatrix} 1 & r_1 & r_2 & \cdots & r_{p-2} & r_{p-1} \\ r_1 & 1 & r_1 & \cdots & r_{p-3} & r_{p-2} \\ \vdots & & & & & \\ r_{p-2} & \cdots & & 1 & r_1 \\ r_{p-1} & \cdots & & r_1 & 1 \end{bmatrix} \quad (2.18)$$

Where ρ_p is the correlation coefficients vector, R_p the Toeplitz matrix of correlation coefficients r_p at lag p and α_p the vector of prediction coefficients a_p [25]. We thus see Equation (2.14) that the Yule-Walker equation represents a linear relationship between the autoregressive parameters a_p and the correlation vector ρ_p .

2.2.4 The Partial Autocorrelation function

The subscript p in Equation (2.14) defining the order of the AR process in the Yule-Walker equation is replaced by the lag k for which we want to compute the prediction coefficient a_k of the model. The Yule-Walker equation (2.14) can be solved for the coefficient vector α_k , which relates the matrix R_k to correlation vector ρ_k . The solution coefficients are referred to as partial correlation coefficients. The last row of Equation (2.14) shows that the term a_k is dependent on the $(k-1)$ previous terms, thus requiring the use of a recursive algorithm [13] [25]:

$$a_k = r_k - [r_{k-1} \cdot a_1 + r_{k-2} \cdot a_2 + \cdots + r_1 \cdot a_{k-1}] \quad (2.19)$$

Then, for the following, a_k will be written as $a_{k,k}$ where the first subscript denotes the total number of lags and the second, the order of the coefficient.

Separating Equation (2.14) into $(k^{\text{th}}-1)$ and k^{th} stage yields:

$$\begin{bmatrix} r_1 \\ r_2 \\ \vdots \\ r_{k-1} \\ r_k \end{bmatrix} = \left[\begin{array}{cccc|c} 1 & r_1 & r_2 & \cdots & r_{k-2} & r_{k-1} \\ r_1 & 1 & r_1 & \cdots & r_{k-3} & r_{k-2} \\ \vdots & & & & & \\ r_{k-2} & & \cdots & & 1 & r_1 \\ \hline r_{k-1} & & \cdots & & r_1 & 1 \end{array} \right] \begin{bmatrix} a_{k,1} \\ a_{k,2} \\ \vdots \\ a_{k,k-1} \\ a_{k,k} \end{bmatrix} \quad (2.20)$$

And

$$\begin{bmatrix} \rho_{k-1} \\ r_k \end{bmatrix} = \begin{bmatrix} R_{k-1} & {}^*\rho_{k-1} \\ {}^*\rho_{k-1}^T & 1 \end{bmatrix} \begin{bmatrix} \alpha'_{k-1} \\ a_{k,k} \end{bmatrix} \quad (2.21)$$

Where the symbol star (*) corresponds to the reversed vector. The correlation vector α'_{k-1} corresponds to the (k-1) dimensional column vector:

$$\alpha'_{k-1} = \begin{bmatrix} a_{k,1} \\ a_{k,2} \\ \vdots \\ a_{k,k-1} \end{bmatrix} \quad (2.22)$$

$$\text{Where } \alpha_k = \begin{bmatrix} \alpha'_{k-1} \\ a_{k,k} \end{bmatrix} \quad (2.23)$$

Expanding (2.21), we obtain:

$$\rho_{k-1} = R_{k-1} \cdot \alpha'_{k-1} + a_{k,k} \cdot {}^*\rho_{k-1} \quad (2.24)$$

$$r_k = {}^*\rho_{k-1}^T \cdot \alpha'_{k-1} + a_{k,k} \quad (2.25)$$

Since R_k is a symmetric matrix with equal diagonal elements, Equation (2.14) is equivalent to:

$$\begin{bmatrix} r_k \\ r_{k-1} \\ \vdots \\ r_2 \\ r_1 \end{bmatrix} = \begin{bmatrix} 1 & r_1 & r_2 & \cdots & r_{k-2} & r_{k-1} \\ r_1 & 1 & r_1 & \cdots & r_{k-3} & r_{k-2} \\ \vdots & & & & & \\ r_{k-2} & & \cdots & & 1 & r_1 \\ r_{k-1} & & \cdots & & r_1 & 1 \end{bmatrix} \begin{bmatrix} a_k \\ a_{k-1} \\ \vdots \\ a_2 \\ a_1 \end{bmatrix} \quad (2.26)$$

Or also

$${}^* \rho_k = R_k \cdot {}^* \alpha_k \quad (2.27)$$

And for the $(k^{\text{th}}-1)$ stage, ${}^* \rho_{k-1} = R_{k-1} \cdot {}^* \alpha_{k-1}$

Now solving (2.24) for the $(k^{\text{th}}-1)$ stage of the correlation vector α'_{k-1} , we have:

$$R_{k-1} \cdot \alpha_{k-1} = R_{k-1} \cdot \alpha'_{k-1} + a_{k,k} \cdot R_{k-1} \cdot {}^* \alpha_{k-1} \quad (2.28)$$

$$\text{Therefore } \alpha'_{k-1} = \alpha_{k-1} - a_{k,k} \cdot {}^* \alpha_{k-1} \quad (2.29)$$

Finally, substituting (2.29) into (2.25) the partial correlation coefficient at lag k can be written as:

$$a_{k,k} = \frac{r_k - {}^* \alpha_{k-1}^T \cdot \rho_{k-1}}{1 - \alpha_{k-1}^T \cdot \rho_{k-1}} \quad (2.30)$$

Note from [25] that the denominator of Equation (2.30) is equal to the predictor error variance and is conveniently used in the recursive algorithm:

$$\sigma_k^2 = 1 - \alpha_{k-1}^T \cdot \rho_{k-1} \quad (2.31)$$

$$\text{Where } \sigma_k^2 = \sigma_{k-1}^2 \cdot (1 - a_{k,k}^2) \quad (2.32)$$

The partial autocorrelation coefficient $a_{k,k}$ represents the direct correlation between a quantity u_n and the same quantity delayed by a lag k . Indeed, Equation 2.19 shows that solving for $a_{k,k}$ removes the effect of the shorter lag correlations from the autocorrelation function r_k .

2.3 STOCHASTIC PROCESSES

Data representing a random physical phenomenon cannot generally be described by a mathematical relationship, because each outcome of the phenomenon cannot be predicted previously [14]. That outcome represents only one solution of all the possible observations. The single time history of one process is called a sample function. Then the collection of all sample records constitutes an ensemble called stochastic process. Figure 2.3 illustrates three time histories of a random process.

In general, a sample record of any particular function $x_k(t)$ is not suitable to represent the entire random process to which it belongs. However, it turns out that for the special type of random process, statistical information can be derived from analysis of a single sample function. A process is said to be ergodic if its properties can be determined by performing a time average of a sample record. These quantities of interest are *mean value* $\mu_x(t)$, *covariance* $C_{xx}(t)$ and *correlation function* $R_{xx}(\tau)$ given by:

$$\mu_x(t) = E[x_k(t)]$$

$$C_{xx}(t) = E[(x_k(t) - \mu_x(t))^2] = \sigma_x^2(t) \quad (2.33)$$

$$R_{xx}(\tau) = E[x_k(t) - x_k(t - \tau)]$$

Where τ is the time lag, $x_k(t)$ is the process to be described and μ_x its conditional mean and σ_x^2 its variance. If these statistical properties yield the same results for different values of time, i.e. independent to time translation, the random process is said to be *weakly stationary*. Our sensor error modeling will be based on the study of the static sensor measurements, and are assumed weakly stationary over time [14]. In the case of

non-stationary data, temperature effect is investigated to explain the measurement drift over time.

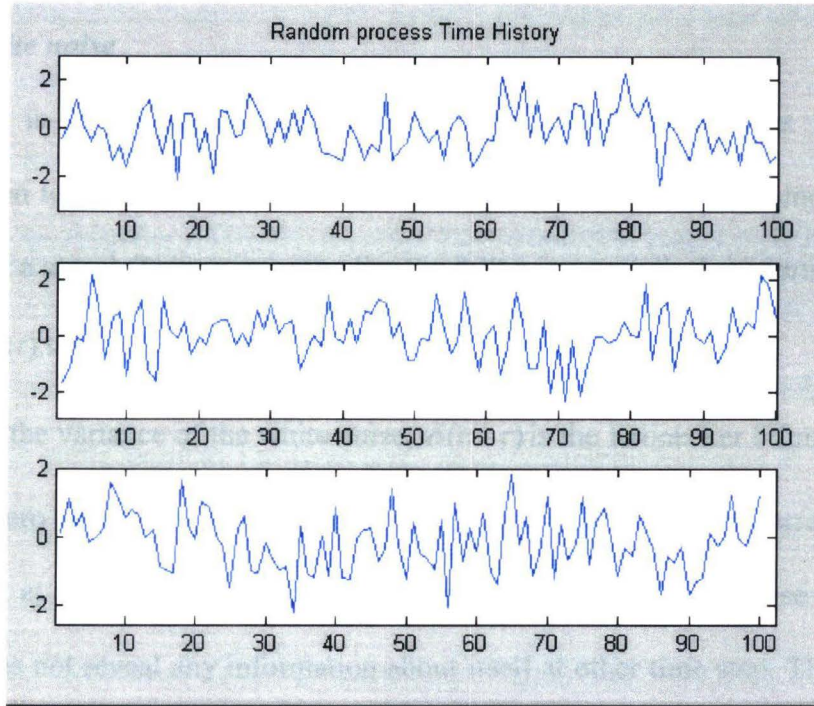


Figure 2.3: Random process

2.3.1 Signal Characteristics

A signal is generally distorted by noise before arriving at the receiver (refer to Equation 2.34). If the statistical properties of the signal and noise are known in advance, it is possible to reduce the effect of the disturbance to a minimum.

A well-known technique for describing the signal in time series analysis was introduced by Box-Jenkins [4] [9] [10]. Any measurement process can be decomposed into two major components: a signal component $f(t)$ and a zero mean gaussian white noise component $v(t)$, i.e.

$$y(t) = f(t) + v(t) \quad (2.34)$$

2.3.2 Noise Characteristics

Any noise can generally be decomposed in two categories, white and colored.

2.3.2.1 White noise

White noise is an idealized concept which does, however, serve as a very useful approximation to situations in which a disturbing noise is wideband compared with the bandwidth of a signal. This noise embodies the following statistical properties [14] [20]:

$$R_{vv}(t) = E[v(t).v(t + \tau)] = \sigma_v^2 .\delta(t - \tau) \quad (2.35)$$

Where σ_v^2 is the variance of the white noise, $\delta(t - \tau)$ is the Kronecker δ function equal to 1 if $t = \tau$, zero otherwise. The occurrence of white noise does not correlate with any measurement at any time step. This implies that measuring a white noise source at one time step does not reveal any information about itself at other time step. The white noise process is therefore unpredictable [20].

2.3.2.2 Colored noise:

All types of noise other than white are called colored noise. These processes usually encompass a strong time autocorrelation meaning that the colored noise is closely related to another at a different time step.

The quantization noise in digital filters, created from continuous to digital discretization via rounding or magnitude truncation errors [14] exhibits a strong correlation with the main signals. Therefore, such noise signal is considered as a sum of both correlated and uncorrelated noise. The uncorrelated component is by definition unpredictable, an effort is focused on characterizing the correlated noise component. We will use a Gauss-Markov process [4] that is capable of characterizing the correlated noise.

2.3.2.2.1 Quantization noise

During any data collection, a process signal is converted from its analog form to a binary word of finite length. Among the infinite continuous values, only finite levels are available for approximation of the measurements. The true value will be offset by this round-off error also called *quantization* error. The standard deviation is given by [14]:

$$\sigma_x = \sqrt{\frac{1}{12}}\Delta x = 0.289.\Delta x \quad (2.36)$$

Where Δx is the measurement resolution.

2.3.2.2.2 Gauss-Markov Process

In our work, the study is based on the data collected from static measurements. The records should in theory be a white noise process as described previously. But in practice, the high frequency component of this noise is removed by effect of signal quantization

[11]. The signal transformation to discrete time then produces a low-frequency random process called Gauss-Markov [31] [32].

By definition, a continuous process $x(t)$ is a *first order* Markov process if for every integer k such that $t_1 < t_2 \dots < t_k$, it is true that [4]:

$$F[x(t_k) | x(t_{k-1}), \dots, x(t_1)] = F[x(t_k) | x(t_k - 1)] \quad (2.37)$$

Where $F[x(t_k)]$ is the probability distribution of the process $x(t)$ at time step t_k and is defined by:

$$F[x(t_k)] = \int_{-\infty}^{x(t_k)} f(u).du \quad (2.38)$$

Equation (2.37) indicates that the probability distribution for the process $x(t_k)$ is dependent only on the value at one point immediately in the past, say $x(t_{k-1})$. In the continuous case, $x(t_k)$ can be represented by the first order differential equation:

$$\dot{x}(t) = -\beta_1 x(t) + w(t) \quad (2.39)$$

Where $w(t)$ is white noise and the first order time-constant β_1 is defined as $\beta_1 = \frac{1}{\tau}$.

The statistics for a 1st order Gauss-Markov process is described using the following autocorrelation function described in 2.2.1:

$$R_{xx}(\tau) = \sigma^2 \cdot \exp(-\beta_1 \cdot |\tau|) + m^2 \quad (2.40)$$

Where σ^2 is the variance. The correlation time τ can be found arithmetically for each process order. The product $\beta_n \cdot \tau$ for any order n should result in the 1/e point of the correlation function. Hence, the analysis of the autocorrelation function for sensor error

can lead to the computation of the time constant and variance for a stationary process, assuming the sensor error is stationary.

An n th order Markov process is defined by the following characteristic equations:

$$\frac{d^n x(t)}{dt^n} + C_n^1 \cdot \frac{d^{n-1} x(t)}{dt^{n-1}} \beta_n^1 + n \cdot \frac{d^{n-2} x(t)}{dt^{n-2}} \beta_n^2 + \dots + C_n^{n-1} \cdot x(t) \cdot \beta_n^n = w(t) \quad (2.41)$$

$$\text{with } C_n^p = \frac{n!}{p!(n-p)!}$$

$$R_{xx}(\tau) = \sigma^2 \cdot e^{-\beta \cdot |\tau|} \cdot \sum_{k=0}^{n-1} \frac{\Gamma(n) \cdot (2\beta_n |\tau|)^{n-k-1}}{(2n-2)! k! \Gamma(n-k)} \quad (2.42)$$

Here, the correlation time is solved arithmetically at each n for $R_{xx}(\tau) = \frac{1}{e}$ [4].

2.3.3 Autoregressive model

A time series $u(n)$, $u(n-1)$, ..., $u(n-p)$ represents a realization of an autoregressive (AR) process of order p if it satisfies the following difference equation [4] [20]:

$$u(n) - a_1 \cdot u(n-1) - \dots - a_p \cdot u(n-p) = v(n) \quad (2.43)$$

where a_1, a_2, \dots, a_p are constants called the AR parameters, and $v(n)$ is a white-noise process. The term $a_k \cdot u(n-k)$ is an inner product of a_k and $u(n-k)$, where $k = 1, \dots, p$.

To explain the reason of the term “autoregressive”, we rewrite the above equation (2.43) in the form:

$$u(n) = [a_1 \cdot u(n-1) + a_2 \cdot u(n-2) + \dots + a_p \cdot u(n-p)] + v(n) \quad (2.44)$$

We notice that u_n is a finite linear combination of past values of the process, $u(n-1), \dots, u(n-p)$, plus an error term $v(n)$ giving the reason for the term “autoregressive”.

Equation (2.43) can also be written as a convolution sum of the input sequence $u(n)$ and the sequence of parameters $\{a_1, \dots, a_p\}$:

$$u_n = \sum_{k=1}^p a_k \cdot u_{n-k} + v_n \quad (2.45)$$

The autoregressive process from the convolution sum Equation (2.45) is schematized in Figure 2.4 in which each of the z^{-1} blocs corresponds to one-time delay. The AR process u_n is related to p previous values by the sequence of AR parameters.

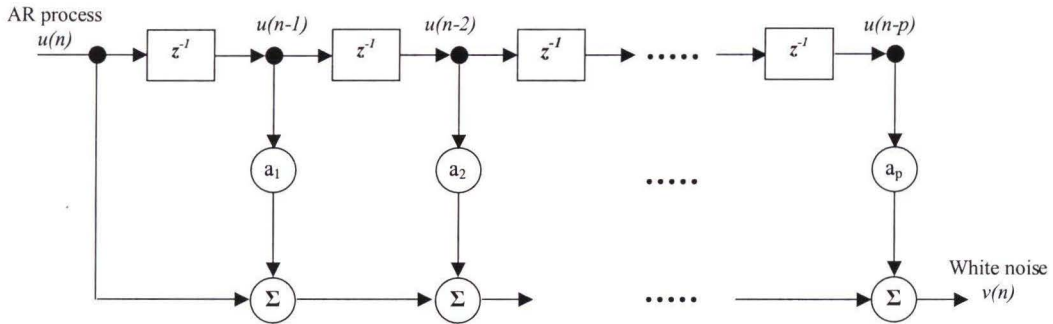


Figure 2.4: AR process

2.3.4 Moving Average model

The second type of noise model is built on parameters called moving-average (MA) parameters [4] [20]. This model resembles closely the AR model but is very different in which the value of the process $u(n)$ is only dependent on the previous white noise values.

A MA model can be formulated as follows:

$$u(n) = v(n) + b_1 v(n-1) + \dots + b_q v(n-q) \quad (2.46)$$

Where b_1, \dots, b_q are constants called the MA parameters, and $v(n)$ is a white-noise process of zero-mean and variance σ_v^2 . Except for $v(n)$, each term on the right-hand side of Equation (2.46) represents an inner product of a white noise at the previous time steps with the MA parameters. The order of the MA process is q .

As for the autoregressive equation (2.45), a moving average can be written as a convolution sum of the input sequence u_n and the sequence of parameters $\{b_1, \dots, b_q\}$:

$$u_n = \sum_{k=0}^q b_k \cdot v_{n-k} \quad (2.47)$$

Where $b_0 = 1$. The MA model bloc scheme is represented in Figure 2.5. Again, the z^{-1} bloc corresponds to one-time delay. As stated before, the MA process u_n is dependent only on q previous values of the white noise v_n .

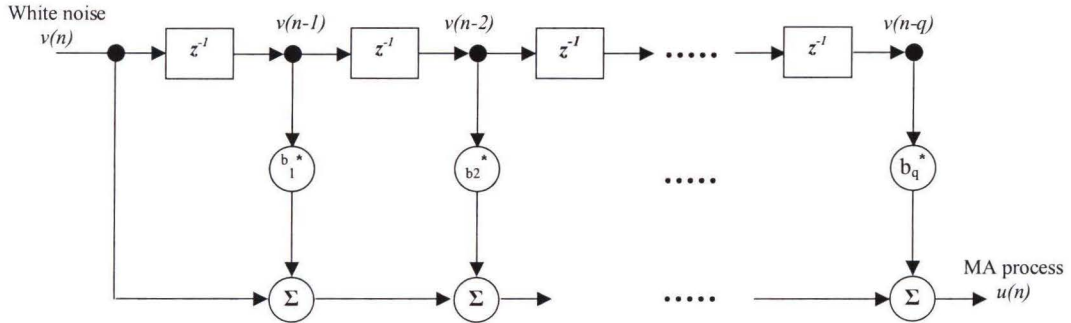


Figure 2.5: MA model

2.3.5 Autoregressive-Moving Average model

A more general model can be written as a combination of both AR and MA processes. Given a white noise process $v(n)$, the autoregressive moving average (ARMA) model $u(n)$ can be described by the difference equation:

$$u(n) - a_1 \cdot u(n-1) - \dots - a_p \cdot u(n-p) = v(n) + b_1 \cdot v(n-1) + \dots + b_q \cdot v(n-q) \quad (2.48)$$

Where a_1, \dots, a_p and b_1, \dots, b_q are constants called the ARMA parameters. Except for $u(n)$ and $v(n)$, all the terms represent scalar versions of time product. The orders of the AR and MA process are p and q and the ARMA order is written as (p, q) .

Taking the convolution formulation of (2.45), we can rewrite the ARMA model as:

$$u_n = \sum_{i=1}^p a_i \cdot u_{n-i} + \sum_{j=0}^q b_j \cdot v_{n-j} \quad (2.49)$$

with $b_0 = 1$.

From Eq. (2.49), we notice that the AR and MA model are particular cases of ARMA model. From a computational viewpoint, the AR model has an advantage over the MA and ARMA models [20]. Specifically, the computation of the AR coefficients involves a system of linear equations known as the Yule-Walker equations. On the other hand, the computation of the MA coefficients and the computation of the ARMA coefficients are more complicated in which they tend to describe a model from an assumed unpredictable noise. Wold in [15] has developed a fundamental theorem, which states that the MA model part can also be represented by an AR model. This type of ARMA estimation is beyond the scope of this thesis but has been developed in [31]. It is for this reason that, in practice, the use of AR models is more popular than the MA or ARMA models.

The ARMA model bloc scheme is represented in Figure 2.6.

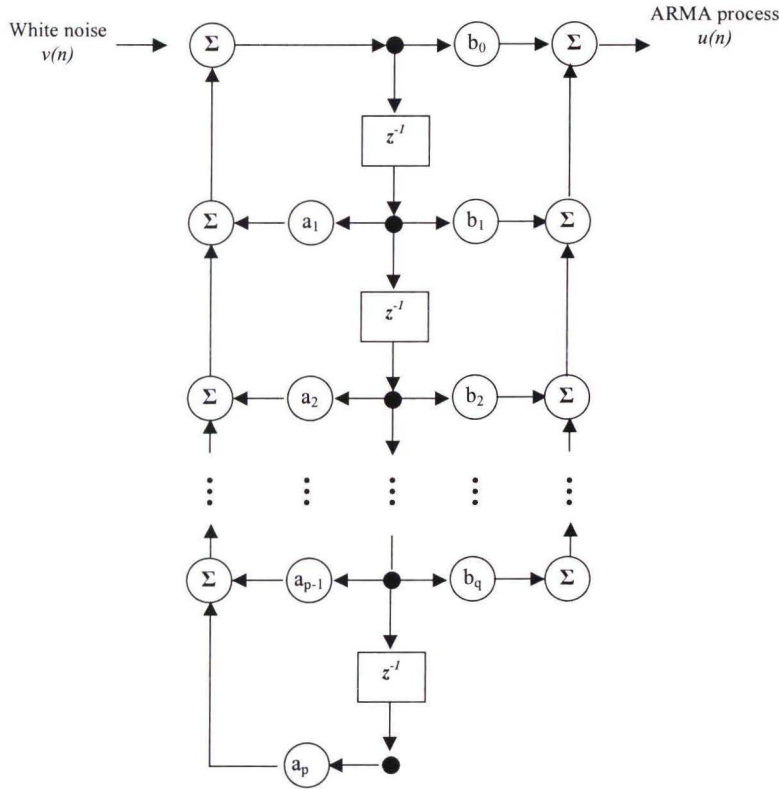


Figure 2.6: ARMA model

2.3.6 Autoregressive-Integrated Moving Average model

In the previous models, an ARMA model was applied to time series, assuming it is stationary over the time interval of interest. In the case of a non-stationary series, an autoregressive integrated moving average ARIMA model can be used. This model differs from an ARMA model by the number of differentiation applied to the series until the stationarity property is achieved. The regular differentiation involves taking a difference z_n between two consecutive values of the process u_n . Hence an ARIMA model of order (p, d, q) corresponds to an ARMA model (p, q) differentiated d times.

$$\sum_{i=0}^p a_i \cdot z_{n-i} = \sum_{j=0}^q b_j \cdot v_{n-j} \quad (2.50)$$

$$\text{Where } z_n = u_n - u_{n-1} \quad (2.51)$$

The process of differencing the time series is equivalent to removing a first order AR parameter from the signal:

$$z_n = u_n - a_1 \cdot u_{n-1} \quad (2.52)$$

With $a_1 = 1$.

2.4 AUTOCORRELATION FUNCTION INTERPRETATION

This section gives valuable insights into the analysis of the autocorrelation (ACF) and partial autocorrelation (PACF) functions. A graphical interpretation based on the knowledge of some ACF and PACF patterns for the various models described earlier is detailed [9] [10] [31] [32].

2.4.1 Interpretation of the Autocorrelation function

In time series forecasting, the autocorrelation function is extremely useful in obtaining a partial description of a time series. The autocorrelation function or ACF tests whether some adjacent observations are auto-correlated. That is, whether there is correlation between observations 1 and 2, 2 and 3, 3 and 4, etc. This is known as autocorrelation of lag one, since one of the pair of observations lags the other by one period or sample. Similarly, it will test at other lags. For instance, the autocorrelation at lag four tests whether observations 1 and 5, 2 and 6, etc. are correlated. The ACF can be computed over the total number of observations in the analysis. But from previous analysis, estimates at longer lags have been shown to be statistically unreliable [12].

Usually, the effect of autocorrelation at small lags will influence the estimate of autocorrelation at longer lags. For an instance, a strong autocorrelation at lag one would cause a higher lag observation to correlate directly with the previous or the next lag. This results in an apparent correlation between observations following high lag autocorrelation coefficient, even though no direct correlation exists. The Partial Autocorrelation Function (PACF) removes the effect of shorter lag autocorrelation from the correlation estimate at longer lags as explained in 2.2.4. This estimate however is only valid for a small portion of the correlation coefficient values.

2.4.2 Interpretation of the Partial Autocorrelation function

The partial autocorrelation function PACF of a series produce patterns that are exactly the reverse of the autocorrelation patterns with respect to AR and MA parameters [8][9]. That is, partial autocorrelation patterns for AR models look like autocorrelation patterns for MA models, and vice versa. A fundamental property of the PACF for the parameterization of a stationary process is described in the following theorem [13].

A process is autoregressive of *order* p , if and only if its PACF Equation (2.30) satisfies:

$$\alpha_k = 0 \text{ for } k > p \quad (2.53)$$

For any coefficient k greater than the AR order p ($k > p$). And for any lag k such that $k < p$, the partial correlation coefficient verifies:

$$\alpha_k \neq 0 \text{ for } k < p \quad (2.54)$$

More explicitly, a model with p AR parameters will generate a series whose PACs have spikes at lags 1 through p and zero spike at remaining lags. The PAC pattern therefore is extremely useful in identifying the presence and number of AR parameters. On the other

hand, a model with q MA parameters will generate a series whose PAC pattern is an exponentially decreasing pattern of some type [9] [10].

Both ACF and PACF will vary between ± 1 , the high values indicating strong correlation. The 95% confidence limits are provided to show when ACF or PACF appears to be significantly different from zero. In other words, lags having values greater than these limits should be considered to have significant correlation.

2.4.3 Simple ACF and PACF patterns

This section illustrates the usage ACF and PACF patterns for AR and MA models of order 1 generated from simulated data.

The standard deviation of the white noise was set to $\sigma = 1/6$. The initial values of the process were set to 1 and the AR and MA parameters were arbitrarily set to $a_1 = 0.8$ and $b_1 = -0.6$. The simulation is performed for a record of 1000 samples.

From the time series representation Figure 2.7, one cannot make any assumption for the model identification. Although a decaying process is obvious for the AR model (depending of the AR parameter used) top plot of Figure 2.7, the other processes are not discernable. The use of the ACF and PACF plots Figure 2.8 to 2.11 will help us recognize these processes. Table 2.2 lists the patterns known for the respective AR, MA and ARMA models.

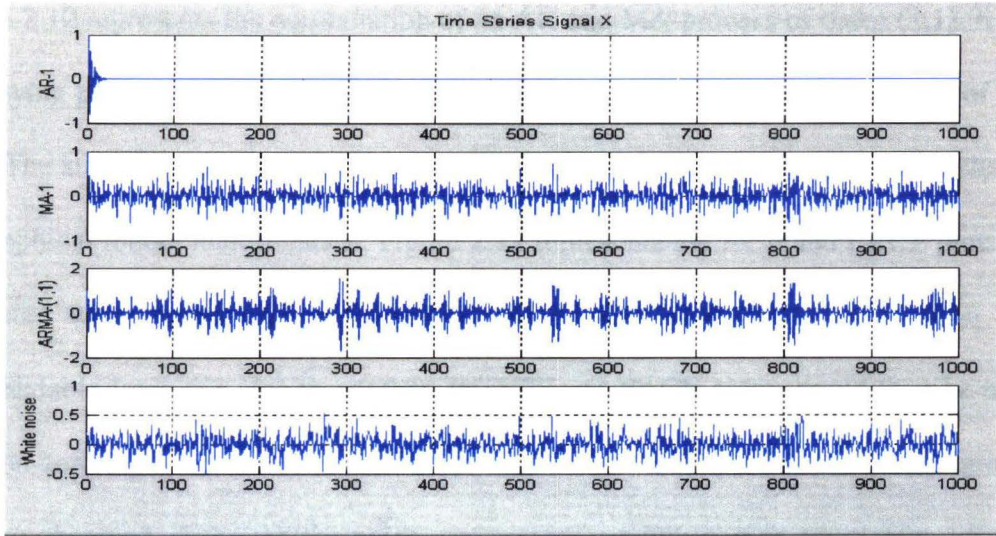


Figure 2.7: Time series signals

Model	Order	ACF	PACF
AR	P	Exponential decay toward zero	Cuts off to zero after lag p
MA	Q	Cuts off to zero after lag q	Exponential decay toward
ARMA	(P, Q)	Tails off toward zero	Tails off toward zero

Table 2.2: Guideline for Box-Jenkins model identification [32]

Figure 2.8 represents the AR process of order 1. It shows a decaying pattern toward zero for the ACF plot, left plot Figure 2.8. The PACF plot, Figure 2.8 shows only one spike at lag 1 as stated for the characteristics of an AR model of order 1. The spike amplitude is 0.8 and verifies the parameter set for a_1 .

Figure 2.9 represents the MA process of order 1. It shows inversely to the AR process a decaying pattern toward zero for the PACF plot Figure 2.9. The ACF plot on left of Figure 2.9 shows a significant spike at lag 1. Here, we cannot deduce the MA parameter value from the spike amplitude contrary to the AR process. Other spikes on both ACF and PACF plots show periodicities eventually driven by the white noise process.

Figure 2.10 represents the combination of an AR and MA process of order (1,1). It shows a decaying pattern toward zero for both the ACF and PACF plots, left and right of Figure 2.10. The statistic properties of the AR and MA shows an increase in the complexity of the graphical model identification. Figure 2.11 represents the ACF and PACF plots of the generated white noise, left and right of Figure 2.11. The white noise is in theory unpredictable from one step to another. Its ACF and PACF plots should then be null for any non-zero lags. However, the spikes found on the PACF plot of the MA (Figure 2.9) are also observed. Although the noise was created randomly, it is practically difficult to generate a pure white noise.

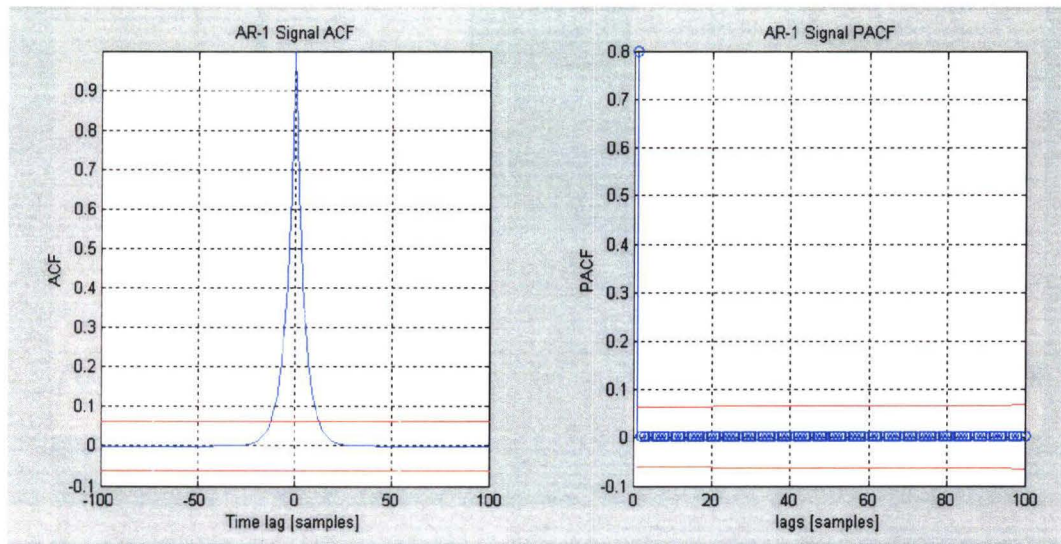


Figure 2.8: AR signal order 1 autocorrelations

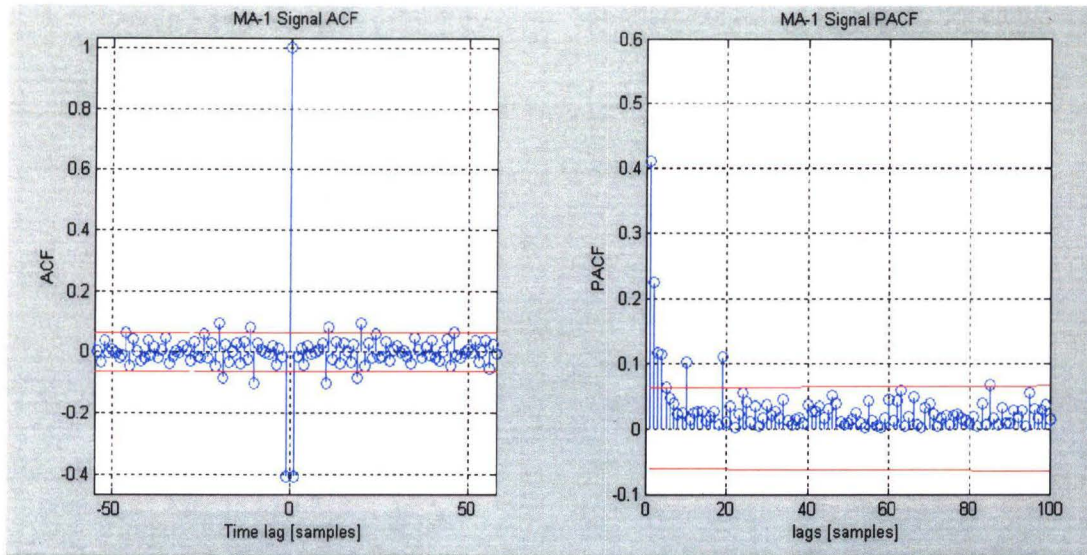


Figure 2.9: MA signal order 1 autocorrelations

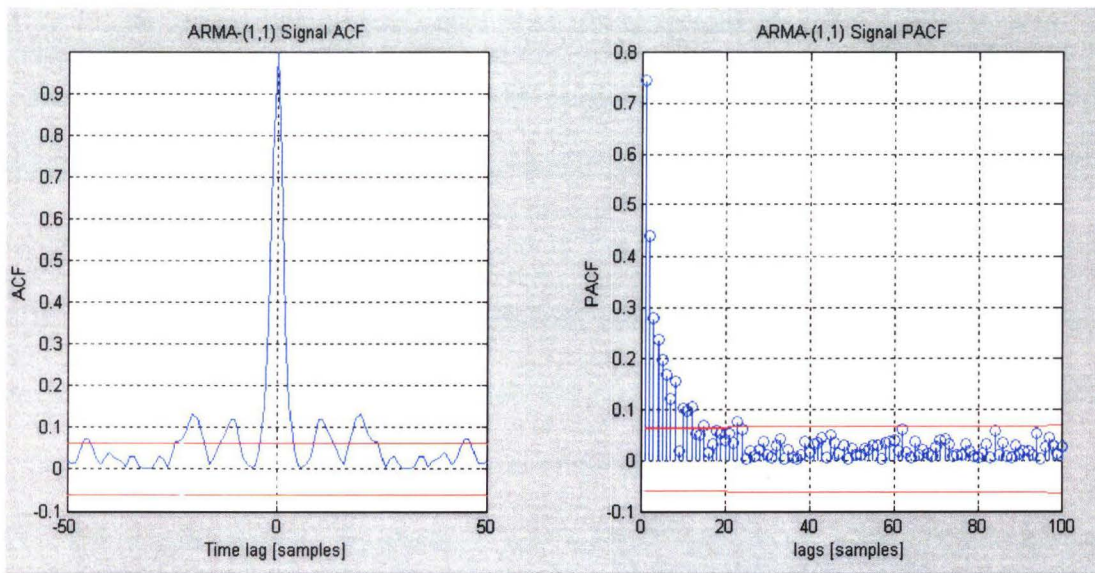


Figure 2.10: ARMA order (1,1) autocorrelations

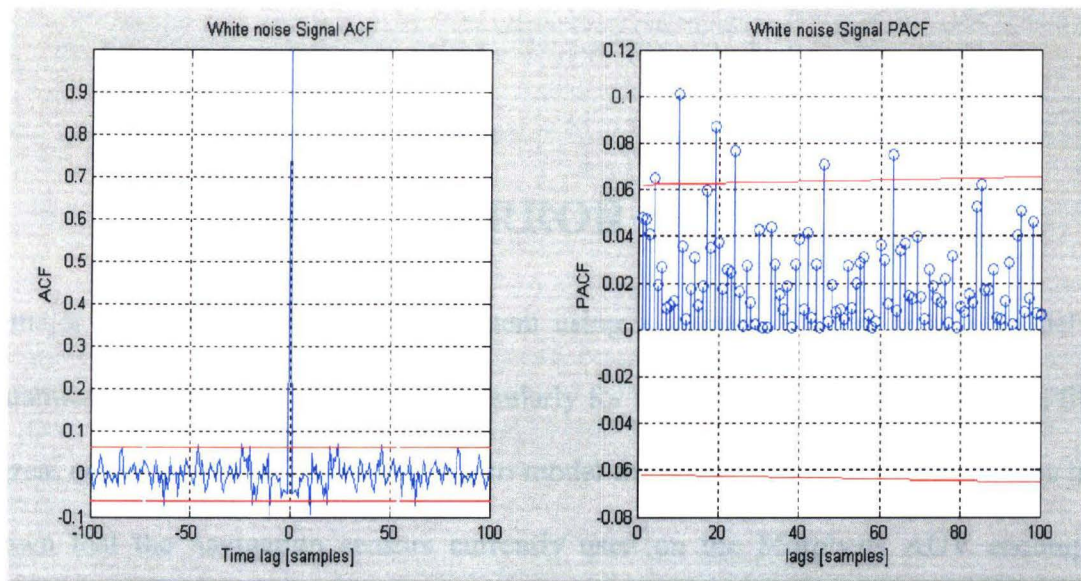


Figure 2.11: White noise signal autocorrelations

3 SENSOR ERROR MODELING

A major concern in the navigation system using a Kalman filter is how to model the dynamics of the system. And more particularly for the use of an error-state Kalman filter, a great emphasis should be put on how to model the sensor errors. Previous studies have shown that the navigation sensors currently used on the Morpheus AUV encompass intrinsic errors [6] [7]. The measurement errors are estimated and modeled in the filter for the: DVL, the magnetic compass, gyroscope, accelerometer and GPS/DGPS system.

A traditional approach was to model the sensor errors by a first order Gauss-Markov process (section 2.3.2.2.2). This method relies on the correlation properties of the noise and appeared sufficient for the applications of the Kalman filter [6]. However, a thorough study of the measurement sensor noise has shown some inadequacies between the theoretical first order Gauss-Markov process and the noise correlation properties. The problem resides in the exact determination of the Gauss-Markov process order.

This section will describe the methodology used to identify an ARMA/ARIMA model. The least-square method used to estimate the ARMA parameters is presented as well as the criteria used to select the model orders.

3.1 BOX-JENKINS BUILDING BLOCKS

For a non-stationary process, an approach to modeling ARIMA processes was proposed by the statisticians G. Box and G. Jenkins in 1970 [9] [10] [31]. Box-Jenkins modeling involves identifying an appropriate ARIMA process, fitting it to the data, and then using the fitted model for forecasting. The original Box-Jenkins modeling procedure involves an iterative three-stage process of model identification, parameter estimation and diagnostic checking.

1. **Data preparation** involves transformations and differencing.

Transformations of the data in the case of logarithmic or exponential trend can help stabilize the variance in a series where the variation changes with the level. The data are then differenced until no obvious patterns such as linear trend or periodicity is observed. “Differencing” meaning taking the difference between consecutive observations, or studying the process derivative.

2. **Model identification** in the Box-Jenkins framework.

Once the time series stationarity has been achieved, it is possible to determine the model of the process by visual inspection. The ACF and PACF provide useful indications for the time series and residual analysis as shown in Table 2.2.

3. **Parameter estimation** involves finding the values of the model coefficients.

This provides the best fit to the data. A least-square algorithm [24] can be used for linear AR processes. For ARMA/ARIMA models, another method using the output prediction error can be applied and will be covered in section 3.4 [33].

4. **Diagnostic checking** tests the assumptions of the model and verifies the adequacy of the model. The model order can be selected with two relevant criteria: the Akaike's Information Criterion and the Mehra's whiteness test (cf. section 3.4). The autocorrelation and partial autocorrelation functions are also used to assess the residual's whiteness. If not the model selection should be redone.
5. **Forecasting** once the model is selected, estimated and checked.

Figure 3.1 summarizes the respective steps of the Box-Jenkins model building blocks.

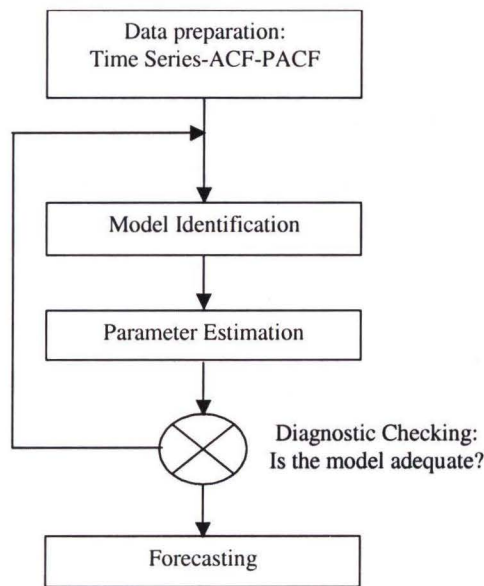


Figure 3.1: Box-Jenkins building blocks

3.2 ESTIMATION STAGE

The method used in this thesis to estimate the ARMA parameters is based on *Multistage Least Squares* also called Extensive Least Square (ELS) and is carried out using the ARMAX function of MATLAB System Identification Toolbox.

It is composed of three steps:

1. Estimate the AR model using a Least Squares algorithm solving for the AR process from Equation (2.43):

$$u_n = \sum_{k=1}^p a_k \cdot u_{n-k} + v_n \quad (3.1)$$

The AR parameter estimates are computed for least-square estimation solution [4] [15] [20] [33]:

$$\hat{a}_k = [X^T X]^{-1} X^T u_k \quad (3.2)$$

Where the hat “^” denotes the estimate.

2. Calculate the prediction error of the AR model:

From the estimated AR parameters, the residuals e_{ARn} can then be sought for:

$$e_{ARn} = \sum_{k=0}^p \hat{a}_k \cdot u_{n-k} \quad (3.3)$$

3. Estimate the ARMA model parameters a_n and b_n with a Recursive Least Square algorithm by approximating the prediction errors of the ARMA model until the residual is equal the AR residual.

$$e_{ARMA_n} \approx e_{ARn} \quad (3.4)$$

The steps 2 and 3 are iterated at most 20 times until the convergence of the residual is reached.

3.2.1 Least Square Estimation

The Least Square approach is commonly used for curve-fitting problems [4] [15] [20] [33], where a best-fit solution is computed for a chosen model order. This technique does

not require any statistical assumption about the source of uncertainty in the problem. It estimates a best fit to the observed measurement by minimization of the loss function.

The ARMA process Equation 2.47 can be formulated as:

$$u_k + a_1 u_{k-1} + \dots + a_n u_{k-p} = b_1 w_{k-1} + \dots + b_n w_{k-q} + v_k, \quad (3.5)$$

Where k denotes the discrete time step. v_k is an white noise term which accounts for the fact that the data never matches the model exactly. p and q are the orders of the ARMA processes.

The problem here is to estimate the parameter vector A from a set of data:

$$A = [-a_1, \dots, -a_p, b_1, \dots, b_q]^T \quad (3.6)$$

Equation (3.5) may be written in a vector form as

$$u_k = \phi_{k-1}^T \cdot A + v_k \quad (3.7)$$

$$\text{With } \phi_{k-1} = [-u_{k-1}, \dots, -u_{k-p}, v_{k-1}, \dots, v_{k-q}]^T \quad (3.8)$$

The vector ϕ_{k-1} represents a sliding window of the signal and noise terms.

We can compute an estimate of the ARMA parameter vector A based on the data set

$U = \{v_0, \dots, v_N, u_0, \dots, u_N\}$ if the N data points are collected. v_k is assumed to be white

noise process. Consequently, if the residual $e_k = u_k - \phi_{k-1}^T \cdot A$ between the data set U and

the estimated data from the model A is assumed to be Gaussian and white, the estimate of

the parameters can then be computed as the least squares solution:

$$\hat{A} = \arg \min_A \sum_{k=1}^N |u_k - \phi_{k-1}^T \cdot A|^2 \quad (3.9)$$

where “ $\hat{}$ ” denotes the estimate.

The solution can be obtained using standard techniques, by writing $\hat{\theta}$ as the least squares solution of the system of linear equations:

$$\begin{bmatrix} u_1 \\ u_2 \\ \vdots \\ u_M \end{bmatrix} = \begin{bmatrix} \phi_1^T \\ \phi_2^T \\ \vdots \\ \phi_M^T \end{bmatrix} . A \quad (3.10)$$

$$\text{Or also } U = \Phi . A \quad (3.11)$$

The solution given by the pseudo-inverse becomes

$$\hat{A} = (\Phi^T \Phi)^{-1} . \Phi^T . U \quad (3.12)$$

For the estimation of the ARMA parameters, a priori knowledge of the residuals is required. Therefore, a first AR estimation is computed for some AR parameters to generate a set of assumed white noise residual e_k .

3.3 SELECTING THE MODEL ORDER

The procedure of statistical model identification may be defined as finding a model which best fits a set of observed data with respect to a chosen criterion. The performance of the sensor error model identification depends very much on the choice of the criterion of fit. In [20] [21] Akaike developed an Information Criterion (AIC) for time series model fitting. This criterion finds an optimal number of ARMA parameters (p,q) which minimizes the maximum likelihood estimation loss function. Another criterion based on Merha's whiteness test of the estimation residual [16] [17] appears to be a very useful tool for the model order selection. Minimal AIC orders and whiteness tests results will be used to determine a sufficient order in the sensor error characterization. The two criteria

3.3.1 The Akaike information theoretic criterion (AIC)

Akaike's Information Criterion is an information theoretic approach for selecting the estimated best approximating ARMA model [20]. In a general sense, the model for which AIC is smallest represents the “best” approximation to the true model. In practice, the model satisfying the AIC criterion may or may not be the “true” model since there is no way of knowing whether the “true” model is included among those being compared [22]. This method contrasts with the typical procedure of testing the correlation significance between different models.

The AIC can be expressed as:

$$AIC = N \cdot \log(\hat{\sigma}^2) + 2K \quad (3.13)$$

$$\text{Where } \hat{\sigma}^2 = \frac{\sum_{i=1}^N (yt_{data} - yt_{fit})^2}{N} \quad (3.14)$$

and yt_{data} is one representation of the N measurements, yt_{fit} is the best fit of the model and $K = p + q$ the sum of the ARMA ($p+q$) model parameters. The term K is simply the number of model parameters and leads to the standard form of the AIC measure used for model selection:

$$AIC = \chi^2 + 2.K \quad (3.15)$$

The function χ^2 is recognized as the logarithm of the maximum likelihood estimates of the model parameters. The term k represents the model complexity penalty. The first term decreases rapidly with N where as the other one increase linearly with N. The representation of the AIC will show a minimum value at an *optimum order* called

minimum AIC. Then when several models are being fitted by the method of least-square estimation, the one with the smallest value of AIC is chosen as best model [21] [22].

3.3.2 Mehra Whiteness Test (WT)

The knowledge of AR or MA autocorrelation patterns [9] [10] can significantly help identify a random process. However, the ACF and PACF plots obtained from real measurement data will never precisely match the theoretical ACF and PACF patterns associated with AR and MA models. While comparing the fitted model with the real data, we then need to find a means, which tells when an autocorrelation function is close enough to zero to be interpreted as zero. Or inversely, we need to know when this value can be considered significant.

For this, a very basic test of time series is the test of whiteness. In the situation of model identification, the whiteness of the residual series after fitting a model is required as a proof of adequacy of the model. This function determines according to the autocorrelation test proposed by Mehra [16] [17], whether a process satisfy the white noise properties.

Considering the normalized autocorrelation function (2.3), the probability for the autocorrelation function to be non-zero with α degree of confidence is given by [14]:

$$\Pr ob \left[z_{1-\alpha/2} < \frac{(x - \mu_x)\sqrt{N}}{\sigma_x} < z_{1-\alpha/2} \right] = 1 - \alpha \quad (3.16)$$

Therefore from the statement that a process is white with 95% degree of confidence, the confidence limits of its autocorrelation function are $\pm \frac{1.96}{\sqrt{N}}$.

For a time series, the whiteness test counts the number of times where the autocorrelation function lies outside the confidence intervals and divide this value by the total number of samples. This ratio is then compared to the 5% value Equation (3.17). If the number greater than 1, the sequence is said to be white. The test is based on the assumption of large number of samples N , [16].

$$WT = \frac{\alpha}{n / N} \quad (3.17)$$

Where $\alpha = 0.05$, n the number of samples lying out of the confidence intervals and N the total number of samples.

The two criteria, minimum AIC and Mehra's maximum whiteness test were used for diagnosis checking at the end of the estimation stage. Each ARMA model order is estimated with its residuals checked and analyzed with the criteria and the ACF, PACF functions.

4 RESULTS AND ANALYSIS

This section presents the data collection procedure and static measurement analysis performed using the two different Morpheus AUVs described in section 2.1. Specifically, the static measurement obtained from the TCM2 compass, GPS, DVL and IMU were analyzed. A model order for each of the quantities recorded is selected. The results obtained from the ARMA process parameter estimation are summarized in Appendix A.

4.1 DATA COLLECTION

This section describes results and analysis of static data collected from the Morpheus AUVs presented in Section 2.1.

Using AUV 1 (refer to section 2.1 for notation), a set of data was extracted on an outdoor field of Seatech, Dania Beach for analysis of the TCM2 and GPS static outputs on November 22nd (see Table 4.1). Although the TCM2 compass is supposed to exhibit steady state measurement, a significant compass heading drift was observed over the record interval (see Figure 4.1). The need to check the redundancy of this phenomenon had to be further investigated. Hence, several other sets of compass measurements were collected from AUV 1 and 2. Other sensor static measurements that were collected on December 18th in the pool of the FAU Ocean Engineering department in Boca Raton came from the Crosbow IMU and the RDI DVL ground and water velocity sensor. AUV 2 was hung by a rope at the water surface to stay stationary. Despite the rope, the pool

data have shown some periodic oscillation, which was assumed due to the wind-induced waves in the pool. Two additional sets of data were recorded indoor on January 24th and February 3rd in the Seatech laboratories in order to obtain better steady state measurements from the IMU and verify the compass heading drift. Table 4.2 lists the data collected from the two Morpheus AUVs.

Date	GPS equipped Morpheus (1)	Bio Morpheus (2)
November 22 nd	Outdoor environment	-
December 18 th	-	Pool
January 24 th	Laboratory (1)	-
February 3 rd	-	Laboratory (2)

Table 4.1: Data collection dates

GPS equipped Morpheus (1)		Bio Morpheus (2)	
OUTDOOR	LAB	POOL	LAB
Case 1	Case 2	Case 3	Case 4
$\Delta t = 0.134$ [sec]	$\Delta t = 0.1551$ [sec]	$\Delta t = 0.11$ [sec]	$\Delta t = 0.11$ [sec]
TimeStamp	TimeStamp	TimeStamp	TimeStamp
auvHeading	auvHeading	auvHeading	AuvHeading
auvRoll	auvRoll	auvRoll	AuvRoll
AuvPitch	AuvPitch	AuvPitch	AuvPitch
Gps status		Acceleration x	Acceleration x
Gps hdop		Acceleration y	Acceleration y
Gps latd		Acceleration z	Acceleration z
Gps latm		Yaw rate	Yaw rate
Gps longd		Roll rate	Roll rate
Gps longm		Pitch rate	Pitch rate
		DVL Velocity x	
		DVL Velocity y	
		DVL Velocity z	
		DVL Altitude	

Table 4.2: Steady State Data collected

Figure 4.1 and 4.2 show the data collected from case 1. Figure 4.3 shows the compass measurements from case 2. Figure 4.4 and 4.5 show the data collected from the pool case

3. The DVL ground velocities were collected only for this set. Figure 4.6 and 4.7 show the data collected from laboratory from case 4.

From figure 4.4, we notice periodic oscillations for the case 3 heading and roll measurements. The DVL x and y-axis ground velocities exhibit the same behavior at the same time instant. The pitch angle and z-axis velocity measurements were on the other hand stationary. We therefore assume that a horizontal wave motion was imposed to the vehicle platform during the data collection. The pool measurements encompass a waveform signal and cannot be treated to model the DVL error. Another approach should be considered to overcome these difficulties. For instance, we can tether the AUV to the 4 corners of an indoor pool. There, the water surface will be steady and the signal characteristics should be essentially white noise driven.

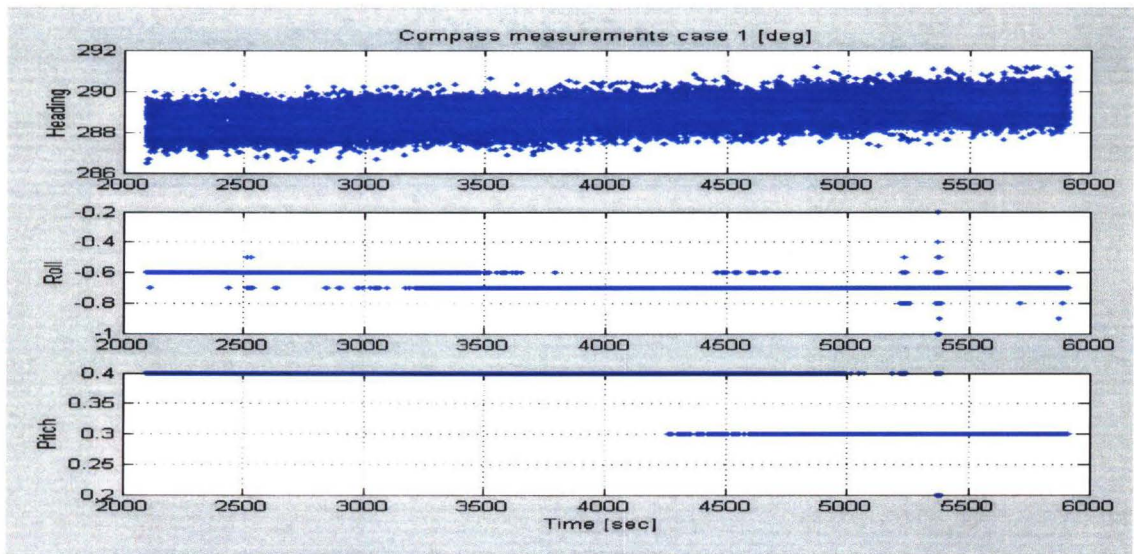


Figure 4.1: Compass measurements case 1

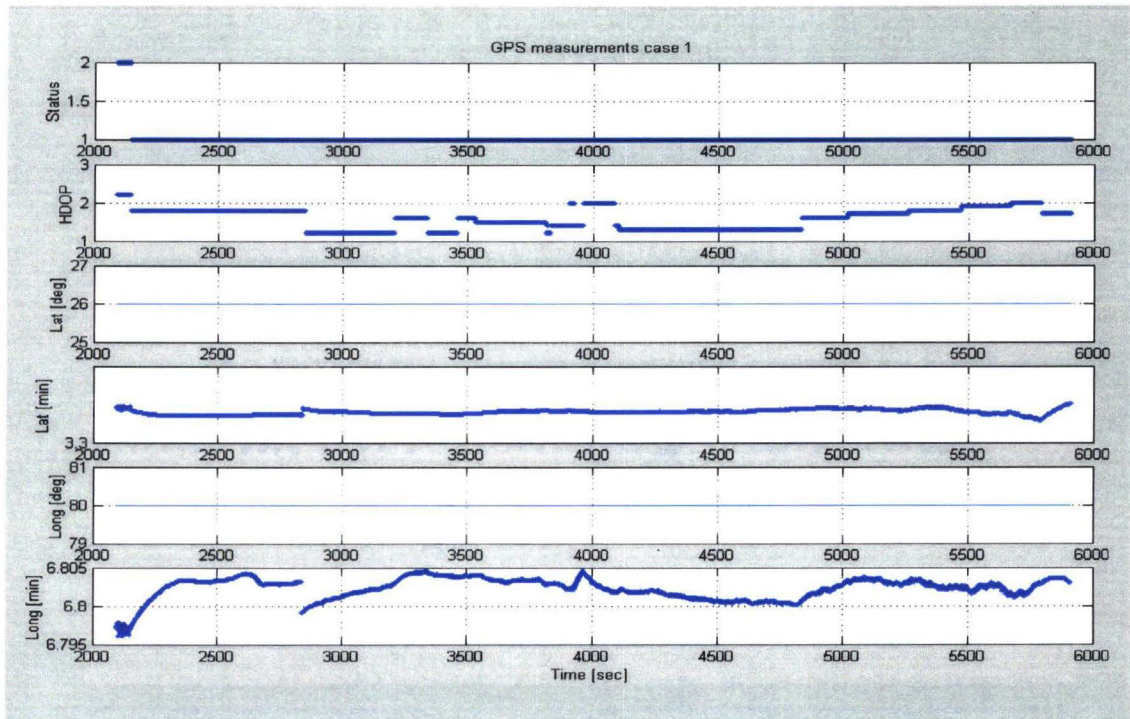


Figure 4.2: GPS measurements case 1

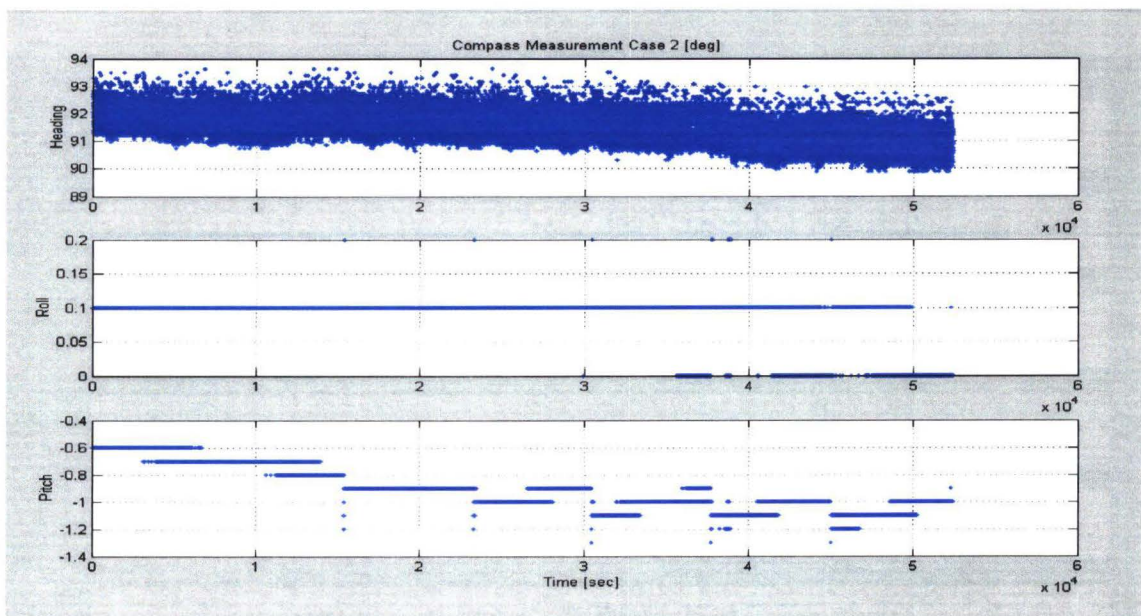


Figure 4.3: Compass measurements case 2

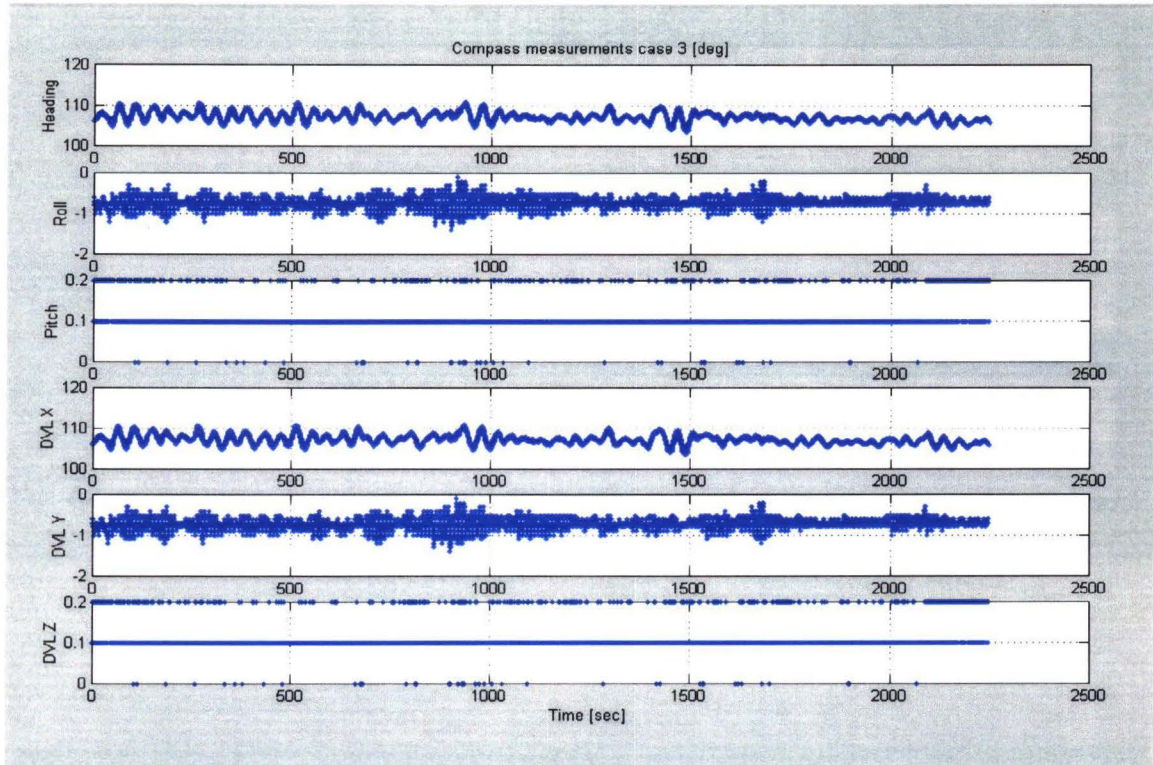


Figure 4.4: Compass and DVL measurements case 3

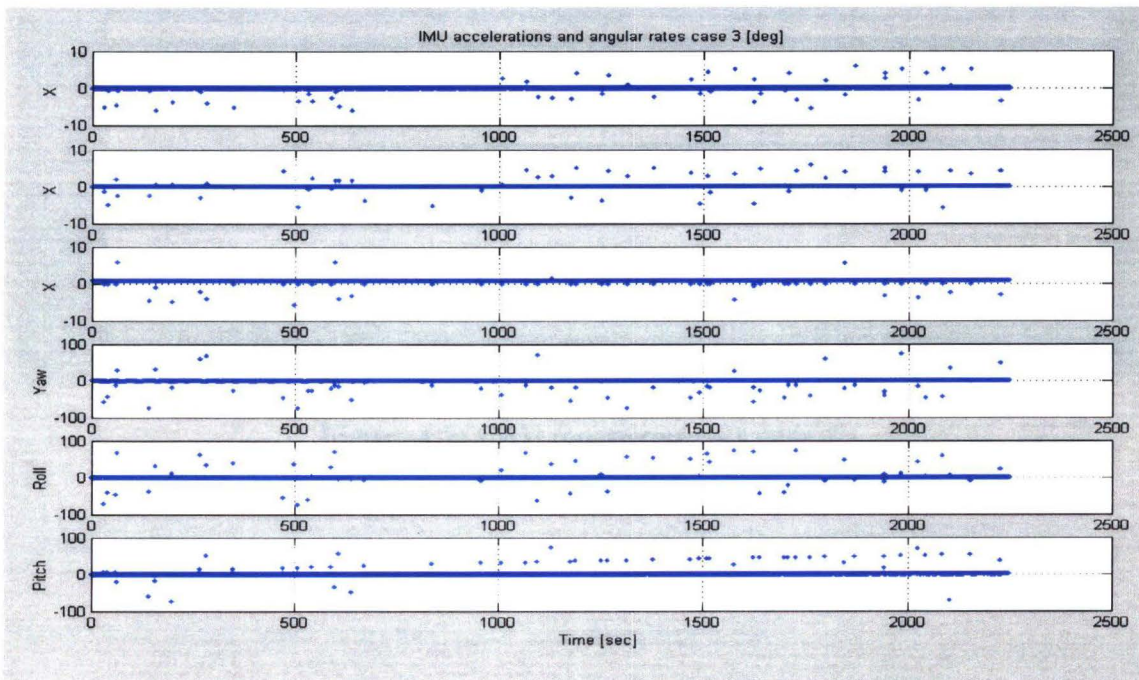


Figure 4.5: IMU measurements case 3

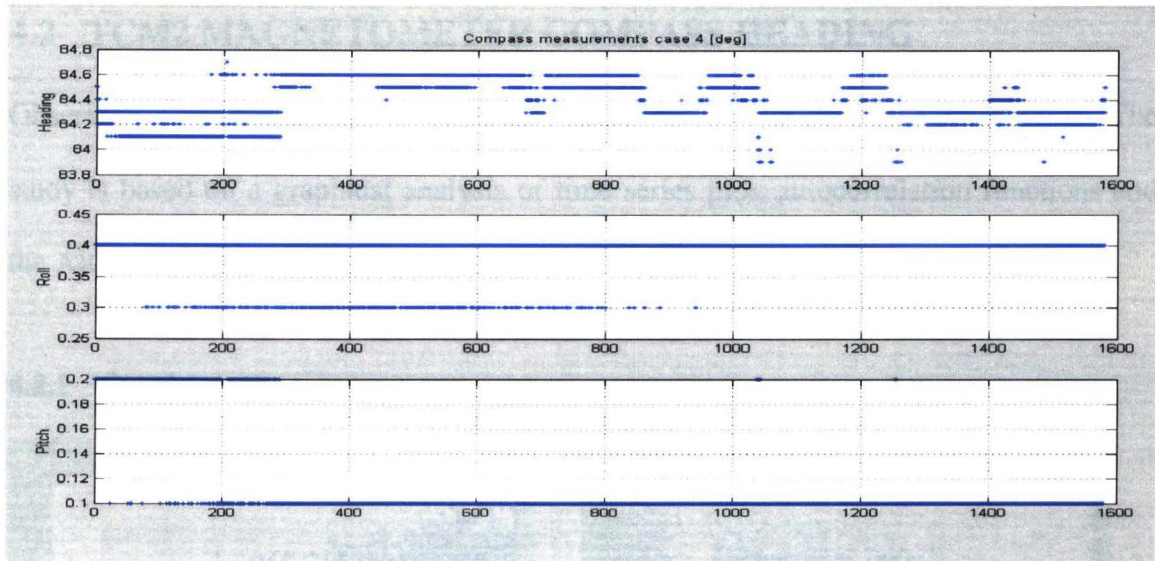


Figure 4.6: Compass measurements case 4

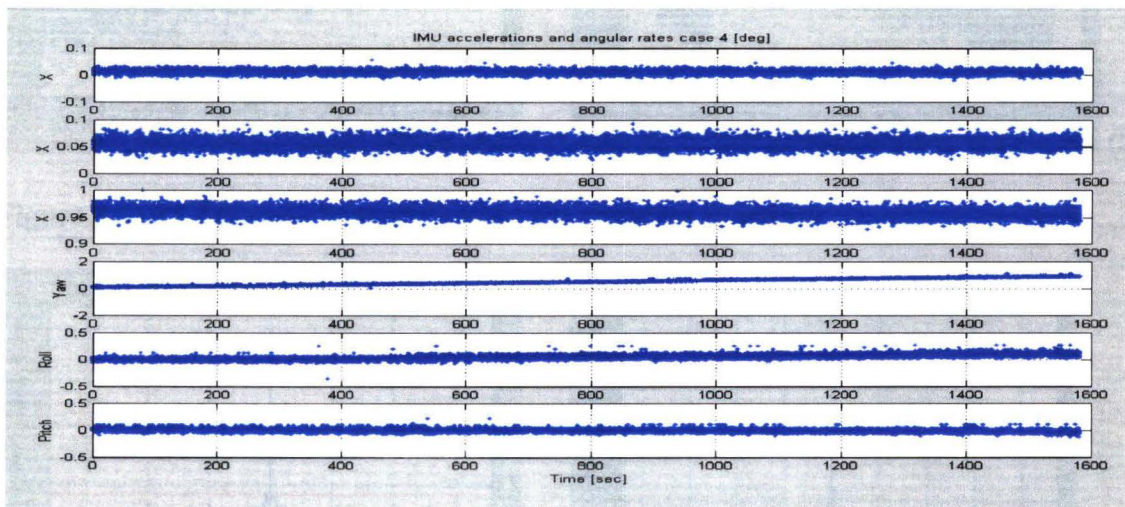


Figure 4.7: IMU measurements case 4

4.2 TCM2 MAGNETOMETER COMPASS HEADING

Observing the compass heading static measurements, we can develop a noise model. The study is based on a graphical analysis of time series plot, autocorrelation functions and the AIC and whiteness test results.

4.2.1 Steady state measurement:

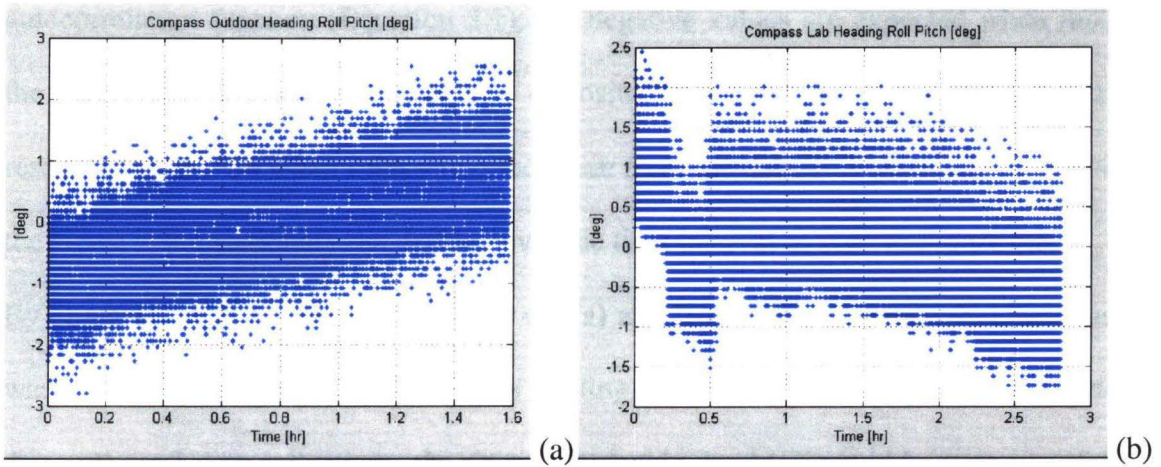


Figure 4.8: TCM2 case 2 (a) and case 1 (b) compass heading

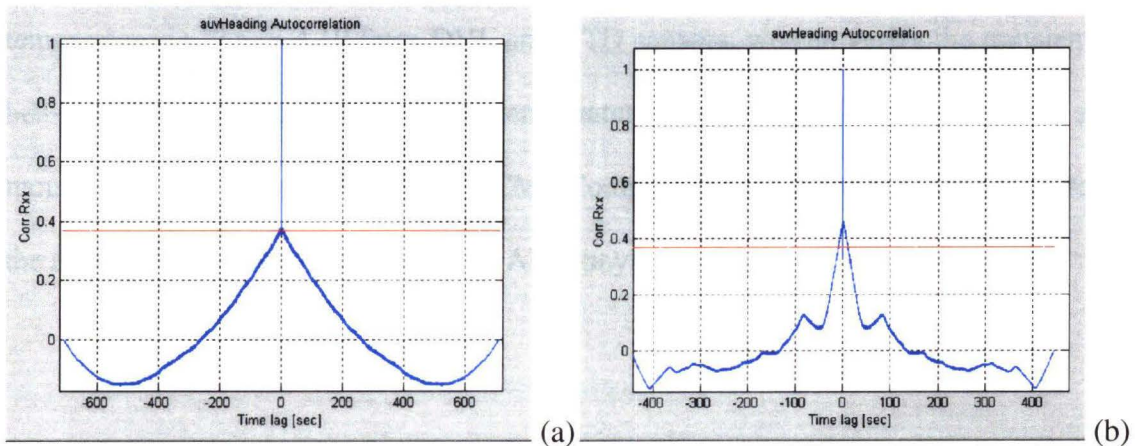


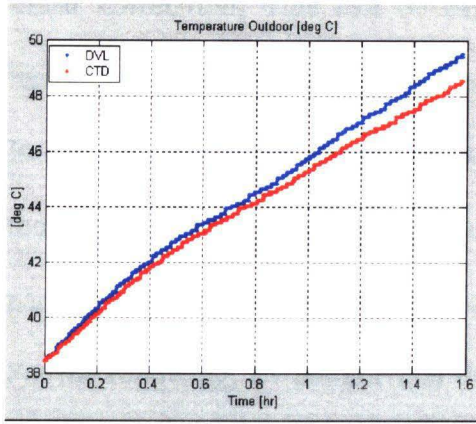
Figure 4.9: TCM2 case 2 (a) and case 1 (b) heading ACF

The two sets of data respectively with case 1 and 2 (see Figure 4.8) exhibit a linear drift with time. The lab heading drifts over a period of 1.53 [hr] with a rate of 1.15 [°/hr]

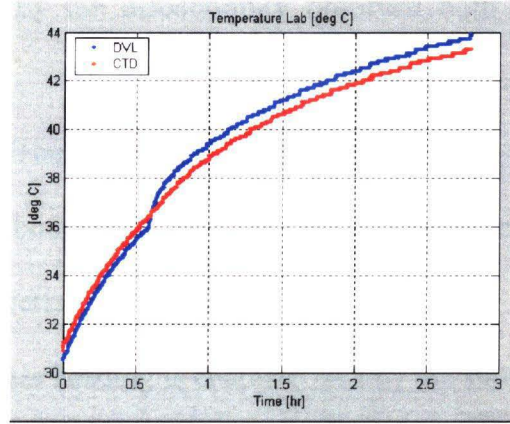
where as the outdoor heading drifts with a rate of -0.45 [$^{\circ}/\text{hr}$] over 2.8 [hr], respectively Figure 4.8 (b) and (a). In general, the statistics property of any random process can easily be described by a probability density and autocorrelation function. Here, an autoregressive pattern for AUV 1 compass heading is deduced from the decaying shape of the two ACF plots in Figure 4.9.

On both plots, the ACF becomes negative at higher lags. From the definition of the autocorrelation function (Equation 2.1), the negative values are expected when most of the integrated product terms have an opposite sign (with respect to their mean for rescaled values). So when subtracting the mean from the data, this generally occurs when the signal is not stationary but drifting over the time interval as seen in Figure 4.8.

By observation of the two plots Figure 4.8 (a) and (b), we may assume that the heading was recorded during a transient state of heating of the AUV electronic devices. Indeed, during these 2 data collections, the rising heat inside the AUV could be a source of drift, as the AUV was not submersed in a sufficiently cooling liquid. By looking at the temperature in Figure 4.10 from DVL and CTD sensors, we can verify the transient state behavior of the process. The DVL temperature was recorded from the DVL sensor mounted in the same payload as the TCM2 Compass. The CTD on the other hand records the ambient temperature outside of the AUV payload.



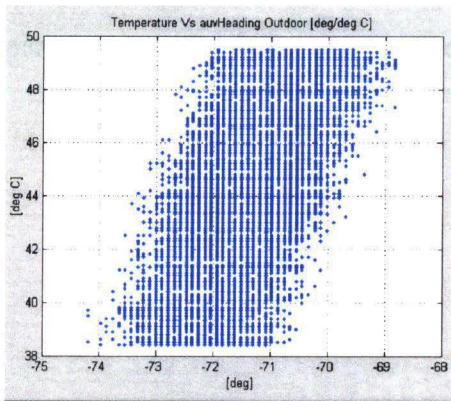
(a)



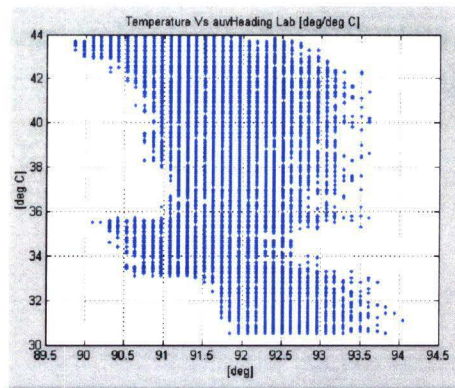
(b)

Figure 4.10: Case 1 (a) and Case 2 (b) DVL-CTD Temperature

The observation of both cross-correlations in Figure 4.10 between the compass heading and the temperature is a good indicator on how to model the heading measurement.



(a)



(b)

Figure 4.11: Case 1 (a) and Case 2 (b) Temperature Vs Heading

The correlation coefficient is computed with MATLAB using the function “corrcoef”:

$\rho_{xy} = 0.6294$ For the outdoor heading and temperature.

$\rho_{xy} = -0.5019$ For the lab heading and temperature.

Figure 4.11 (a) shows a moderate linear correlation between the compass heading and the temperature. This is verified by a pretty high correlation coefficient of 0.6294. On the other hand, the cross correlation in Figure 4.10 (b) is close to a scatter pattern than a

linear correlation. This can be explained by the discontinuity observed both in the temperature and the heading measurements.

In addition, the two cross-correlation coefficients obtained have an opposite sign even though the temperature was increasing in both cases. We assume that other external parameters may also be considered to characterize the heading drift.

For the following, we assume that the compass heading is characterized by the sum of an ARMA model and a linear temperature term.

$$\sum_{k=0}^p a_k \cdot \psi(n - k) + K_T \cdot T = \sum_{k=0}^q b_k \cdot v(n - k) + v(n) \quad (4.1)$$

Where K_T is to be computed experimentally, T represents the temperature, p and q are the parameter order of the ARMA process ψ is compass heading and $v(n)$ is white noise.

4.2.2 Order and parameter estimation:

The ARMA parameters (p,q) were computed using the ARMAX Matlab function. The Akaike AIC criterion (top of Figure 4.12) was computed from the residual of the estimation for each combination of p and q orders. The whiteness test described by Merha [16] is represented on the lower side of Figure 4.12.

4.2.2.1 Case 2 data set

The data set collected from the AUV 1 case 2 was studied for the original and differenced cases (ARMA and ARIMA models). The estimation performances are compared regarding the stationarity of the signal.

4.2.2.1.1 Original Signal Parameter Estimation:

On top of figure 4.12, the AIC criterion and Whiteness test are found to be respectively the minimum and maximum for the parameter orders (see Appendix A for the parameter estimation results):

$$\begin{bmatrix} p = 6 \\ q = 10 \\ d = 0 \end{bmatrix} \Rightarrow AIC : -1.91168 \qquad \begin{bmatrix} p = 10 \\ q = 8 \\ d = 0 \end{bmatrix} \Rightarrow WT : 3.5970$$

With p being the AR order, q the MA order, and d the number of signal differentiations.

Although the heading measurement seemed to be temperature dependent in Figure 4.11 (b), an ARMA model can be used to remove the linear trend created by the increasing heat. As we can see on the top right hand side of Figure 4.12, the AIC criterion is higher along the q -axis. This indicates that the model is “best-fitted” with an AR process model of order 1 at minimum. The whiteness test on lower part of Figure 4.12 confirms this

assumption. Indeed, on these plots the 95% degree of confidence for which the innovation residual is white is reached for an AR order $p \geq 1$.

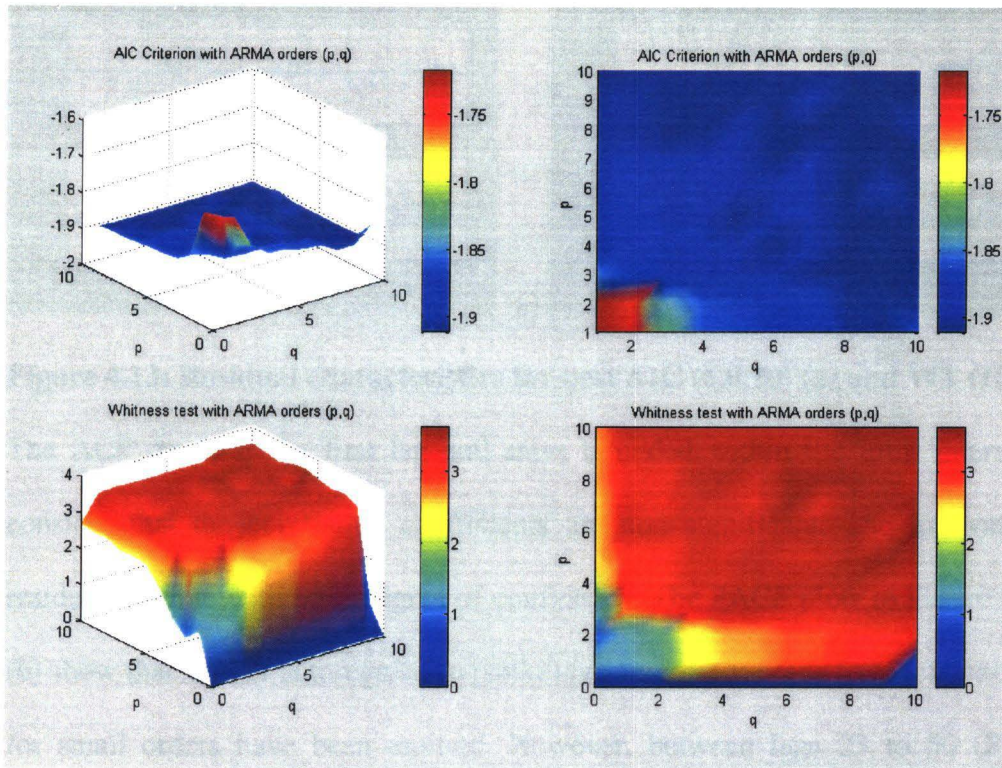


Figure 4.12: Lab case 2 heading residual AIC (above) and WT (below)

Figure 4.13 shows the time series, autocorrelation function ACF and the partial autocorrelation function PACF based on the data from case 2. The plots on the left-hand side were computed for the best AIC criterion and for the best whiteness test result on the right hand side.

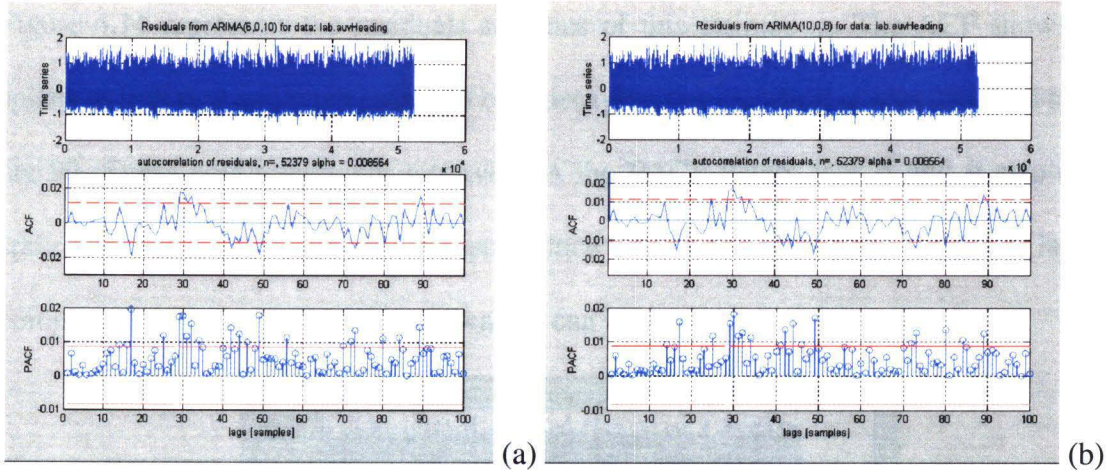


Figure 4.13: Residual characteristics for best AIC (6,0,10) (a) and WT (10,0,8) (b)

The ACF drops at the first lag and stays bounded within the limit interval. We can consider that the correlation coefficients are non significant. The innovation process residual is white with 95% degree of confidence. The PACF plots in Figure 4.13 (a) and (b) show that neither autoregressive (spike) nor moving average term (exponential decay) for small orders have been omitted. However, between lags 23 to 50 (Figure 4.13), several terms are not characterized. They can be considered with a higher order differentiation, but in our case, they are relatively insignificant. In both cases (a) and (b), the variance of the signal has been halved (from 0.3263 to 0.1473).

From figure 4.5, we have seen that a white noise residual was obtained with 98% confidence interval for $(p,d,q) = (4,0,4)$ (whiteness test > 3 , in our case $WT = 3.3231$) and may be a sufficient order for estimation.

The results from the AIC and whiteness test criteria yield an ARMA process order of 10. A comparison is made with lower order terms to check whether the model was over fitted. The significance of the residual spikes from the ACF and PACF plots will be the reference for this analysis.

Figure 4.14 represents the residuals statistics of this estimation. The ACF shows some spikes at lags 6, 9 and what seems to be a decaying term starting at lags 29 and a spike at lag 90. These coefficients are retrieved on the PACF where lags 6 and 9 also exhibit spikes without any decaying shape. Since then, the graphical analysis is more complicated and we'll assume these values can be neglected.

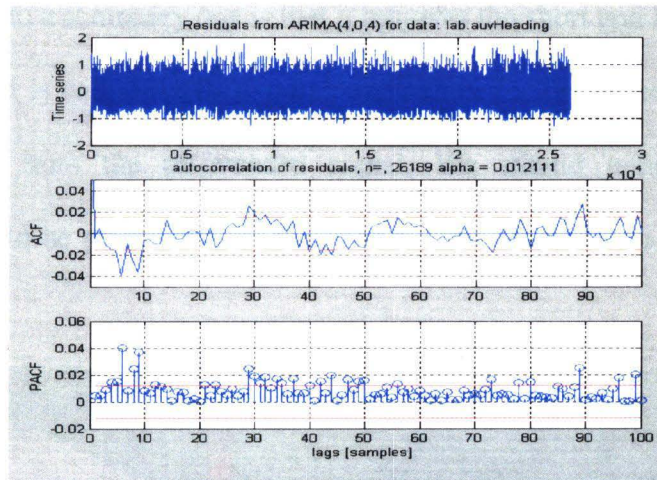


Figure 4.14: Residual characteristics for order (4,0,4)

4.2.2.1.2 Regular Differenced Signal Parameter Estimation:

Another method proposed by Jenkins [9] [10], is to use a regular or seasonal differentiation for non-stationary processes. This consists of taking the difference between consecutive values (for regular differencing) or between assumed periodical values (seasonal differencing). The reason differencing can be used to convert non-stationary series into a stationary one is that it removes the short and long-term trends in a series. The method is called ARIMA parameterization for the values are estimated and then “integrated” from the differenced signal. We should note that the seasonal differentiation could be performed for the periodicities observed on the PACF of figure 4.13.

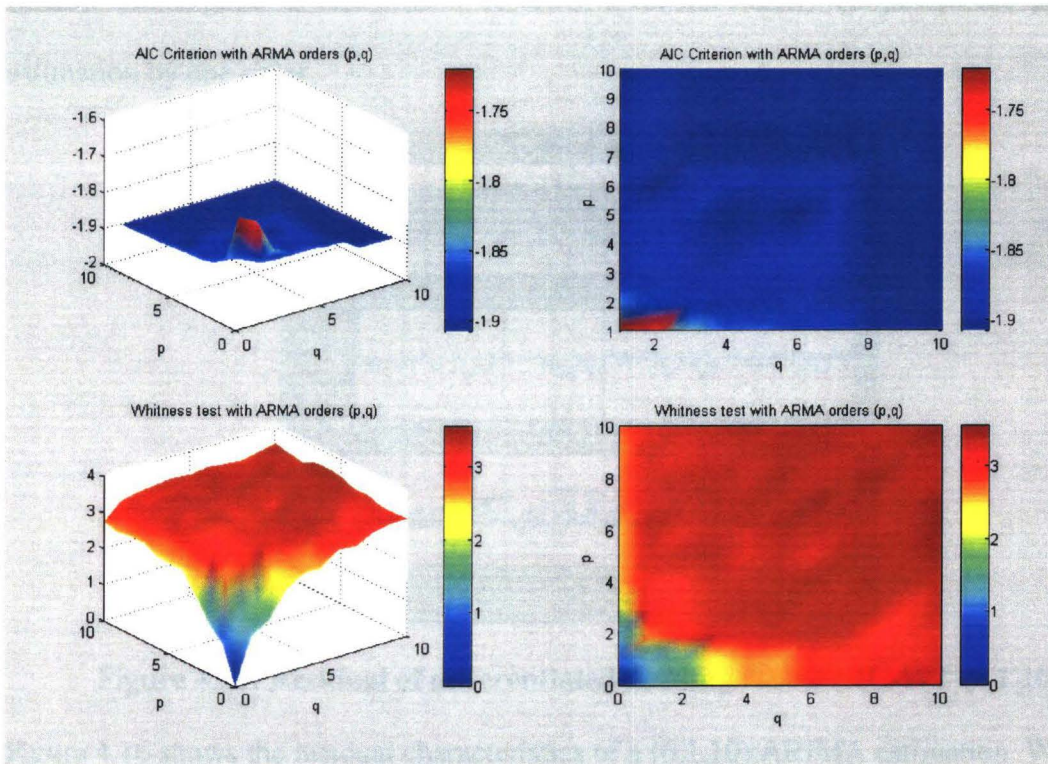


Figure 4.15: Differentiated heading residual case 2 AIC (above) and WT (below)

Figure 4.15 displays the AIC criterion and whiteness test results of a regular differentiation of order 1 for the heading case 2. The AIC criterion and Whiteness test were found to be respectively minimum and maximum for the same parameter orders:

$$\begin{bmatrix} p = 6 \\ q = 10 \\ d = 1 \end{bmatrix} \Rightarrow \begin{matrix} AIC : -1.9077 \\ WT : 3.5384 \end{matrix}$$

Same parameter orders were obtained as for the AIC non-differenced signal results. However, while looking at the plots of whiteness test Figure 4.15, we observe that the residual becomes non-white since an estimation order of (2,1,2) where as in the non differenced signal in Figure 4.12, the whiteness is obtained ($WT > 1$) for higher orders i.e. (3,0,3). The regular differentiation of order 1 indeed mainly simplifies the parameter estimation by one order.

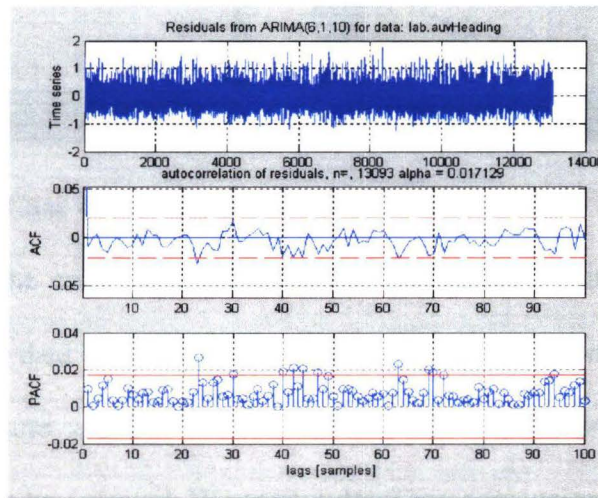


Figure 4.16: Residual of differentiated heading case 2 AIC-WT (6,1,10)

Figure 4.16 shows the residual characteristics of a (6,1,10) ARIMA estimation. We notice the same spike on the PACF plot at lag 23. This means that an AR or MA term was omitted at lag 23 and would require a model of order 23. Noting from section 2.4.2 that a

pure white noise cannot practically be obtained, we consider the (6,1,10) ARMA orders as sufficient. However, the residual of the ACF plot remain within the confidence limit of 95%. Between Figure 4.13 and 4.16, the regular differentiation of order 1 improved the residual whiteness. The ARIMA estimation then verifies the order found for the original signal. The sensor error model for the heading case 2 is assumed to be an ARMA model of order $(p, q) = (6, 10)$.

4.2.2.2 Case 4 data set

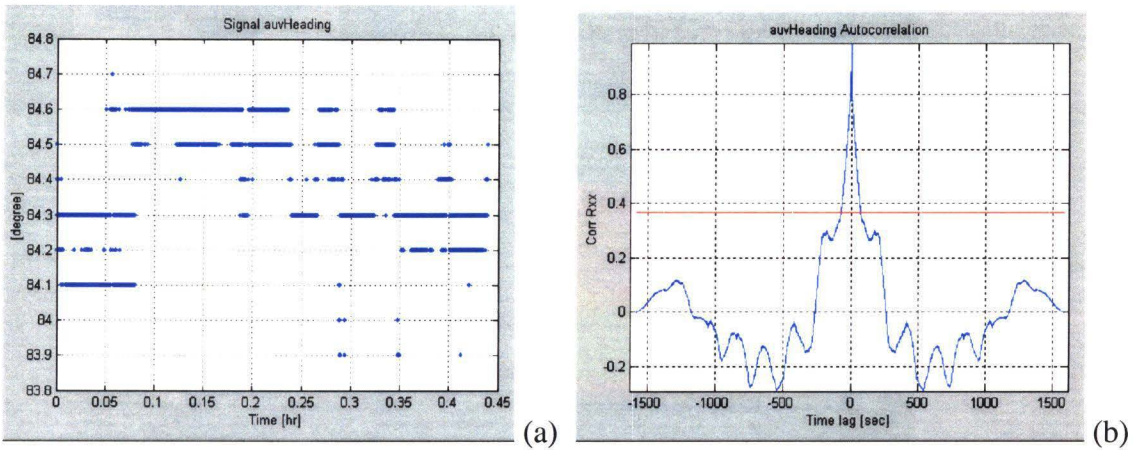


Figure 4.17: Signal Case 4 heading (a) and ACF (b)

In Figure 4.17 (a), the compass time series data case shows stationary characteristics. However the heading data has been filtered to remove the impulsive noise response of the signal. The temperature was not recorded during this experiment and so the heading dependency could not be assessed. We cannot draw any conclusion regarding the trend of the compass heading, as the data seems to oscillate around $\psi = 84.3$ [deg] with a variance $\sigma_{\psi} = 0.0257$ [deg²].

The autocorrelation function of the signal in Figure 4.17 (b) highlights the presence of an autoregressive process. This pattern is recognized as a band-pass white noise process in

[14] resulting in a sine cardinal autocorrelation function. Modeling with a 1st order Gauss Markov process appears to be insufficient for this signal, as it doesn't exhibit an exponentially decaying autocorrelation function. We will investigate the model order selection in the following.

4.2.2.2.1 Original Signal Parameter Estimation

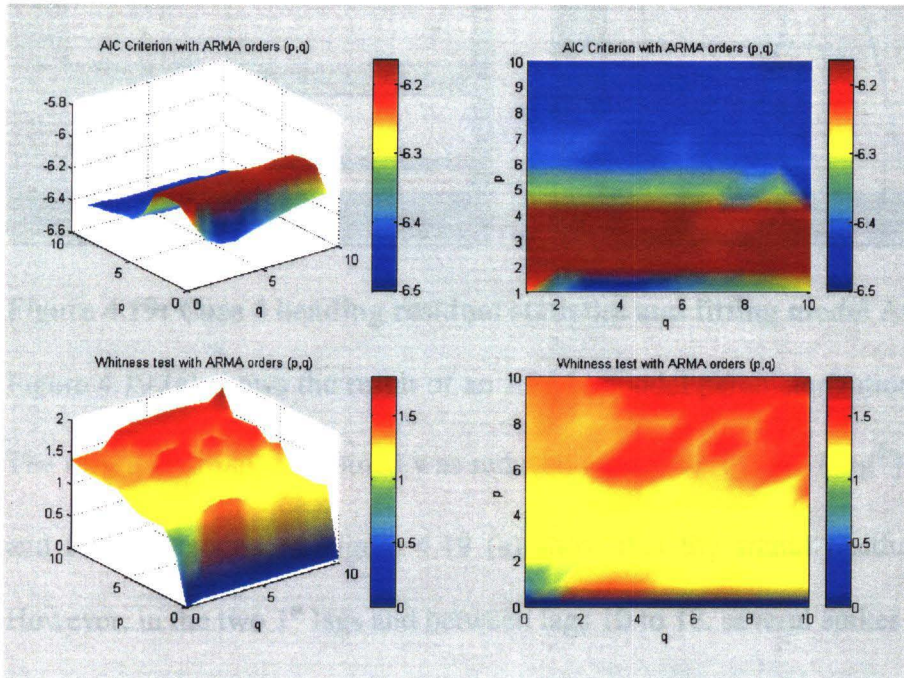


Figure 4.18: Lab case 4 residual AIC (above) and WT (below)

The AIC criterion appears to be minimum for the parameter orders $(p,d,q) = (10,0,9)$ in Figure 4.18. Like in Figure 4.5, the AIC criterion is higher along the q -axis and highlights the need to fit the data with an AR process. But in this case, for model estimations of p values ranging between 2 and 5, the AIC criterion is maximal. The whiteness test shows that the prediction error is not white with 95% of confidence ($WT < 1$) for an AR model less than 2. The best AIC criterion was found for the parameters $(p,d,q)=(10,0,9)$

and $(p,d,q)=(10,0,10)$ for the whiteness test. For these parameters, the residuals characteristics were assumed to be white with 97% confidence interval ($WT \sim 1.7$).

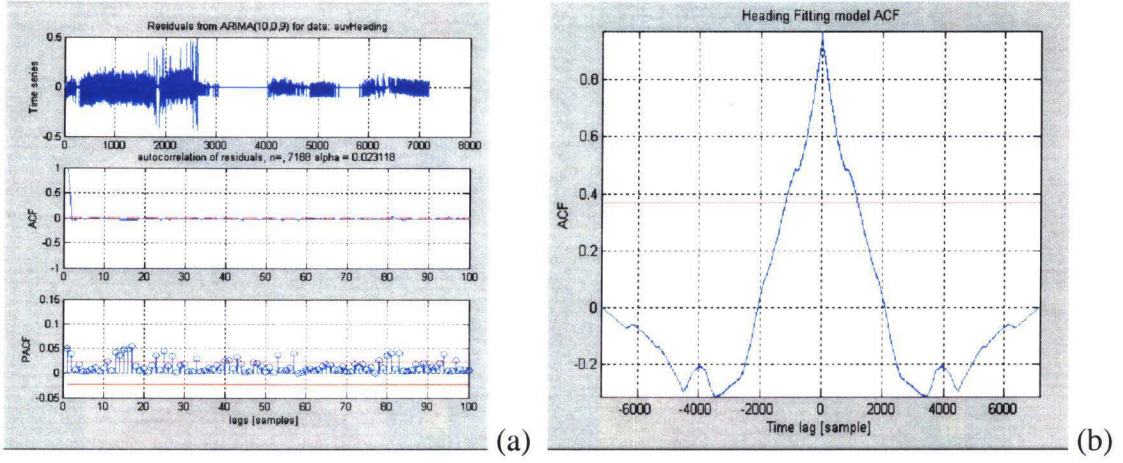


Figure 4.19: Case 4 heading residual statistics and fitting model ACF (10,0,9)

Figure 4.19 (a) shows the result of an ARMA model parameterization of order $(10,0,9)$. The residual variance obtained was reduced to $\sigma_{resid} = 0.0049 \text{ [deg}^2\text{]}$. The residual ACF and PACF function in Figure 4.19 (a) show that the signal residual is almost white. However, in the two 1st lags and between lags 10 to 18, several spikes occur on the PACF plot. This indicates that a higher order model should be used for a parameterization enhancement. Figure 4.19 (b) shows the ACF plot of the model used to fit the heading signal. We notice that this function is almost identical to the band-pass white noise pattern of Figure 4.17 (b).

4.2.2.2.2 Regular Differenced Signal Parameter Estimation

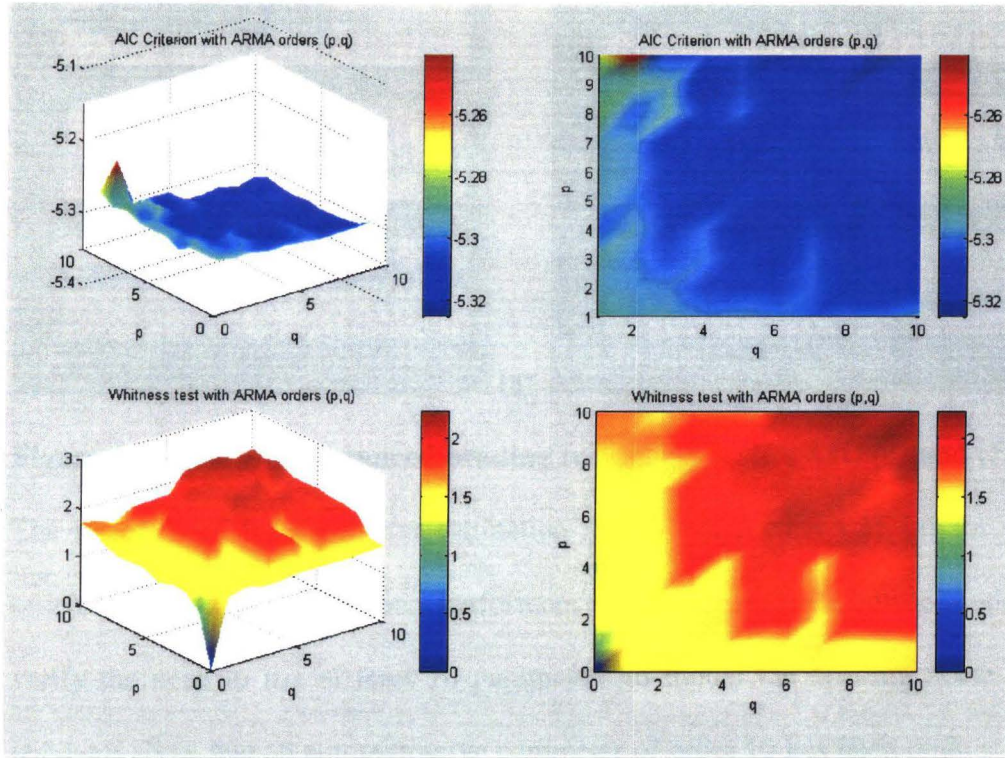


Figure 4.20: Differenced case 4 residual AIC (above) and WT (below)

The AIC and whiteness test study of the heading case 4 differenced signal in Figure 4.20 shows similar results (10,1,9) as for the non-differenced signal (10,0,9). As previously, the signal differentiation hasn't shown much improvement in the signal order estimation. We can therefore assume that we can represent the sensor error model of the compass heading measurement from the AUV 2 by an ARMA model of order $(p,q) = (10,9)$.

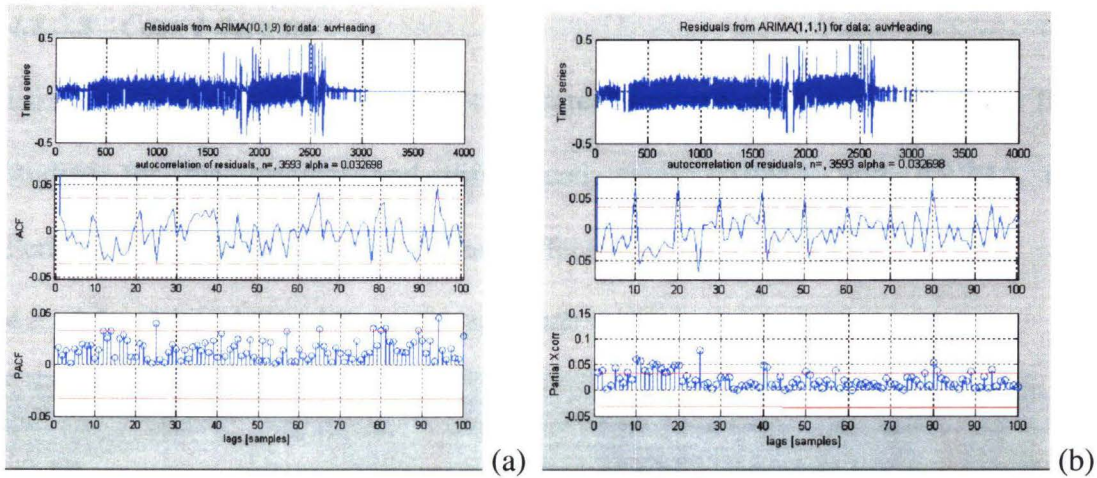


Figure 4.21: Case 4 differenced heading residual statistics AIC (a) and (1,1,1) (b)

The residuals of the parameter estimation are shown Figure 4.21 (a) for the ARIMA orders (10,1,9). The estimation performance is compared to a lower model (1,1,1) to verify the need to use at least 10 parameters to model the heading noise. The (1,1,1) residuals show that an autoregressive parameter of order 10 has been omitted on the ACF plot indicating the need to parameterize the model until order 10.

4.2.2.3 Case 1 data set

Like the previous cases, the data set collected from the AUV 1 in an outdoor field was studied for the original and differenced cases (ARMA and ARIMA models). Performances between the original and differenced signal were compared.

4.2.2.3.1 Original Signal Parameter Estimation:

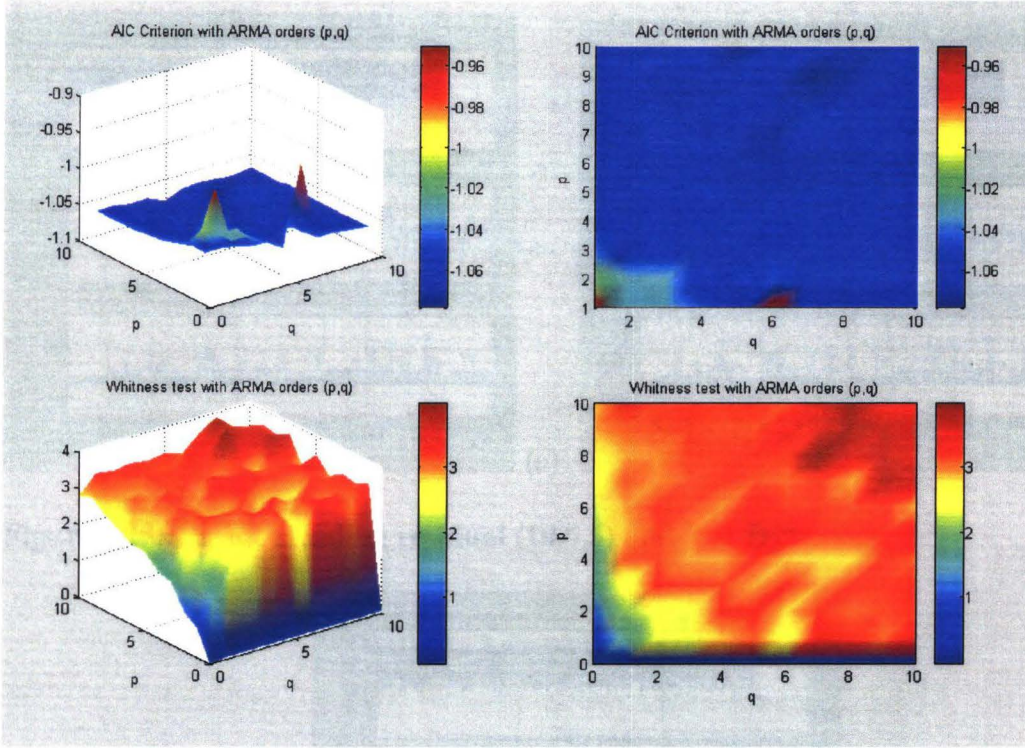


Figure 4.22: Case 1 Heading residual AIC (above) and WT (below)

The AIC criterion is minimum for the parameter orders $(p, d, q) = (10, 0, 5)$ in Figure 4.22. Like that in Figure 4.12, the AIC criterion has several peaks along the q -axis. This is confirmed on the below plots of figure 4.22 where the whiteness test increases with the AR orders p . For this signal, the best model is obtained from the WT criterion for the orders $(p, d, q) = (8, 0, 7)$. It also seems necessary to estimate the sensor error with a

minimum order (4,0,2). There, the residual whiteness is guaranteed with 95% confidence interval (WT>1).

Figure 4.23 shows the residuals characteristics of estimation with the best AIC criterion and whiteness test results. These residuals are compared to the lower order parameter estimation $(p,d,q) = (4,0,2)$ chosen graphically from Figure 4.24.

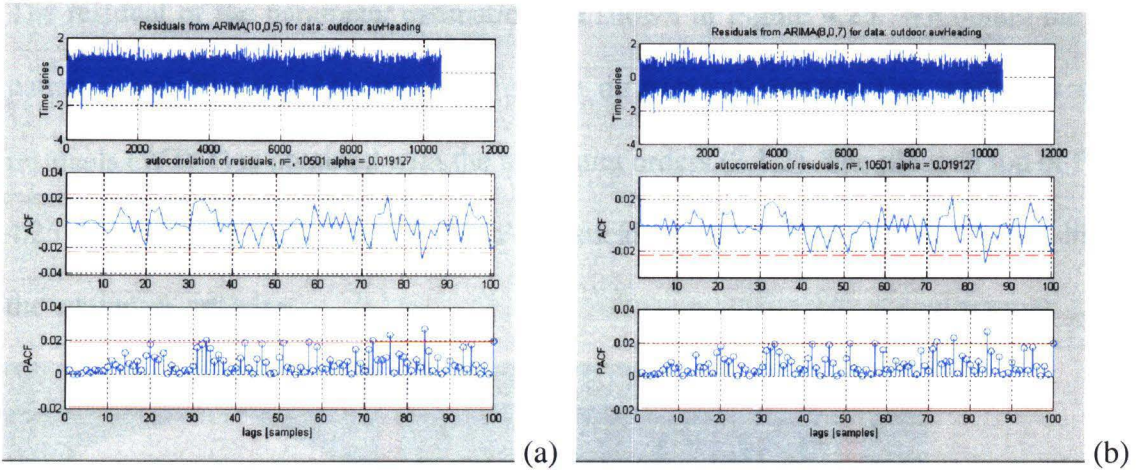


Figure 4.23: Case 1 Heading residual (10,0,5) and (8,0,7)

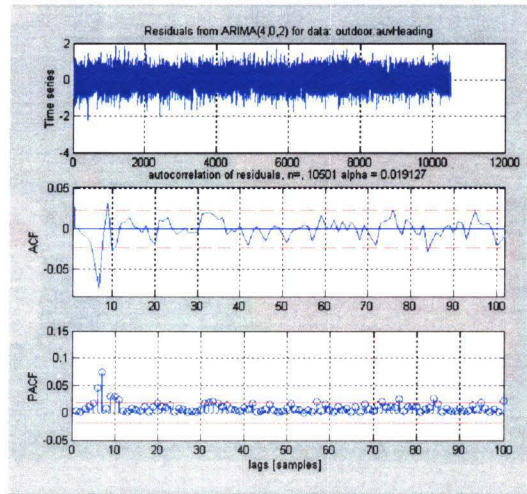


Figure 4.24: Case 1 Heading residual (4,0,2)

The variance of the heading signal has been reduced from $\sigma_{signal} = 0.4017$ to $\sigma_{resid} = 0.3417$ for the white noise. Despite the assumption that the drift is temperature

dependent the major part of the heading fluctuation is due to white noise. Figure 4.24 shows a residual with a spike at lag 7 on the PACF plot. Even if the whiteness is attained for the parameters $(4,0,2)$, a moving average of order 7 has been omitted and should be considered as shown in Figure 4.23 (b).

4.2.2.3.2 Regular Differenced Signal Parameter Estimation

The residual of the parameter estimation are shown in Figure 4.25. We obtain the same pattern as in Figure 4.15 and 4.20 for the differenced signals. The whiteness of the residuals ($WT > 1$) is obtained with the minimum orders $(2,1,2)$. The plots on top of Figure 4.25 show that the AIC criterion doesn't drastically improve beyond order $(2,1,2)$ like for the whiteness criterion.

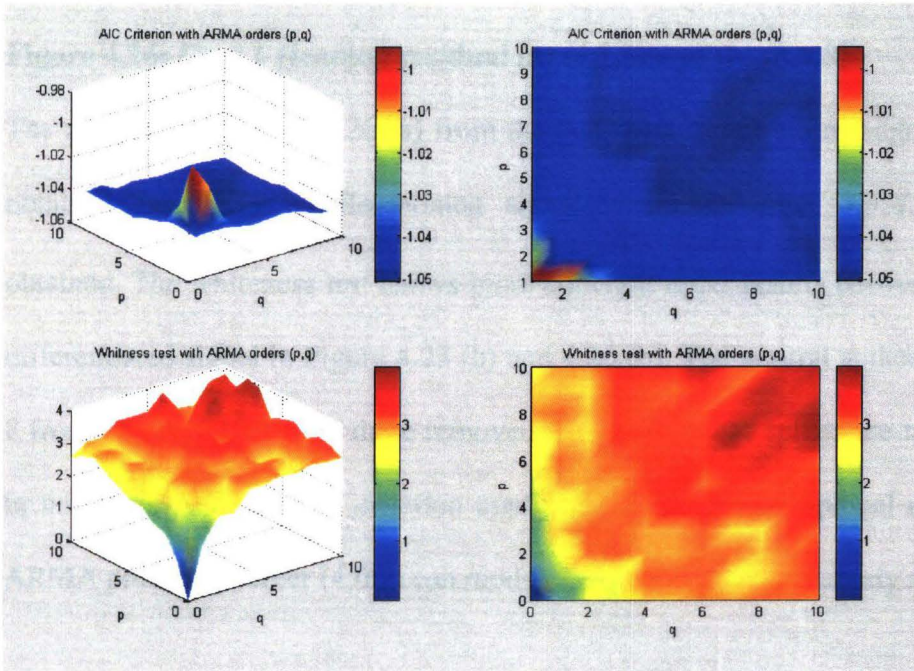


Figure 4.25: Differenced Case 1 heading residual AIC (above) and WT (below)

The best AIC criterion and whiteness test are respectively obtained for the orders:

$$\begin{bmatrix} p = 4 \\ q = 6 \\ d = 1 \end{bmatrix} \Rightarrow AIC : -1.509 \quad \begin{bmatrix} p = 8 \\ q = 8 \\ d = 1 \end{bmatrix} \Rightarrow WT : 3.9758$$

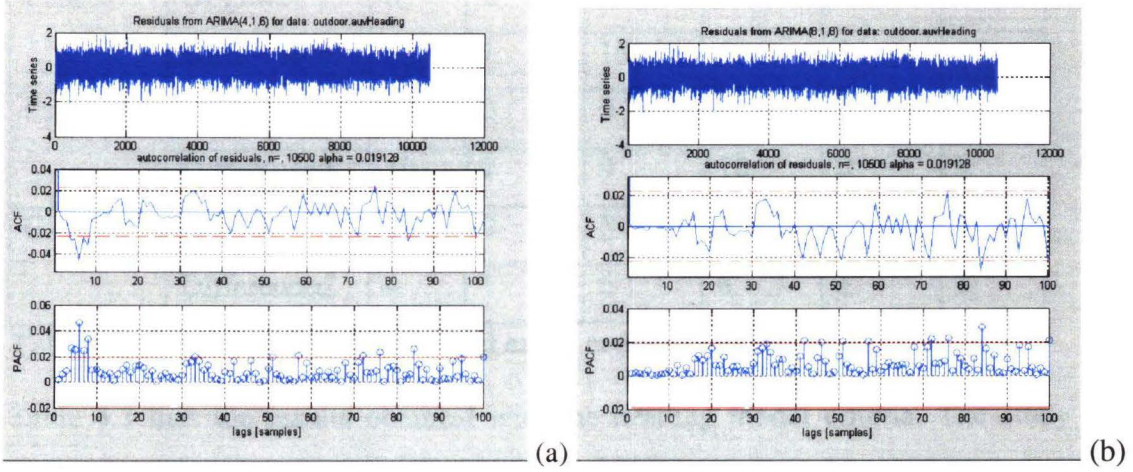


Figure 4.26: Case 1 Heading residual (a) (4,1,6) and (b) (8,1,8)

The residuals in Figure 4.26 (a) from the AIC best orders do not agree with the results obtained for the non-differentiated signal where an order $(p,d,q) = (10,0,5)$ was obtained. The whiteness test shows more coherent order results between the original and differentiated signal in Figure 4.23 (b) and 4.26 (b). The several spikes between lags 4 to 8 from Figure 4.19 (a) are there removed. However, these spikes are not very significant in this case. And the AIC criterion confirms the previous graphical assumption that an ARMA process of order (4,0,2) can model the outdoor heading steady state signal.

4.2.3 Conclusion

Heading		Order					
		AIC criterion			Whiteness test		
		P	D	Q	P	D	Q
Case 2	Original	6	0	10	10	0	8
	Differenced	6	1	10	6	1	10
Case 4	Original	10	0	9	10	0	10
	Differenced	10	1	9	10	0	9
Case 1	Original	10	0	5	8	0	7
	Differenced	4	1	6	8	1	8

Table 4.3: Results of heading model error order selection

Table 4.3 lists the results obtained with the heading model criteria. The study of the heading error model has shown various results depending on the experiments. A fixed number of models have not been set to be optimum. The order parameterization has been evaluated until order 10 as it was found that the correlation was more significant for the shorter lags. It also removes most of the periodic terms of the signal. As a result, an order estimate encompassing 10 AR and/or MA components was able to guarantee whiteness of the residual. It has been shown from graphical analysis of the whiteness test that acceptable error modeling was performed with an ARMA process of minimal order 4. The parameters results obtained are given in Appendix A.

The variability of the parameters values with the experiments suggests that online parameter estimation with the vehicle steady state is preferable using a maximum of order 10.

Heading	Case 2	Case 4	Case 3
Signal std [°]:	0.5712	0.1604	0.6338
Residual std [°]:	0.4358	0.0588	0.5846

Table 4.4: Standard deviation of the heading signal

We remark from table 4.4 that the white noise fluctuations still represent a large amount of the heading noise error on the Morpheus AUV 1. On the Morpheus AUV 2, the fluctuation magnitudes are much smaller and enable the characterization of 2/3 of the variations.

4.3 GPS SENSOR NOISE CHARACTERISTICS

As we have seen in section 2.1.1.2, the major part of error in GPS measurements can be assigned to: satellite clock errors, ephemeris error, receiver errors and atmospheric or ionospheric delay. However, in spite of these noise characteristics that can be partially corrected with the HDOP and consequently the number of satellites, the position data are still accompanied with a low-frequency noise that is investigated in this section.

4.3.1 Steady state measurement

A set of GPS measurements were collected on the AUV 1 in an outdoor field, see Table 4.1. In this field, the AUV was partially surrounded by the buildings of Seatech University. Despite that the GPS signals emitted by the satellites can be affected by the high buildings, tunnels or bridges, the Horizontal Dilution of Precision, Figure 4.28, shows a satisfactory reception. We will describe a noise model of GPS from these static data tests and its statistics properties.

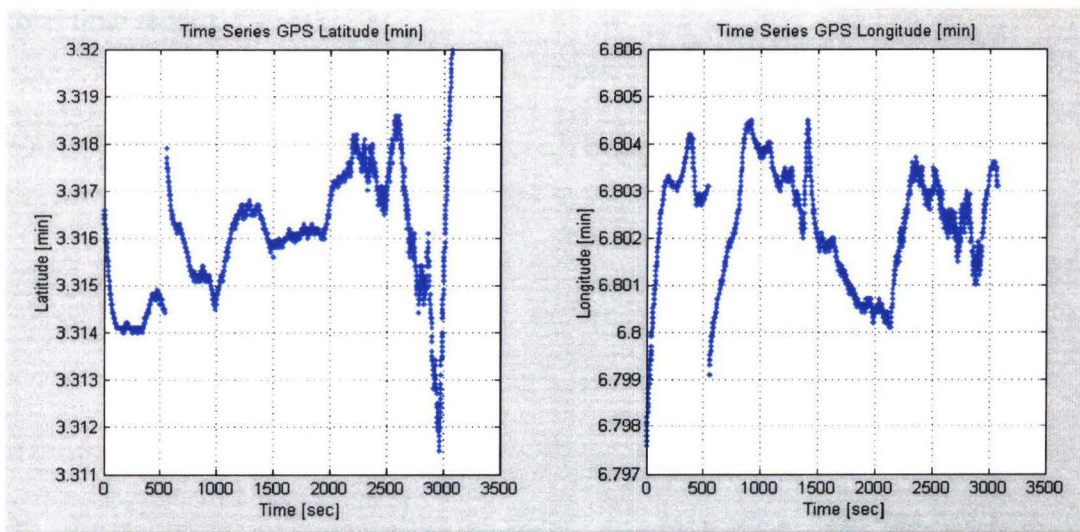


Figure 4.27: GPS latitude (left) and Longitude (right) [min]

Figure 4.27 shows the latitude and longitude position recorded on the steady state AUV while being stationary in an outdoor field at Seatech campus. The very high resolution of the GPS data should enable a precise positioning ($10^{-4}[\text{min}] \leftrightarrow 3.10^{-3}[\text{meter}]$). However, the observed fluctuations and data inaccuracies are caused by ionospheric delay, satellite multipath, orbital error and satellite geometry. The Horizontal Dilution Of Precision HDOP fluctuations (Figure 4.28) measures how the available satellite geometry influences the latitude and longitude data accuracy:

$$HDOP = \sqrt{\frac{\sigma_x^2 + \sigma_y^2}{\sigma}} \quad (4.2)$$

Where σ_x is the latitude standard deviation, σ_y the longitude standard deviation and σ is the global position standard deviation. For a HDOP greater than 4, the data are usually disregarded. A statistical analysis would have been ideal on a set with the same HDOP values. But the results on the two large spans for $HDOP = 1.8$ and 1.3 have not shown satisfactory parameter estimation (see Figure 4.28). We then applied the analysis on the total time record.

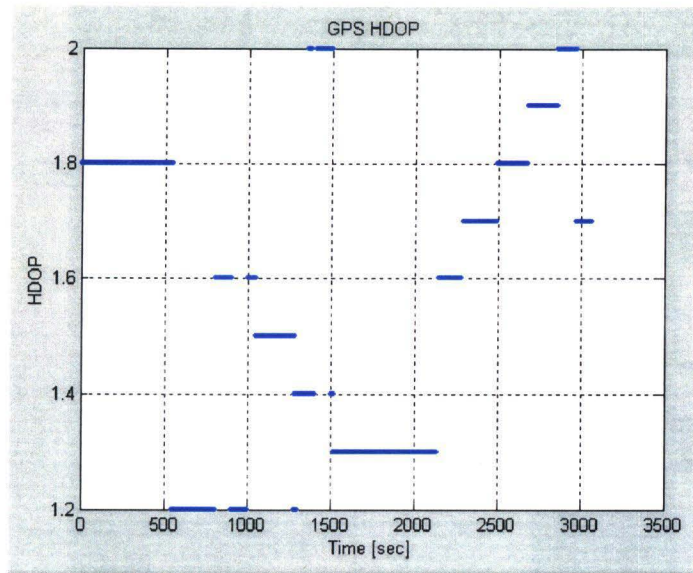


Figure 4.28: GPS HDOP

The ACF plots for latitude and longitude measurements on top of Figure 4.29 resembles an autoregressive model with a pass-band white noise ACF pattern [14], similar to that in Figure 4.19 (b). The PACF plots (middle of Figure 4.29) show a spike at lag 1 and indicate that a Gauss-Markov process of order 1 may describe the model, which will be discussed later.

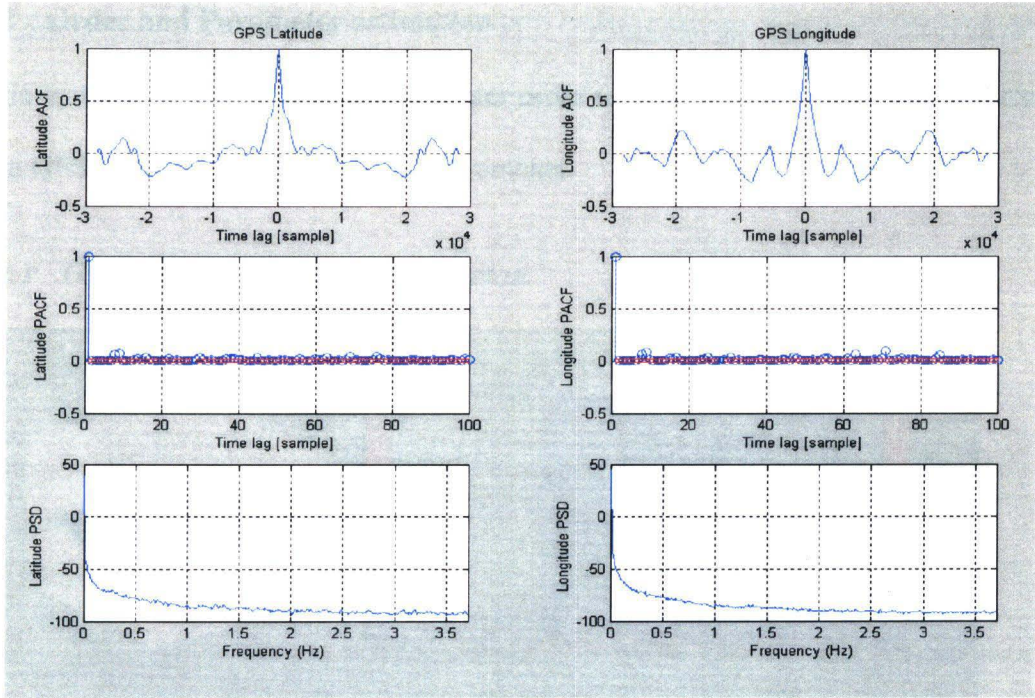


Figure 4.29: GPS Latitude (left) and Longitude (right) statistics

From the logarithmic PSD plots, below of Figure 4.29, we notice that the signal is carried by low-frequency energies and the remaining higher frequencies represent the background noise. This pattern usually corresponds to the frequency representation of a bias, a constant, or a long-term drift. The model of a wave signal as emitted for a GPS sensor error model [23] with a very long period ranging from 1200 to 2400 [seconds] appears suitable at first sight. But in our case, although the ACF plots exhibit some periodic oscillations, their amplitude tends to decay with the lags. The PACF plots, in Figure 4.29, give a more accurate answer regarding the sensor error model. The strong spike at lag 1 indicates the presence of an autoregressive term of order 1. Several other spikes of minor amplitude are observed at lags 8, 9 and at further lags 63, 71 and 85.

4.3.2 Order and Parameter estimation

In this section, we select the best parameter order to adequately represent the error model of the GPS latitude and longitude measurements.

4.3.2.1 GPS Latitude parameter estimation

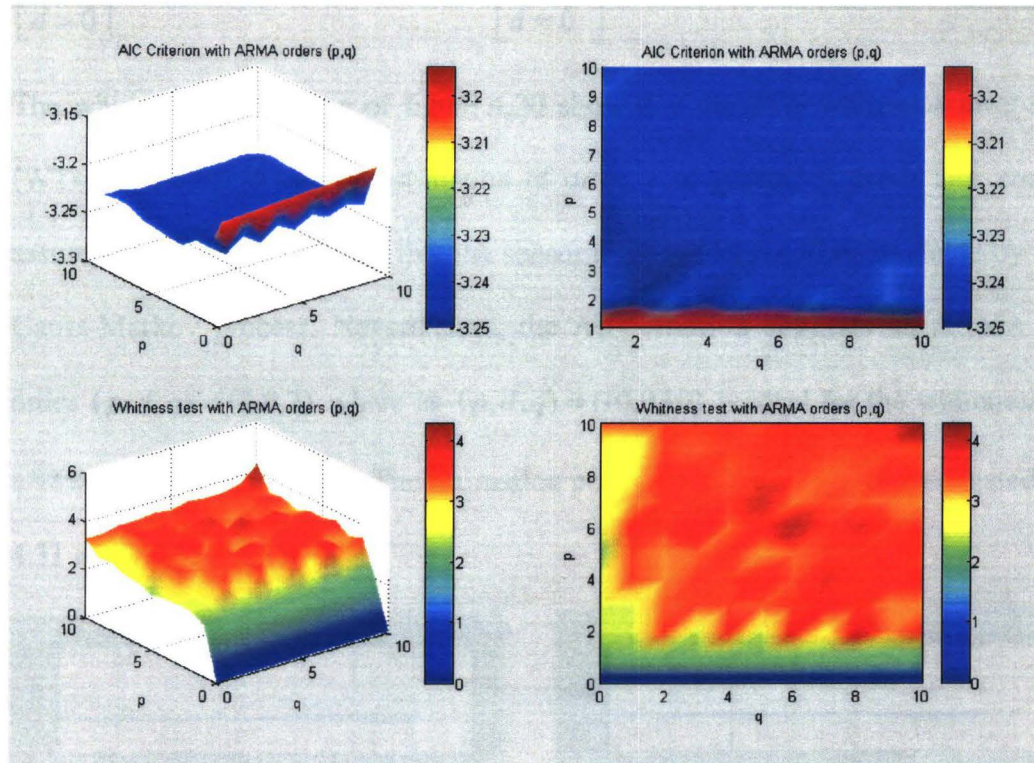


Figure 4.30: GPS Latitude residual AIC (above) and WT (below)

In Figure 4.30, the AIC criterion and Whiteness test are found to be respectively minimum and maximum for the following parameter orders (see Appendix A for the parameter estimation results):

$$\begin{bmatrix} p = 2 \\ q = 2 \\ d = 0 \end{bmatrix} \Rightarrow AIC : -3.2502 \qquad \begin{bmatrix} p = 10 \\ q = 10 \\ d = 0 \end{bmatrix} \Rightarrow WT : 4.2639$$

The whiteness test, below of figure 4.30 show that the 95% whiteness level is reached (WT=1) as soon as an AR estimation of order 1 or greater is used. This confirms the assumption made in 2.3.2.2.2 that the sensor error model could be modeled by a 1st order Gauss-Markov process. Nevertheless, the AIC criterion suggests an ARMA model of order $(p,d,q) = (2,0,2)$ where as $(p,d,q) = (10,0,10)$ is ideal for the whiteness test with a 98% confidence interval. The estimation performance results are investigated in Figure 4.31 and 4.32.

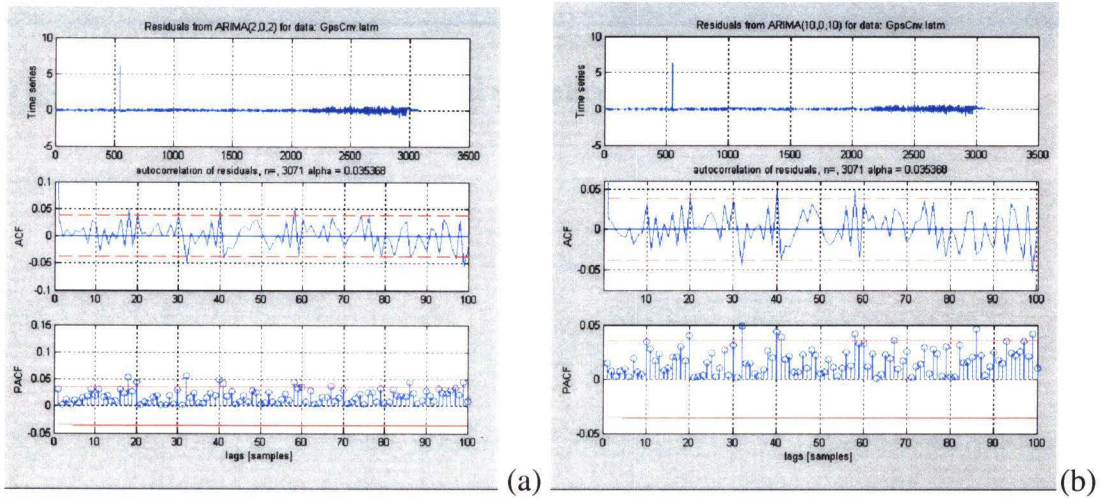


Figure 4.31: GPS Latitude residual statistics (a) (2,0,2) and (b) (10,0,10)

From the middle plots in figure 4.31, the ACF are shown for parameter order of (2,0,2) and (10,0,10). Figure 4.32 shows the residual time series, ACF and PACF plots of $(p,d,q) = (1,0,1)$ and $(p,d,q) = (2,0,0)$ signal estimations. A significant peak at lag 1 of 0.185 is observed on the PACF and ACF plots of Figure 4.32 (a). Contrary to our previous assumptions, the sensor error model is not sufficiently described with an order 1 AR model solely. This implies that the residual is still correlated.

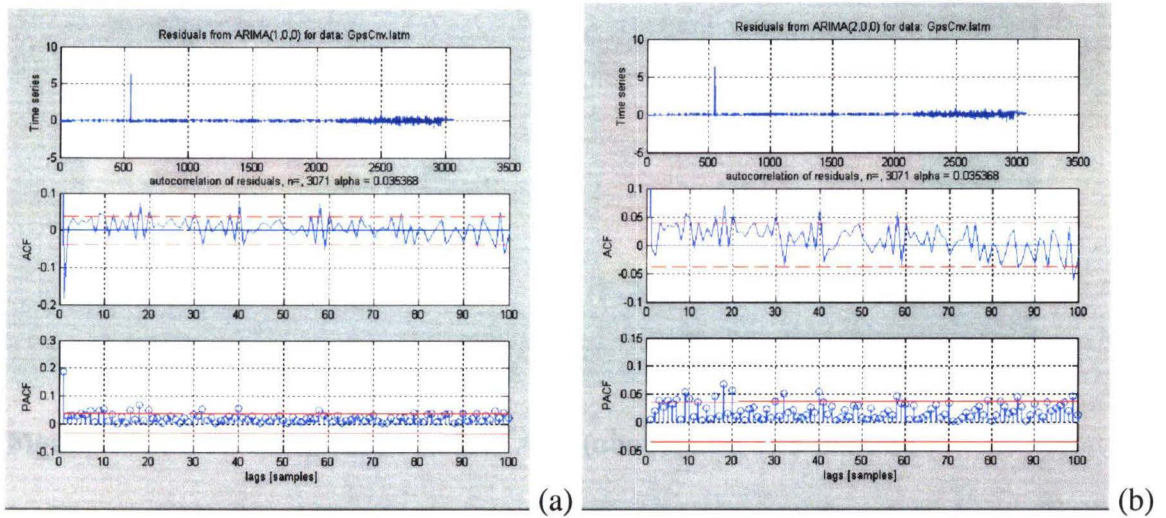


Figure 4.32: GPS Latitude residual statistics (a) (1,0,1) and (b) (2,0,0)

4.3.2.2 GPS Longitude parameter estimation

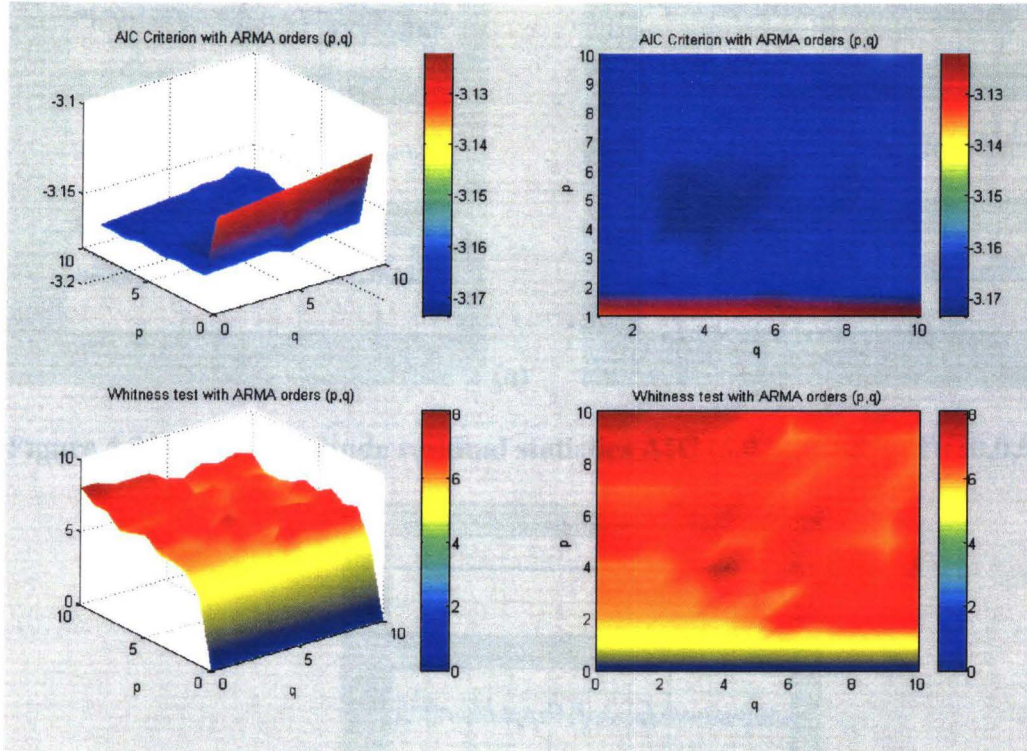


Figure 4.33: GPS Longitude residual AIC (above) and WT (below)

In Figure 4.33, the AIC criterion and Whiteness test are found to be respectively minimum and maximum for the following parameter orders (see Appendix A for the parameter estimation results):

$$\begin{bmatrix} p = 5 \\ q = 5 \\ d = 0 \end{bmatrix} \Rightarrow AIC : -3.1736 \qquad \begin{bmatrix} p = 10 \\ q = 0 \\ d = 0 \end{bmatrix} \Rightarrow WT : 8.0789$$

As previously, the whiteness is reached for AR orders ≥ 1 . The Whiteness test contrary to the AIC criterion, suggests the use of AR parameters only for the model estimation. In both cases, the whiteness performances are very high. It appears sufficient to use an AR model of order 2. In this case, the whiteness confidence is almost 99% (WT~5), see Figure 4.35.

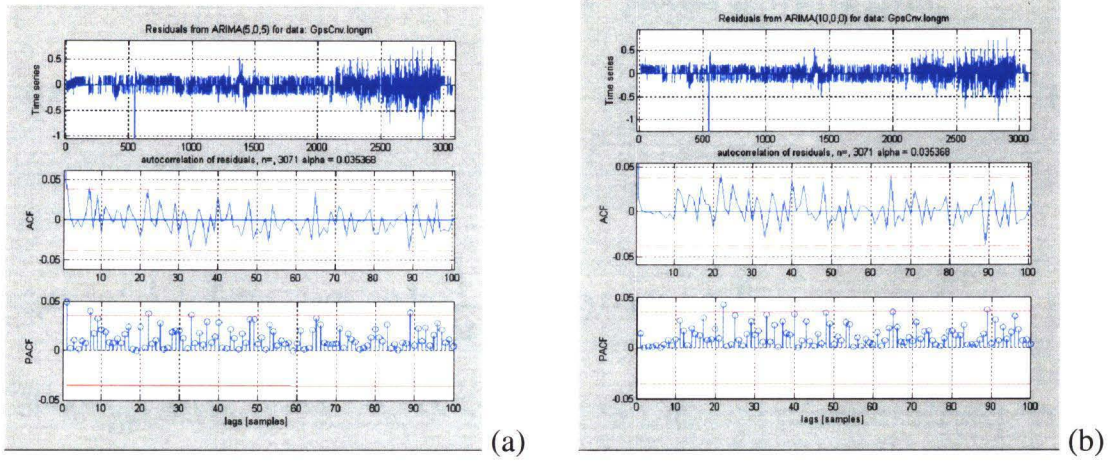


Figure 4.34: GPS Longitude residual statistics AIC (5,0,5) (a) & WT (10,0,0) (b)

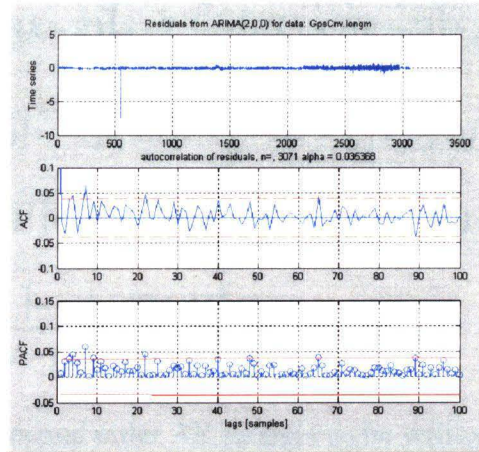


Figure 4.35: GPS Longitude residual statistics (2,0,0)

4.3.3 Conclusion

Table 4.5 summarizes the parameter estimation results obtained with the AIC criterion and Whiteness test respectively. An autoregressive process of order 2 appears to be an adequate model for the GPS position error model. Then the GPS sensor error can be modeled in continuous time domain as a 2nd order Gauss Markov process. Deriving equation 2.41 for $n = 2$, we obtain:

$$\ddot{x}(t) = -2\beta_2(t)\dot{x}(t) + \beta_2^2(t)x(t) + w(t) \quad (4.3)$$

The discrete time formulation of the 1st and 2nd process derivative gives:

$$\dot{x}(k) = \frac{1}{\Delta t} \cdot [x(k) - x(k-1)] \quad (4.4)$$

$$\begin{aligned} \ddot{x}(k) &= \frac{1}{\Delta t} \cdot [\dot{x}(k) - \dot{x}(k-1)] \\ \ddot{x}(k) &= \frac{1}{\Delta t} \cdot \left[\frac{1}{\Delta t} \cdot [x(k) - x(k-1)] - \frac{1}{\Delta t} \cdot [x(k-1) - x(k-2)] \right] \\ \ddot{x}(k) &= \frac{1}{\Delta t^2} \cdot [x(k) - 2 \cdot x(k-1) + x(k-2)] \end{aligned} \quad (4.5)$$

Replacing the terms on both side of Equation (4.3), we have:

$$\frac{1}{\Delta t^2} \cdot [x(k) - 2 \cdot x(k-1) + x(k-2)] = -2 \cdot \frac{\beta_2}{\Delta t} \cdot [x(k) - x(k-1)] + \beta_2^2 \cdot x(k) + w_k \quad (4.6)$$

$$[x(k) - 2 \cdot x(k-1) + x(k-2)] = -2 \beta_2 \cdot \Delta t \cdot [x(k) - x(k-1)] + \beta_2^2 \cdot \Delta t^2 \cdot x(k) + \Delta t^2 \cdot w_k \quad (4.7)$$

$$x(k) \cdot [1 + 2 \cdot \beta_2 \cdot \Delta t - (\Delta t \cdot \beta_2)^2] = x(k-1) \cdot [2 + 2 \Delta t \cdot \beta_2] - x(k-2) + \Delta t^2 \cdot w_k \quad (4.8)$$

$$x(k) = \frac{x(k-1) \cdot [2 + 2 \Delta t \cdot \beta_2] - x(k-2) + \Delta t^2 \cdot w_k}{[1 + 2 \cdot \beta_2 \cdot \Delta t - (\Delta t \cdot \beta_2)^2]} \quad (4.9)$$

From Equation (2.44), a second order AR model can be written as:

$$x_k = a_1 \cdot x_{k-1} + a_2 \cdot x_{k-2} + w_k \quad (4.10)$$

The constant time is computed by $\tau = \frac{2.146}{\beta_2}$ for the order 2 [4], Δt is the time step

interval and the AR parameters should verify the following equalities:

$$\begin{aligned} a_1 &= \frac{2 + 2 \Delta t \cdot \beta_2}{1 + 2 \Delta t \cdot \beta_2 - (\Delta t \cdot \beta_2)^2} \\ a_2 &= \frac{-1}{1 + 2 \Delta t \cdot \beta_2 - (\Delta t \cdot \beta_2)^2} \end{aligned} \quad (4.11)$$

GPS		Order					
		AIC criterion			Whiteness test		
		P	D	Q	P	D	Q
Latitude	Original	2	0	2	10	0	10
Longitude	Original	5	0	5	10	0	0

Table 4.5: Results of GPS model error order selection

Table 4.6 compares the standard deviation between the GPS measurements and the residual prediction errors. As we can see, a tenth of the deviation is recognized as white noise. This indicates that a major part of the oscillation is efficiently characterized by an ARMA process.

GPS measurements:	Latitude	Longitude
Signal std [min]:	2.3720	2.2708
Residual std [min]:	0.1965	0.2036

Table 4.6: Standard deviation of the GPS signals

4.4 IMU SENSOR NOISE CHARACTERISTICS

The Crossbow IMU quantities were collected solely on Morpheus AUV 2 as the other AUV did not encompass any Inertial Measurement Unit at this time. Two sets of IMU data (acceleration and angular rates) were available for analysis. They were collected from AUV 2 respectively in the pool and in laboratory. The analysis was performed only on the latter set of data as (section 4.4.1), the wave oscillation highly corrupts the steady state data analysis.

4.4.1 Accelerometer characteristics

An acceleration error model will be constructed based on the similar analysis as that from the compass data.

4.4.1.1 *Steady state measurement*

Table 4.7 shows the statistics of the residuals of acceleration (mean and variance). The high resolution enables the output of a very precise acceleration reading. The acceleration readings in X and Y seem to remain stationary on left of Figure 4.36, the Z axis however outputting the gravity term tends to drift over the time span. Last rows of Table 4.7 show that the whiteness tests of first differenced signals are assumed white noise. It favors the minimum use of a 1-order AR model (see section 2.3.6).

Accelerometer		X acceleration	Y acceleration	Z acceleration
Sampling rate [sec]:		0.11	0.11	0.11
Resolution [g']:		10^{-6}	10^{-6}	10^{-6}
Mean [g']:		0.007038	0.055706	0.957941
Variance [g'] ² :		0.009236	0.021534	0.014305
Standard deviation [g']:		0.096092	0.146746	0.119603
Whiteness	Signal	0.0514	0.0508	0.0508
	1 st Difference	1.3359	1.5390	1.4788

Table 4.7: Acceleration whiteness test

By observing the logarithmic PSD plots of acceleration along the three axes, right in Figure 4.36, we assume that the signal high frequency oscillations are due to white noise shown by the energy level present along the whole frequency span. The sample ACF plots, left in Figure 4.37, show that the noise is close to white but the decaying trends observed resembles to the AR model pattern. The z-axis acceleration ACF plot decay is more accentuated and becomes negative around the lags 5000 of the 14400 total samples. The signal autocorrelation was computed for the signal minus its mean (see section 2.2.1). Consequently, for time-drifting data the product of opposite sign values will result in a negative autocorrelation function for higher lags.

The sensor error residuals show few autoregressive terms (spikes) in the PACF plots, right of Figure 4.37.

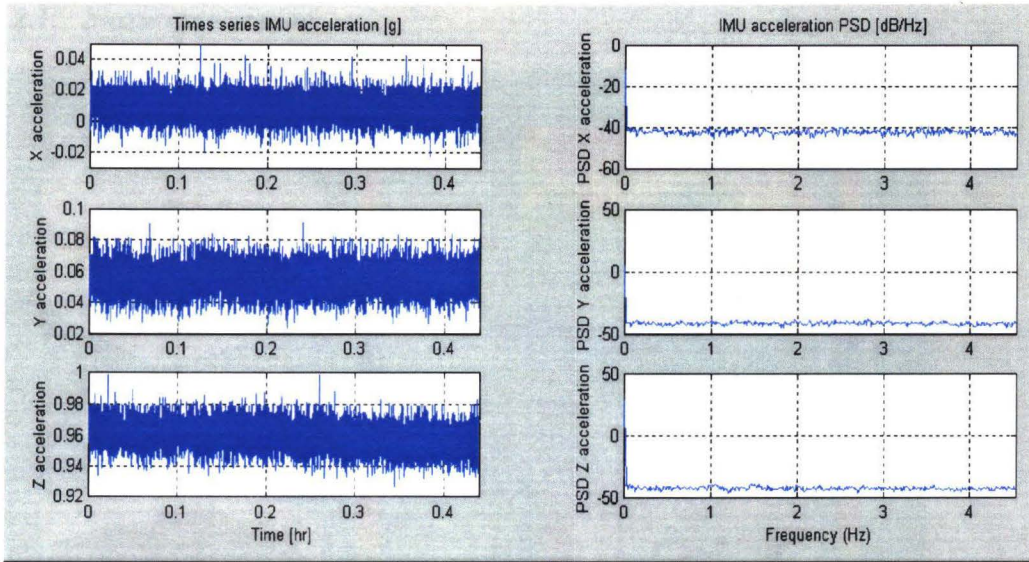


Figure 4.36: X, Y, Z Acceleration signals time series (left) and PSD (right)

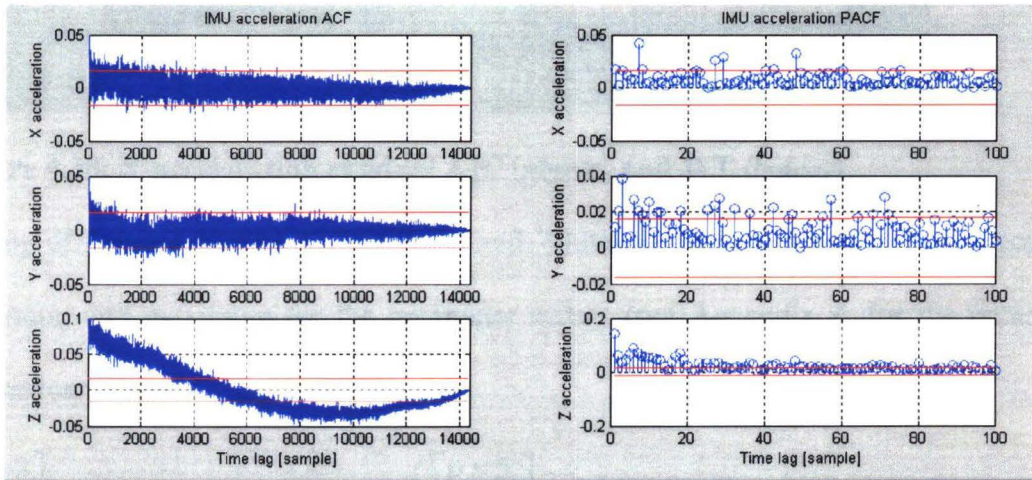


Figure 4.37: X, Y, Z Acceleration signals ACF (left) and PACF (right)

4.4.1.2 Order and parameter estimation

In this section, we select the best parameter order to adequately represent the error model of the acceleration measurements.

4.4.1.2.1 X-axis acceleration

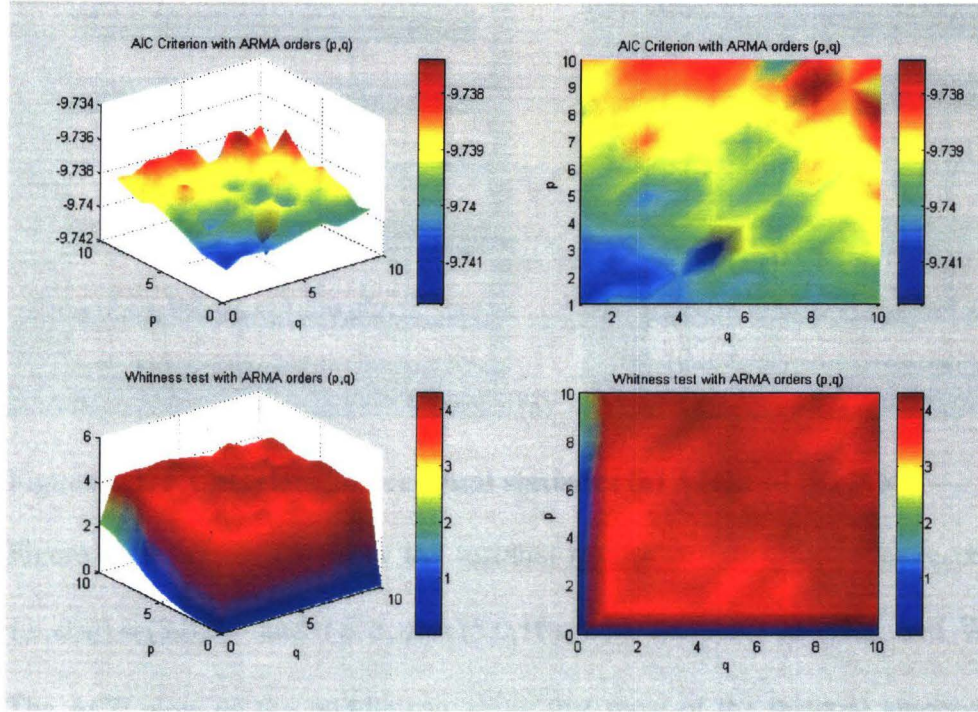


Figure 4.38: X-acceleration residual AIC (above) and WT (below)

On top of figure 4.38, the AIC criterion and Whiteness test are found to be respectively minimum and maximum for the parameter orders (see Appendix A for the parameter estimation results):

$$\begin{bmatrix} p = 3 \\ q = 5 \\ d = 0 \end{bmatrix} \Rightarrow AIC : -9.7482$$

$$\begin{bmatrix} p = 5 \\ q = 10 \\ d = 0 \end{bmatrix} \Rightarrow WT : 4.2780$$

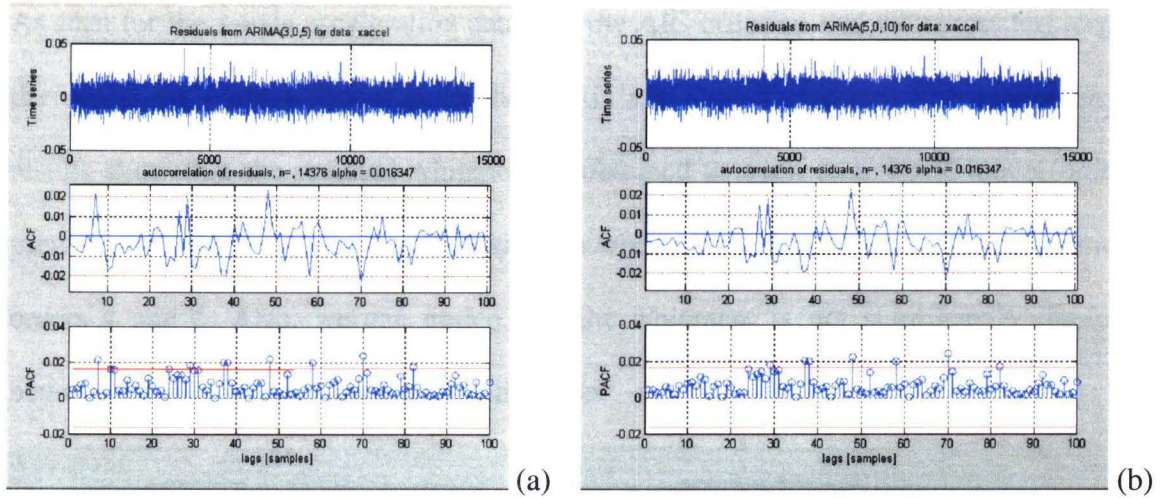


Figure 4.39: X acceleration residual statistics (a) AIC and (b) WT

Figure 4.39 (a) and (b) show the residual results statistics for order respectively found $(p,d,q) = (3,0,5)$ and $(p,d,q) = (5,0,10)$ with the AIC criterion and Whiteness test. The ACF plots on the middle row show that most of the residual autocorrelation terms stay within the confidence interval. Some few spikes within this region are retrieved on the PACF plots last row in Figure 4.39. When using the optimum order from the AIC criterion, we have omitted a minor autoregressive term at lag 7 and a $(p,d,q) = (5,0,10)$ order estimation obtained with the whiteness test shows a residual significantly uncorrelated for the first 24 lags.

4.4.1.2.2 Y-axis acceleration

From Figure 4.40, the AIC criterion and Whiteness test are found to be respectively minimum and maximum for the parameter orders (see Appendix A for the parameter estimation results):

$$\begin{bmatrix} p = 3 \\ q = 3 \\ d = 0 \end{bmatrix} \Rightarrow AIC : -9.3977$$

$$\begin{bmatrix} p = 10 \\ q = 4 \\ d = 0 \end{bmatrix} \Rightarrow WT : 4.3823$$

As seen for the x-axis acceleration analysis, the AIC criterion and whiteness test suggest the use of an ARMA model to fit the y-axis acceleration process. The whiteness test results show that the residual whiteness is obtained as soon as a 4 AR model order is used. This is confirmed by the AIC criterion where the best orders are obtained between orders 4 and 6. Also, we can notice that the whiteness is not significantly improved beyond a $(p,d,q)=(2,0,2)$ parameter estimation.

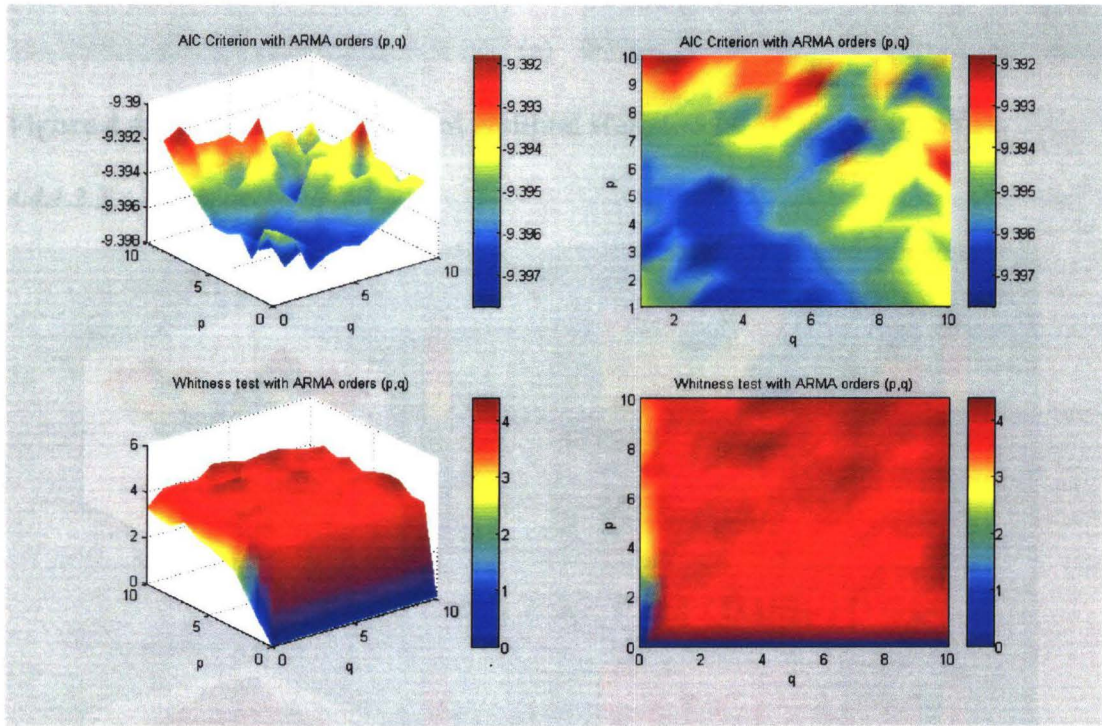
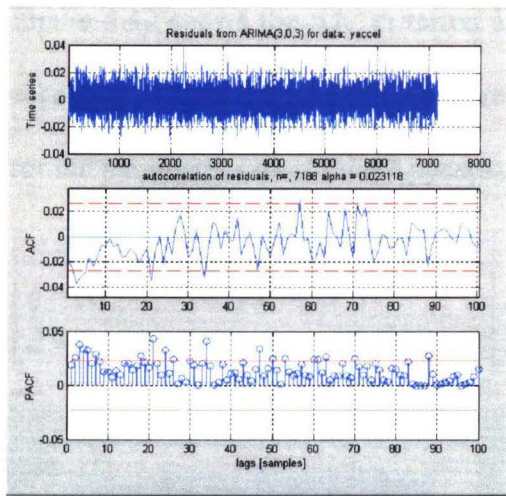
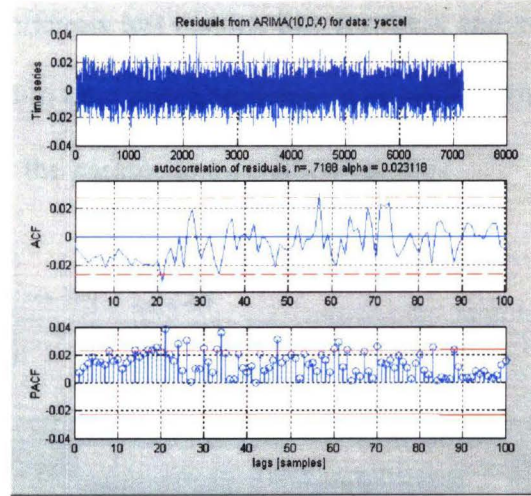


Figure 4.40: Y-acceleration residual AIC (above) and WT (below)

Left of Figure 4.41 shows the estimation result with $(p,d,q)=(3,0,3)$ ARMA parameters. The ACF plot is almost completely contained under the confidence limits apart some peaks starting at lag 3, same is observed on the PACF plot below. The parameterization until order $(p,d,q)=(10,0,4)$ seems preferable for an almost perfect modeling.



(a)



(b)

Figure 4.41: Y acceleration signal residual statistics (a) AIC and (b) WT

4.4.1.2.3 Z-axis acceleration

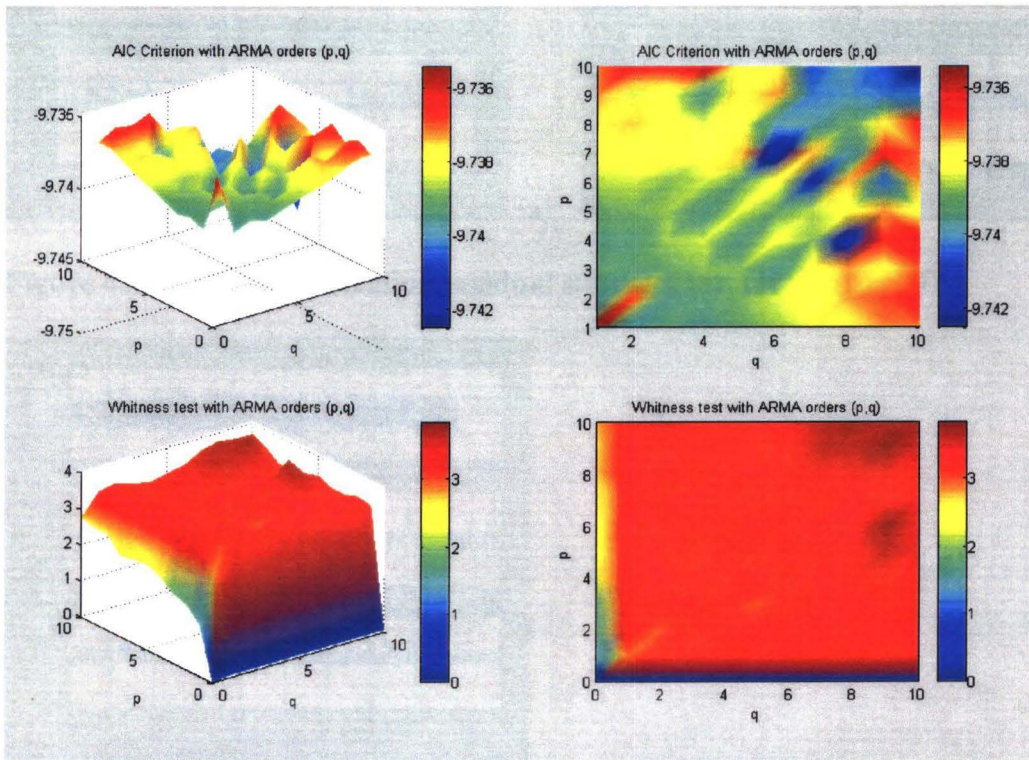


Figure 4.42: Z-acceleration residual AIC (above) and WT (below)

Figure 4.42 shows the AIC criterion and Whiteness test results, like for the x and y-axis acceleration data. These indicators are found to be respectively minimum and maximum for the parameter orders (see Appendix A for the parameter estimation results):

$$\begin{bmatrix} p = 10 \\ q = 10 \\ d = 0 \end{bmatrix} \Rightarrow AIC : -9.7425 \quad \begin{bmatrix} p = 6 \\ q = 9 \\ d = 0 \end{bmatrix} \Rightarrow WT : 3.8228$$

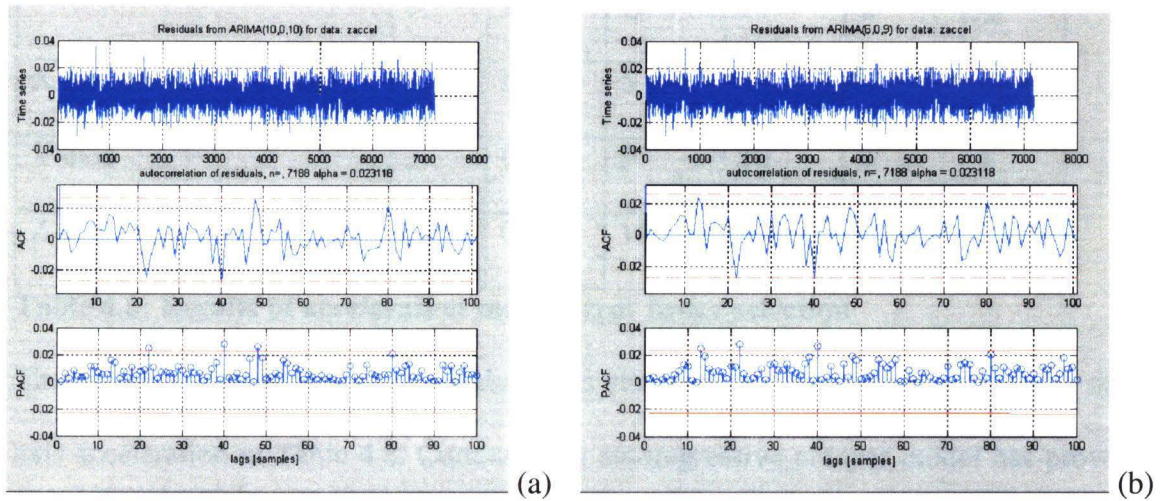


Figure 4.43: Z-axis acceleration residual statistics (a) AIC & (b) WT

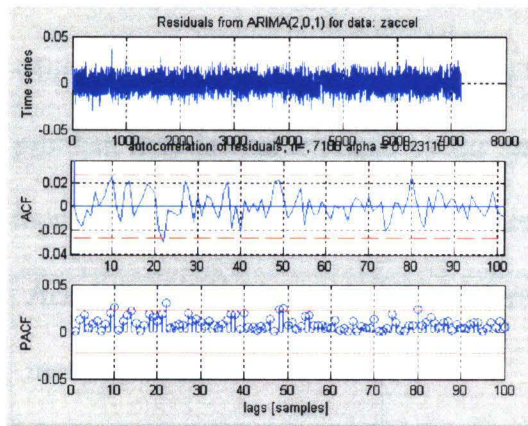


Figure 4.44: Z-axis acceleration residual statistics (2,0,1)

Figure 4.43 show the best results obtained from the two criteria. Figure 4.44 shows the results for an ARMA model estimation with orders $(p,d,q)=(2,0,1)$. The results do not

show any spike over the confidence level for the smaller lags. A MA order 1 is still needed in this case to take in account the drift revealed in Figure 4.36 (left below row).

4.4.1.3 Conclusion

Acceleration		Order					
		AIC criterion			Whiteness test		
		P	D	Q	P	D	Q
X-axis		3	0	5	5	0	10
Y-axis		3	0	3	10	0	4
Z-axis		10	0	10	6	0	9

Table 4.8: Results of acceleration model error order selection

The accelerometer sensor model analysis has yielded to various results for the x, y and z-axis acceleration in Table 4.8. Currently, an autoregressive process model has proven to characterize the errors correctly. A moving average parameter seems required for the drift models and unexpectedly, even for the apparently stationary process. In the last case, the white noise fluctuation amplitude may be too large compared to the signals'. Indeed the problem here is characterized by the standard deviations listed in table 4.9 showing that most of the signal fluctuation is attributed to the white noise.

Accelerometer measurements:	X acceleration	Y acceleration	Z acceleration
Signal std [g']:	0.007633	0.008712	0.008153
Residual std [g']:	0.007640	0.008912	0.007670

Table 4.9: Standard deviation of the accelerometer signals

4.4.2 Gyroscope characteristics

Table 4.10 shows the statistics of the static residuals of the angular rate measurements (mean and variance). Like the accelerometer, the high resolution enables the output of a very precise observation reading. The whiteness test in table 4.14 suggests that the yaw rate can be modeled with 1-order ARMA parameter (of value around 1) since the whiteness is verified for the differenced signal (see section 2.3.6). The roll and pitch rate on the other hand have a differenced signal still correlated and suggest $p > 1$.

Gyroscope		Yaw rate	Roll rate	Pitch rate
Measurements:				
Resolution [°/sec]:		10^{-6}	10^{-6}	10^{-6}
Mean [°/sec]:		0.411180	0.0149180	0.001239
Variance [°/sec] ² :		2.188923	3.870713	2.421427
Standard deviation [°/sec]:		1.479501	1.967413	1.556094
Whiteness test:	Signal	0.0537	0.0583	0.0580
	1 st Difference	1.6792	0.3912	0.4936
	signal			

Table 4.10: Angular rates characteristics

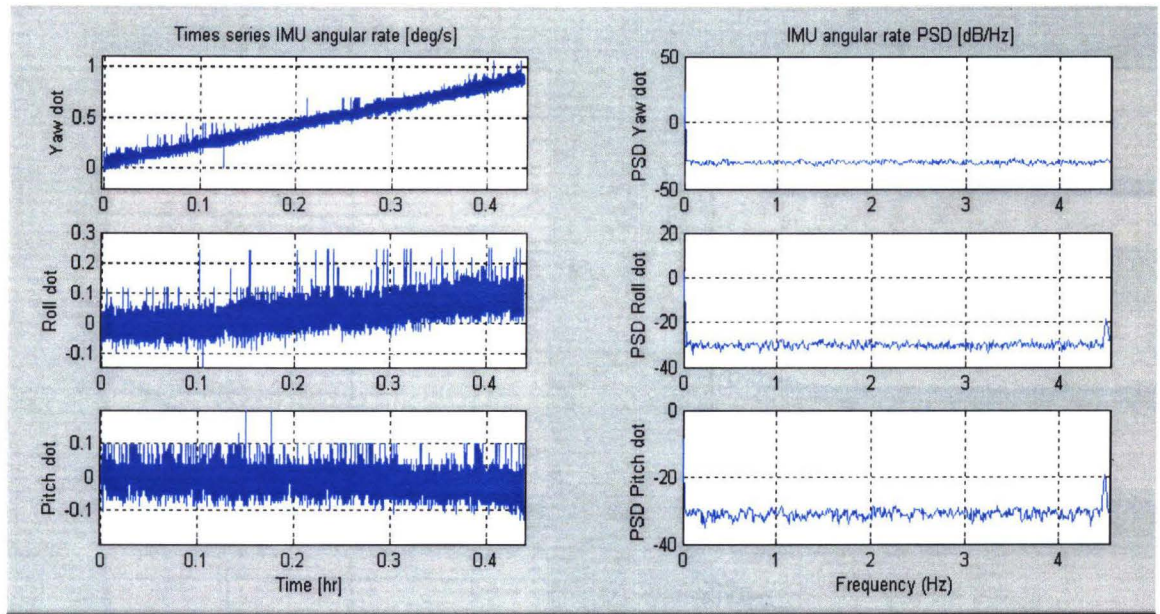


Figure 4.45: Gyroscope signals (left) and PSD (right)

As stated previously, the angular rates recorded from the ring-laser gyroscope exhibit a long-term drift, left of Figure 4.45. In the yaw rate signal, this drift is greater than usual value expected. The yaw rate drift rescaled on 1 hr is about $2.5 [^{\circ}/\text{hr}]$. For the roll and pitch rate, these values are 10 times smaller. Right of Figure 4.45 shows the logarithmic PSD functions of yaw pitch and roll over time. The signal and drift are supposedly contained in the lower frequency of the spectrum.

Figure 4.46 shows the ACF plots of the angular rates. The PACF function, right of Figure 4.46 exhibits some decaying patterns for the 3 angular rates. The yaw rate PACF (top row Figure 4.46) displays an auto regression at every lag whereas the pitch rate PACF (middle row Figure 4.46) displays another one every other lag and for the roll rate (last row Figure 4.46), an auto regression for both lags 1 and 2. This implies the use of MA process of order 1 to parameterize the yaw rate, and of order 2 for the pitch and roll rate.

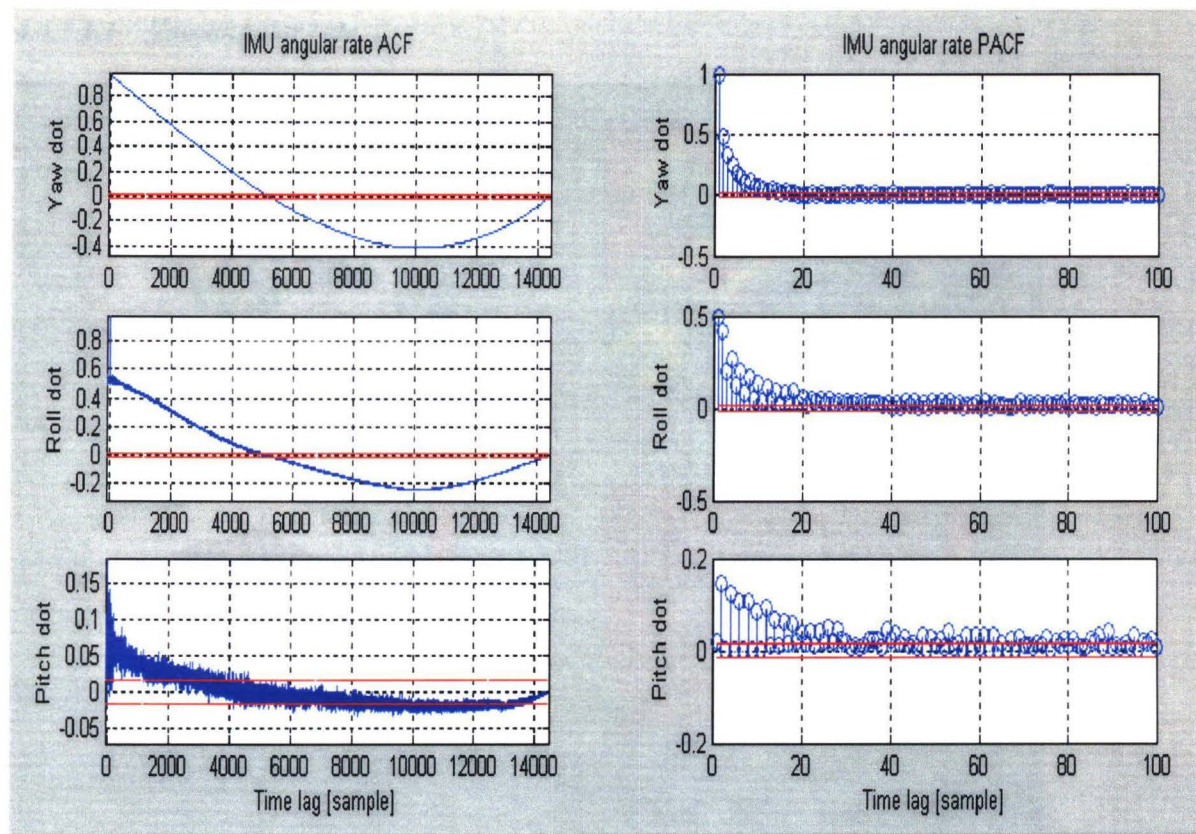


Figure 4.46: Gyroscope signals ACF (left) and PACF (right)

4.4.2.1.1 Yaw angular rate

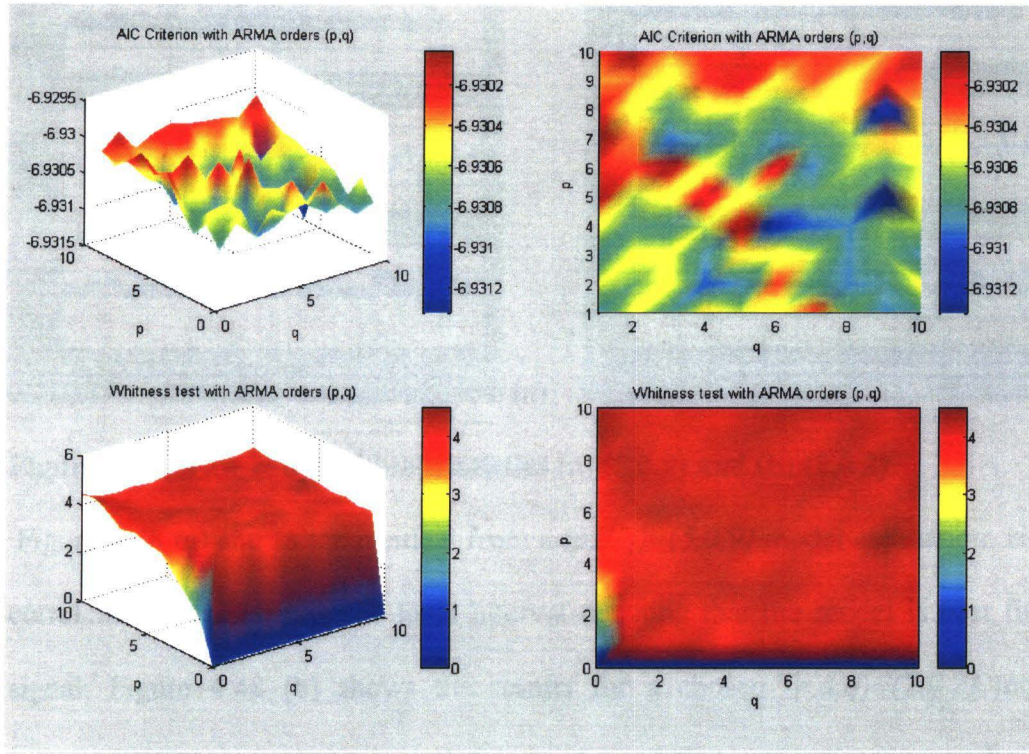
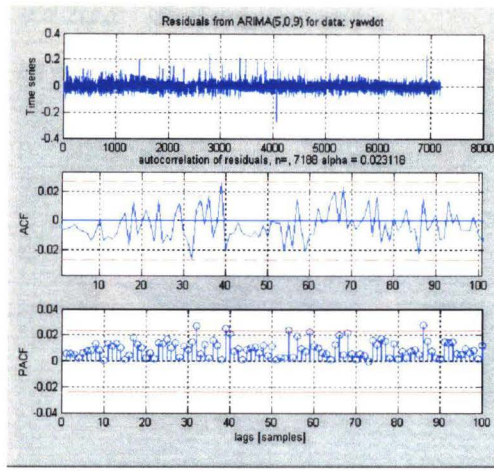


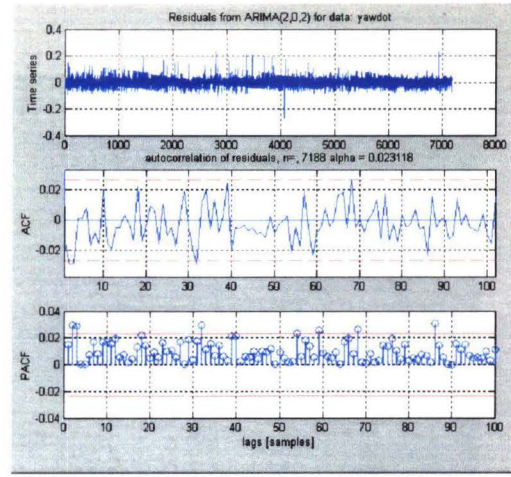
Figure 4.47: Yaw rate residual AIC (above) and WT (below)

On top of figure 4.47, the AIC criterion and Whiteness test are found to be respectively minimum and maximum for the same parameter orders (see Appendix A for the parameter estimation results):

$$\begin{bmatrix} p = 5 \\ q = 9 \\ d = 0 \end{bmatrix} \Rightarrow \begin{matrix} AIC : -6.9313 \\ WT : 4.4642 \end{matrix}$$



(a)



(b)

Figure 4.48: Yaw rate residual statistics (a) (5,0,9) and (b) (2,0,2)

Figure 4.48 (a) shows the residual from a $(p,d,q)=(5,0,9)$ model estimation. None of the correlation terms crosses the level interval meaning that the model is best fitted to the signal. Figure 4.48 (b) shows the results for a chosen $(p,d,q)=(2,0,2)$ model order estimation. Other tests not included here showed that any estimation under this order exhibits a significant correlation term at lag 2. It is necessary to model the signal with a second order at least in spite of the first analysis highlighting the only need of 1 MA parameter.

4.4.2.1.2 Roll angular rate

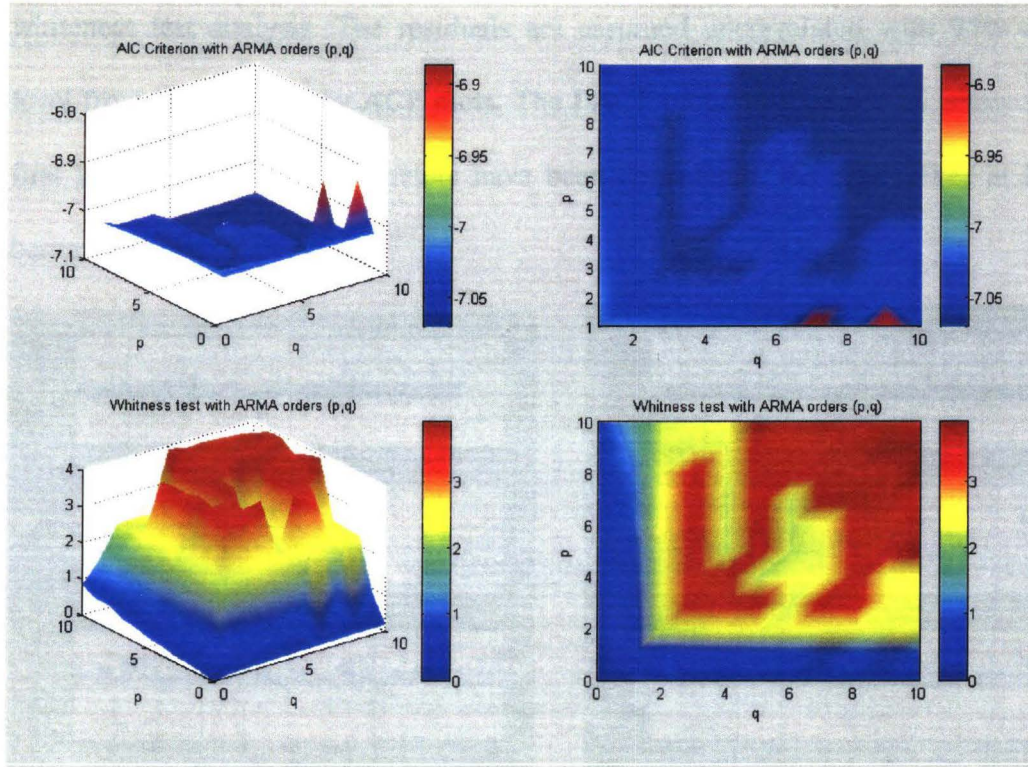


Figure 4.49: Roll angular rate AIC and WT

On top of figure 4.49, the AIC criterion and Whiteness test are found to be respectively minimum and maximum for the parameter orders (see Appendix A for the parameter estimation results):

$$\begin{bmatrix} p = 3 \\ q = 3 \\ d = 0 \end{bmatrix} \Rightarrow AIC : -7.0698$$

$$\begin{bmatrix} p = 8 \\ q = 10 \\ d = 0 \end{bmatrix} \Rightarrow WT : 3.9059$$

We can see that unlike the characteristics for the yaw rate measurements 4.4.2.1.1, the roll angular rate needs MA terms added to the AR to model adequately the correlation of the noise ($WT < 1$ for $p, q < 1$). The ACF plot of the original signal already highlighted the 2-order minimum MA model.

Figure 4.50 (a) and (b) show the residuals obtained from the best AIC criterion and whiteness test analysis. The residuals are assumed uncorrelated with 95% confidence level from the middle row ACF plots. The PACF plots, in Figure 4.50, show that all the first lags AR and MA parameters have been considered, the few spikes at larger lags being insignificant.

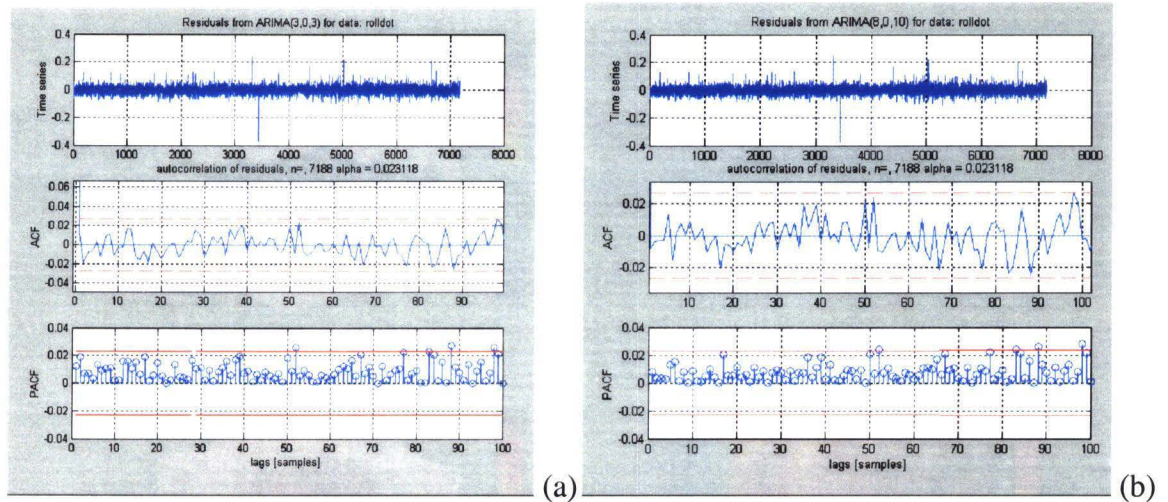


Figure 4.50: Roll rate residual statistics (3,0,3) and (8,0,10)

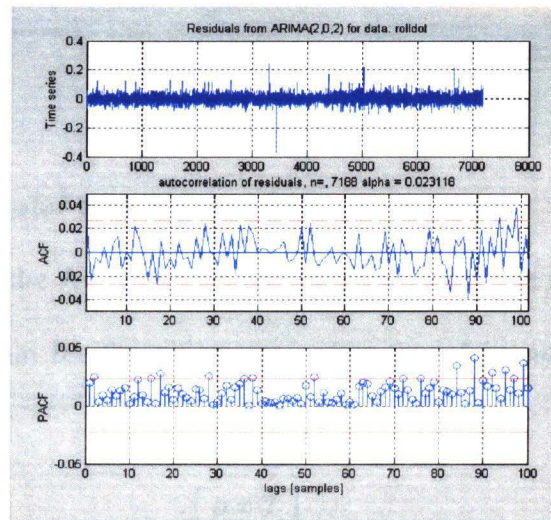


Figure 4.51: Roll rate residual statistics (2,0,2)

Figure 4.51 shows the analysis residual obtained with a second order ARMA model as presume in Figure 4.46 (b). Here, the whiteness performances, respectively on the ACF and PACF plots have shown satisfactory for the first lags until the series of spikes beyond lag 80.

4.4.2.1.3 Pitch angular rate

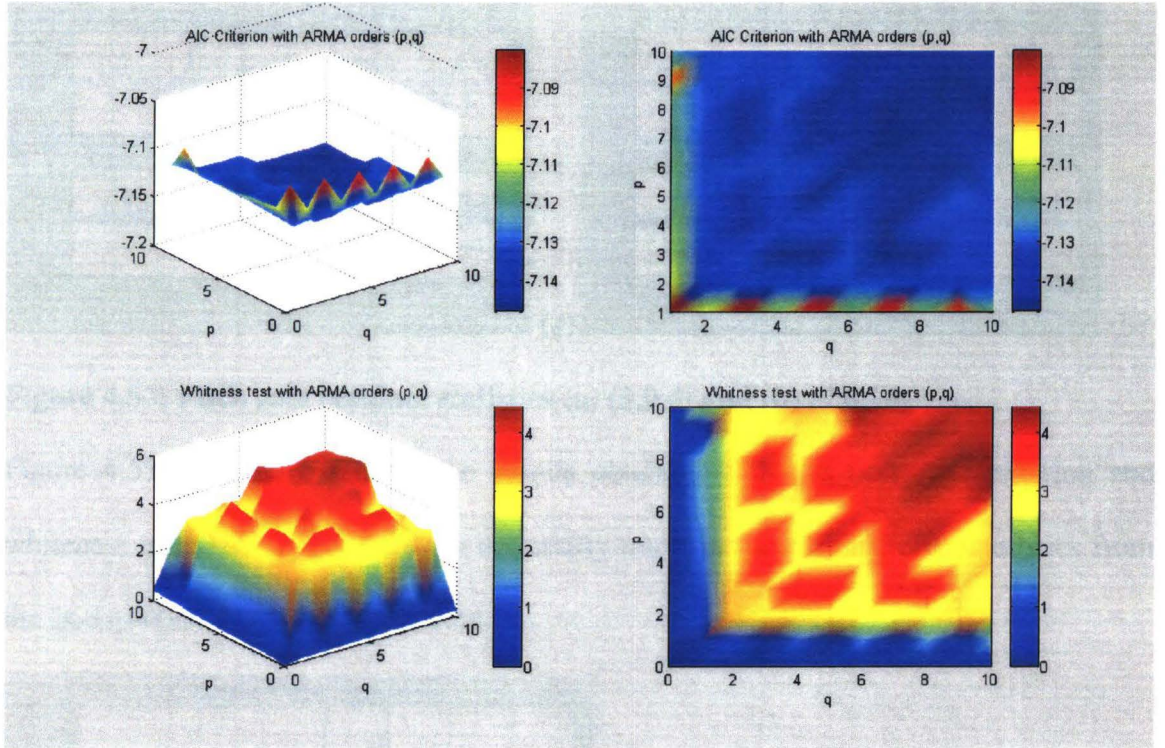


Figure 4.52: Pitch angular rate AIC and WT

On top of figure 4.52, the AIC criterion and Whiteness test are found to be respectively minimum and maximum for the parameter orders (see Appendix A for the parameter estimation results):

$$\begin{bmatrix} p = 3 \\ q = 4 \\ d = 0 \end{bmatrix} \Rightarrow AIC : -7.1457$$

$$\begin{bmatrix} p = 7 \\ q = 10 \\ d = 0 \end{bmatrix} \Rightarrow WT : 4.4364$$

The AIC criterion exhibits peaks along the q -axis for the odd MA parameters. The AR terms do not show any improvement when used solely. The combination of the AR and MA parameters seems necessary for all the angular rate measurements.

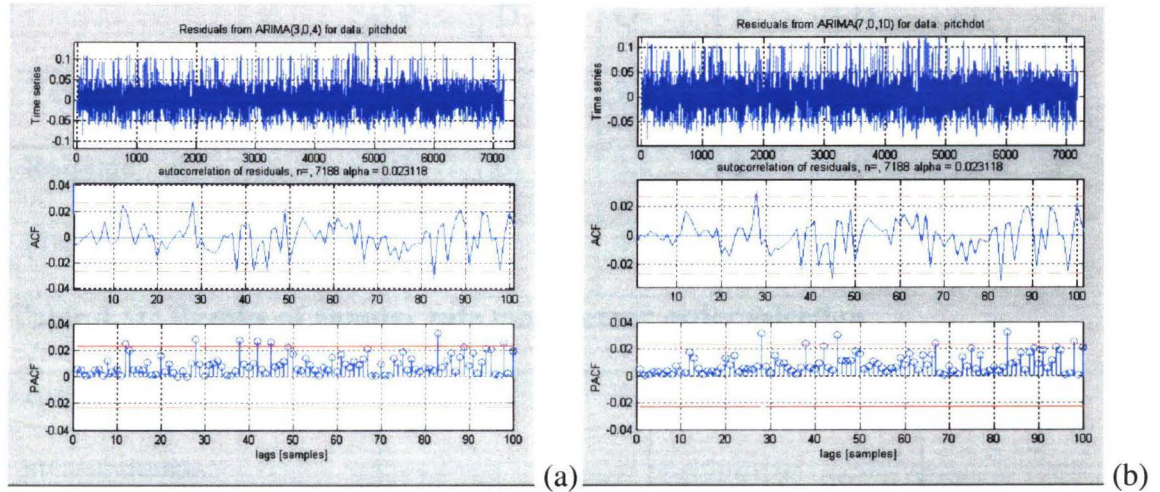


Figure 4.53: Pitch rate residual statistics (a) (3,0,4) and (b) (7,0,10)

Figure 4.53 (a) and (b) shows the results obtained with the best AIC criterion and whiteness test. The results does not drastically improve the residual characteristics from the $(p,d,q)=(2,0,2)$ model Figure 4.54.

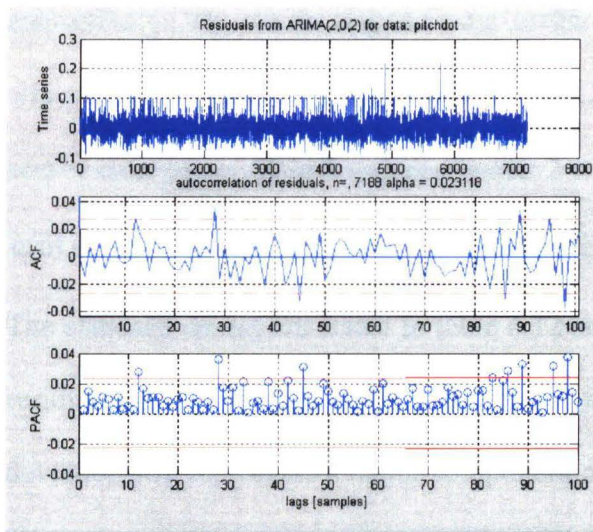


Figure 4.54: Pitch rate residual statistics (2,0,2)

4.4.2.2 Conclusion

Angular rates	Order					
	AIC criterion			Whiteness test		
	P	D	Q	P	D	Q
Yaw rate	5	0	9	5	0	9
Roll rate	3	0	3	8	0	10
Pitch rate	3	0	4	7	0	10

Table 4.11: Results of angular rate model error order selection

Angular rate measurements:	Yaw rate	Roll rate	Pitch rate
Signal std [°/sec]:	0.247457	0.046969	0.029928
Residual std [°/sec]:	0.031187	0.029114	0.028192

Table 4.12: Standard deviation of the angular rate signals

Table 4.11 resumes the best parameters found with AIC criterion and whiteness test respectively. The three angular rate errors despite these results, showed acceptable whiteness characteristics with a $(p,d,q)=(2,0,2)$. It seems suitable to model the gyroscope sensor error by an ARMA model of order 2 with:

$$u(n) + a_1 \cdot u(n-1) + a_2 \cdot u(n-2) = b_1 \cdot v(n-1) + b_2 \cdot v(n-2) + v(n) \quad (4.12)$$

The standard deviations listed in table 4.12 show that the model accounts for most of the residual error for the yaw rate where as for the roll and pitch rate, the residual standard deviation still represents a major component of the total signal fluctuation.

The results of the parameter estimation are given in Appendix A.

5 CONCLUSIONS

The goal of this research was to develop an error model for the navigation sensors used on the Morpheus AUV. Following the work done in [6] using an error state Kalman Filter; my contribution was focused on modeling the sensor errors.

The method applied was based on the Box-Jenkins building block processes. The use of graphical autocorrelation analysis has been a useful tool for model identification. Two criteria were used to select the model order, and were applied to the prediction error residual. The consistency of the model was checked with both the ACF and PACF functions.

The model orders and parameters estimates are included in Appendix A. Model orders have shown to be very different from one sensor to another. This confirms the assumption that a 1st order Gauss-Markov process is not adequate to characterize most of the sensors except for the acceleration quantities.

The DVL measurements collected in the pool did not enable the sensor error modeling. We assumed that a horizontal wave motion was imposed to the vehicle platform during the data collection. The pool measurements encompass a waveform signal and cannot be treated to model the DVL error. Another approach should be considered to overcome

these difficulties. For instance, we can tether the AUV to the 4 corners of an indoor pool. There, the water surface will be steady and the signal characteristics should be essentially white noise driven. However, if the signal component still remains significant, another approach is proposed. The method based on power spectrum subtraction described in [17] can be applied if the signal still encompasses a periodic wave oscillation. This method consists in subtracting from the signal its background noise through the power spectrum estimation. Following, an ARMA model can then be estimated.

The ARMA model estimated from the MATLAB ARMAX function did not characterize accurately the measurements from one data set to another. The model parameters obtained give the best fit from the Least-Square Estimation but do not guarantee that this is the true model. This suggests an online parameter estimation of the sensor errors. A model can also be developed to incorporate these error models into the process model used for the error-state Kalman Filter [6].

For further work on sensor modeling, it is suggested to investigate the sampling rate effect over the model orders. A simple case Equation 3.1 showed that the correlation time is directly related to the sampling rate Δt . The dependency of the model order and therefore the ARMA parameter values with the sampling rate can be the next step of a complete sensor error modeling.

REFERENCES

- [1] R.E.Kalman, "*A New Approach to Linear Filtering and Prediction Problems*", Trans ASME, Ser. D: Journal of Basic Engineers 82, March 1960, pp. 35-46.
- [2] R.E.Kalman and R.S. Bucy, "*New Results in Linear Filtering and Prediction Theory*", Trans ASME, Ser. D: Journal of Basic Engineers 83, 1961, pp. 95-108.
- [3] Peter S. Maybeck, "*The Kalman Filter: An Introduction To Concepts*" Academic Press Inc., 1979.
- [4] A.Gelb et al., "*Applied Optimal Estimation*", MIT Press, 1986
- [5] R.B Brown and P.Y.C. Hwang, "*Introduction to Random Signals and Applied Kalman Filtering*", 3rd Edition, Wiley, 1997
- [6] E.I.Gustafson, "*A post-processed Kalman Smoother for Underwater Vehicle Navigation*", Thesis, FAU Ocean Engineering Department, 2001
- [7] G.Grenon, "*Enhancement of the Inertial Navigation System for the Florida Atlantic University Autonomous Underwater Vehicle*", Thesis, FAU Ocean Engineering Department, 1999
- [8] M.S Grewal and A.P Andrews, "*Kalman Filtering: Theory and Practice*", Englewood Cliffs, NJ: Prentice-Hall, 1993
- [9] John C.HOFF, "*A Practical Guide To Box-Jenkins Forecasting*", Lifetime learning publication, 1983.

- [10] Walter Vandaele, "*Applied Time-Series And Box-Jenkins Models*", Academic Press, 1983.
- [11] M. Niedzwiecki, K. Cisowski, "*Adaptive scheme for elimination of broadband noise and impulsive disturbances from AR and ARMA signals*", IEEE Trans. on Signal Processing, Vol.44, March 1996, pp. 528-537.
- [12] G. Doblinger, "*An adaptive Kalman filter for the enhancement of noisy AR signals*", Proc.1998 IEEE Intl. Symp. ISCAS '98, May 31- June 3, 1998, Vol.5, pp. 305-308.
- [13] S. Degerine, S. Lambert, "*Characterization Of The Partial Autocorrelation Function Of Nonstationary Time Series*", Laboratoire LMC-IMAG, Grenoble, France.
- [14] J.S. Bendat, A.G. Piersol "*Random Data: Analysis and Measurement Procedure*" 3rd edition, WILEY Inter-Science.
- [15] J.S. Riedel, "*Seaway Learning And Motion Compensation In Shallow Waters For Small Auvs*", Thesis, Naval Postgraduate School Monterey CA., 1999.
- [16] Raman K. Merha, "*On The Identification Of Variances And Adaptive Kalman Filtering*" IEEE Transactions on automatic control, 1970, Vol. 15 Issue: 2, pp. 175-184.
- [17] Bc. Jan Kybic, "*Kalman Filtering and Speech Enhancement*", Thesis, Ecole Polytechnique Federale de Lausanne, 1998.
- [18] Wold, H (1938), "*A Study In The Analysis Of Stationary Time Series*", Almqvist and Wiksell, Uppsala, Sweden.
- [19] B.D.Ripley, "*Appendix A in Pattern Recognition and Neural Networks*", Cambridge University Press, 1996.
- [20] Simon Haykin, "*Adaptive Filter Theory*", Prentice Hall 3rd Edition 1996.

- [21] Akaike, H. (1973), "*Information theory and an extension of the maximum likelihood principle*". In B.N. Petrov and F. Csake (eds.), Second International Symposium on Information Theory. Budapest: Akademiai Kiado, pp. 267-281.
- [22] Akaike, H., "*A New Look at the Statistical Model Identification*". IEEE Transactions on automati Control, Dec. 1974, Vol. 19 Issue: 6, pp. 716-723.
- [23] J. Wang, S.Y. Chao, A.M. Agogino, "*Sensor Noise Model Development of a Longitudinal Positioning System for AVCS*", 1999 ACC Session FM11-1, Berkeley, CA, pp. 3760-3764 Vol.4.
- [24] L.Ljung, "*Analysis of recursive stochastic algorithms*", Automatic Control, IEEE Transactions on Automatic Control, Volume: 22 Issue: 4, Aug 1977 pp. 551-575.
- [25] A. ARCESE, "*On the Method of Maximum Entropy Spectrum Estimation*", IEEE Transactions on Information Theory, Vol IT-29, January 1983, pp. 161-164.
- [26] S. Smith, P.E. AN, K. Holappa, J. Whitney, A. Burns, K. Nelson, E. Heatzig, O. Kempfe, D. Kronen, T. Pantelakis, E. Henderson, G. Font, R. Dunn, and S.E. Dunn, "*The Morpheus Ultramodular Autonomous Underwater Vehicle*", IEEE Journal Of Oceanic Engineering, vol. 26, no. 4, Oct. 2001, pp. 453-465.
- [27] Manhar R. Dhanak, P.E. An, and K. Holappa, "*An AUV Survey in the Littoral Zone: Small-Scale Subsurface Variability Accompanying Synoptic Observations of Surface Currents*", IEEE Journal Of Oceanic Engineering, vol. 26, no. 4, Oct. 2001, pp. 752-768.
- [28] "*TCM2 Electronic Compass Module – User's Manual*", Precision Navigation, Inc, June 1995.
- [29] "*Workhouse Navigator DVL 1200, 600 or 300 kHz*" RD Instruments.

- [30] “*DMU User’s Manual*”, Crossbow Technology, Inc, San Jose CA.
- [31] K.M, Malladi, K.; R.V.R. Kumar, K.V. Rao, “*Gauss-Markov model formulation for the estimation of ARMA model of time-varying signals and systems*” IEEE International Conference on Global Connectivity in Energy, Computer, Communication and Control, Vol.1, 1998, pp 166-169.
- [32] Y.K. Wong, A.B. Rad, “*Gauss-Markov models for forecasting and risk evaluation*” IEEE Proceeding of EMPD, March 98, pp. 287-292.
- [33] O. Nelles, “*Nonlinear System Identification*”, Springer, Berlin 2001.
- [34] L.Ljung,” *From data to model: A guided Tour*”, International Conference on Control, Vol. 1, Mar 1994, pp. 422-430.
- [35] “VP Oncore GPS Receiver”, Motorola. www.oncore.motorola.com

APPENDIX A

ARMA Parameter Orders and Estimates:

1 – Sensor Error Model Orders

2 – TCM2 Compass Heading parameters

3 – GPS parameters

4 – Crossbow IMU parameters

APPENDIX A – 1

SENSOR ERROR MODEL ORDERS

Measurement	Set	P	D	Q	AIC	WT
Compass Heading	Laboratory (1)	6	0	10	-1.7317	3.5579
		10	0	8	-1.9106	3.5970
	Outdoor	10	0	5	-1.0782	3.4539
		8	0	7	-1.0717	3.9773
	Laboratory (2)	10	0	9	-6.0531	1.6486
		10	0	10	-6.4937	1.7970
Compass Heading Differentiated	Laboratory (1)	6	1	10	-1.9077	3.5384
		6	1	10	-1.9077	3.5384
	Outdoor	4	1	6	-1.0509	3.3641
		8	1	10	-1.0497	3.9758
	Laboratory (2)	10	1	9	-5.3254	2.1012
		10	1	8	-5.3185	2.2317
GPS	Latitude	2	0	2	-3.25018	3.3370
		10	0	10	-3.2413	4.2639
	Longitude	5	0	5	-3.1736	6.3958
		10	0	0	-3.1708	8.0789
IMU	X acceleration	3	0	5	-9.7482	3.9710
		5	0	10	-9.7385	4.2780
	Y acceleration	3	0	3	-9.3977	3.7432
		10	0	4	-9.3932	4.3823
	Z acceleration	10	0	10	-9.7425	3.6668
		6	0	9	-9.7403	3.8228
	Yaw rate	5	0	9	-6.9313	4.4642
		5	0	9	-6.9313	4.4642
	Roll rate	3	0	3	-7.0698	3.7046
		8	0	10	-7.0673	3.9059
	Pitch rate	3	0	4	-7.1457	3.7432
		7	0	10	-7.1443	4.4364

APPENDIX A – 2

TCM2 Compass Heading parameters

Laboratory 1 Heading

Original signal:

AIC CRITERION: (6,0,10)

Order	1	2	3	4	5	6	7	8	9	10
A	-2.203	1.251	0.483	-1.302	1.234	-0.463				
Order	1	2	3	4	5	6	7	8	9	10
B	-2.149	0.846	0.964	-1.034	0.654	-0.428	0.164	0.0620	-0.108	0.028

WHITENESS TEST: (10,0,8)

Order	1	2	3	4	5	6	7	8	9	10
A	-0.986	0.580	-0.615	-0.652	0.783	-0.355	0.377	-0.0180	0.020	-0.133
Order	1	2	3	4	5	6	7	8		
B	-0.931	0.239	-0.518	-0.515	0.849	-0.164	0.191	-0.144		

Difference signal:

AIC CRITERION – WHITENESS TEST: (6,1,10)

Order	1	2	3	4	5	6	7	8	9	10
A	0.0427	0.4656	0.2463	-0.446	0.0654	0.190				
Order	1	2	3	4	5	6	7	8	9	10
B	-0.930	0.0639	-0.028	-0.548	0.4477	-0.081	0.113	-0.064	-0.024	0.058

OUTDOOR Heading

Original signal:

AIC CRITERION: (10,0,5)

Order	1	2	3	4	5	6	7	8	9	10
A	0.293	0.2880	-0.457	0.040	-0.911	-0.088	-0.157	0.0662	-0.120	0.0456
Order	1	2	3	4	5					
B	0.0413	0.134	-0.382	0.056	0.830					

WHITENESS TEST: (8,0,7)

Order	1	2	3	4	5	6	7	8		
A	-1.092	1.043	-0.164	-0.216	-0.165	0.182	-0.435	-0.153		
Order	1	2	3	4	5	6	7			
B	-1.352	1.257	-0.173	-0.590	0.303	-0.016	0.416			

1st difference:**AIC CRITERION: (4,1,6)**

Order	1	2	3	4	5	6	7	8	9	10
A	0.801	1.058	0.924	0.5756	-	-	-	-	-	-
Order	1	2	3	4	5	6	7	8	9	10
B	-0.438	0.243	0.0146	-0.483	-0.336	0.081	-	-	-	-

WHITENESS TEST: (8,1,10)

Order	1	2	3	4	5	6	7	8	9	10
A	1.596	1.471	2.183	2.518	1.723	1.458	1.288	0.578	-	-
Order	1	2	3	4	5	6	7	8	9	10
B	0.354	-0.335	0.893	0.155	-0.953	0.0845	-0.084	-0.683	-0.286	0.117

Laboratory 2 Heading**Original signal:****AIC CRITERION: (10,1,9)**

Order	1	2	3	4	5	6	7	8	9	10
A	1.438	1.145	0.417	-0.466	-1.159	-1.419	-1.133	-0.420	0.431	0.168
Order	1	2	3	4	5	6	7	8	9	10
B	1.990	2.403	2.098	1.202	0.075	-0.870	-1.268	-0.988	-0.168	-

WHITENESS TEST: (10,0,10)

Order	1	2	3	4	5	6	7	8	9	10
A	1.507	1.182	0.405	-0.524	-1.237	-1.487	-1.168	-0.407	0.488	0.241
Order	1	2	3	4	5	6	7	8	9	10
B	2.052	2.464	2.125	1.176	0.001	-0.967	-1.359	-1.044	-0.171	0.0342

Difference signal:**AIC CRITERION: (10,1,9)**

Order	1	2	3	4	5	6	7	8	9	10
A	-1.604	1.657	-0.995	0.0463	1.004	-1.583	1.646	-0.993	0.0448	0.029
Order	1	2	3	4	5	6	7	8	9	10
B	-2.279	2.668	-2.043	0.673	0.930	-2.138	2.533	-1.952	0.643	

WHITENESS TEST: (10,1,8)

Order	1	2	3	4	5	6	7	8	9	10
A	1.461	1.197	-0.693	-0.173	0.841	-0.829	0.739	-0.162	-0.113	-0.073
Order	1	2	3	4	5	6	7	8	9	10
B	-1.461	1.197	-0.693	-0.052	0.911	-1.345	1.190	-0.606		

APPENDIX A – 3

GPS parameters

GPS Latitude

AIC CRITERION:

Order	1	2	3	4	5	6	7	8	9	10
A	-1.977	0.644								
Order	1	2	3	4	5	6	7	8	9	10
B	-1.210	0.242								

WHITENESS TEST:

Order	1	2	3	4	5	6	7	8	9	10
A	-0.985	-0.151	0.035	-0.067	0.116	0.112	0.167	-0.207	0.664	0.643
Order	1	2	3	4	5	6	7	8	9	10
B	-0.198	-0.141	-0.041	-0.130	0.013	0.079	0.249	-0.038	-0.616	0.136

GPS Longitude

AIC CRITERION:

Order	1	2	3	4	5	6	7	8	9	10
A	-1.343	0.2859	-0.239	0.0359	0.260	-	-	-	-	-
Order	1	2	3	4	5	6	7	8	9	10
B	-0.597	0.042	-0.249	-0.172	0.018					

WHITENESS TEST:

Order	1	2	3	4	5	6	7	8	9	10
A	-0.787	-0.177	-0.062	-0.022	0.068	0.021	-0.061	0.048	-0.026	0.041
Order	1	2	3	4	5	6	7	8	9	10
B	-	-	-	-	-	-	-	-	-	-

APPENDIX A – 4

Crossbow IMU parameters

IMU X acceleration

AIC CRITERION:

Order	1	2	3	4	5	6	7	8	9	10
A	-0.089	0.080	-0.990	-	-	-	-	-	-	-
Order	1	2	3	4	5	6	7	8	9	10
B	-0.055	0.080	-0.977	-0.011	0.015	-	-	-	-	-

WHITENESS TEST:

Order	1	2	3	4	5	6	7	8	9	10
A	-0.861	-0.243	0.634	-0.654	0.124	-	-	-	-	-
Order	1	2	3	4	5	6	7	8	9	10
B	-0.831	-0.269	0.634	-0.626	0.102	0.001	0.035	-0.009	-0.016	0.003

IMU Y acceleration

AIC CRITERION:

Order	1	2	3	4	5	6	7	8	9	10
A	-0.439	0.020	-0.581	-	-	-	-	-	-	-
Order	1	2	3	4	5	6	7	8	9	10
B	-0.356	-0.108	-0.507	-	-	-	-	-	-	-

WHITENESS TEST:

Order	1	2	3	4	5	6	7	8	9	10
A	-0.534	0.365	-1.084	0.326	-0.388	-0.004	0.019	-0.041	0.006	-0.014
Order	1	2	3	4	5	6	7	8	9	10
B	-0.464	0.316	-1.006	0.285	-	-	-	-	-	-

IMU Z acceleration

AIC CRITERION:

Order	1	2	3	4	5	6	7	8	9	10
A	-0.333	0.170	0.069	-0.683	0.797	-0.356	0.176	0.0217	-0.712	-0.150

Order	1	2	3	4	5	6	7	8	9	10
B	-0.260	0.134	0.070	-0.668	0.748	-0.279	0.151	0.021	-0.695	-0.199

WHITENESS TEST:

Order	1	2	3	4	5	6	7	8	9	10
A	-2.154	2.214	-1.170	-0.231	1.038	-0.697	-	-	-	-
Order	1	2	3	4	5	6	7	8	9	10
B	-2.081	2.050	-1.006	0.3033	0.998	-0.583	-0.096	0.032	-0.007	-

IMU Yaw rate

AIC CRITERION:

Order	1	2	3	4	5	6	7	8	9	10
A	-0.162	0.178	-0.111	-0.029	-0.877	-	-	-	-	-
Order	1	2	3	4	5	6	7	8	9	10
B	-0.138	0.174	-0.093	-0.014	-0.856	-0.003	0.003	0.020	-0.013	-

WHITENESS TEST:

Order	1	2	3	4	5	6	7	8	9	10
A	-0.122	-0.008	-0.177	0.012	-0.313	-0.093	-0.130	-0.101	-	-
Order	1	2	3	4	5	6	7	8	9	10
B	-	-	-	-	-	-	-	-	-	-

IMU Roll rate

AIC CRITERION:

Order	1	2	3	4	5	6	7	8	9	10
A	0.998	-1.000	-0.999	-	-	-	-	-	-	-
Order	1	2	3	4	5	6	7	8	9	10
B	0.990	-0.987	-0.979	-	-	-	-	-	-	-

WHITENESS TEST:

Order	1	2	3	4	5	6	7	8	9	10
A	-1.296	0.014	1.941	-2.259	0.474	0.993	-1.128	0.261	-	-
Order	1	2	3	4	5	6	7	8	9	10
B	-1.284	0.004	1.922	-2.206	0.422	1.007	-1.087	0.204	0.023	0.005

IMU Pitch rate

AIC CRITERION:

Order	1	2	3	4	5	6	7	8	9	10
A	0.996	-1.000	-0.997	-	-	-	-	-	-	-
Order	1	2	3	4	5	6	7	8	9	10
B	0.976	-1.003	-0.973	0.008	-	-	-	-	-	-

WHITENESS TEST:

Order	1	2	3	4	5	6	7	8	9	10
A	-0.000	-1.094	0.375	-0.696	-0.650	0.788	0.273	-	-	-
Order	1	2	3	4	5	6	7	8	9	10
B	-0.021	-1.081	0.387	-0.699	-0.628	0.785	0.265	0.011	-0.003	-0.014

